

# Development of an Inhalable Dry Powder Platform for mRNA Therapeutics

**Dissertation**

zur Erlangung des Doktorgrades  
der Mathematisch-Naturwissenschaftlichen Fakultät  
der Christian-Albrechts-Universität zu Kiel

vorgelegt von  
**Jana Karin Schembera**

Kiel, 2024



## Vorbemerkung

Die vorliegende Arbeit wurde unter Anleitung von Prof. Dr. Regina Scherließ in der Zeit von April 2020 bis April 2024 an der Mathematisch-Naturwissenschaftlichen Fakultät der Christian-Albrechts-Universität zu Kiel angefertigt.

1. Gutachterin: Prof. Dr. Regina Scherließ

2. Gutachterin: Assoc. Prof. Jenny Lam

Tag der mündlichen Prüfung: 04.06.2024



*Für meine Familie*



*„Man braucht im Leben nichts zu fürchten, man muss es nur verstehen.“*

*Marie Curie*



Lack of a specific mark or a reference to trademark or a patent does not imply that this work or part of it can be used or copied without copyright permission.



Parts of this work have already been published:

## Conference Contributions

### Poster Presentations

#### **Transfection of Calu-3 cells with mRNA/DOTAP:DOPE lipoplexes: influence of weight ratio and forming media**

Schembera J., Scherließ R.

13<sup>th</sup> World Meeting on Pharmaceutics, Biopharmaceutics and Pharmaceutical Technology, Rotterdam, The Netherlands (2022)

#### **A functional study of tubing material for the spray drying of mRNA lipoplexes**

Schembera J., Leister R., Scherließ R.

Drug Delivery to the Lungs, Edinburgh, Scotland (2022)

#### **Spray drying mRNA lipoplexes for inhalation: finding the highest possible process temperature**

Schembera J., Leister R., Müller C., Scherließ R.

10<sup>th</sup> Polish-German Symposium on Pharmaceutical Sciences, Düsseldorf, Germany (2023)

#### **Spray drying of mRNA lipoplexes to produce an inhalable dry powder formulation for mRNA therapeutics**

Schembera J., Leister R., Müller C., Scherließ R.

Drug Delivery to the Lungs, Edinburgh, Scotland (2023)

#### **Optimising aerodynamic performance of spray dried mRNA lipoplexes in mannitol and lactose matrix**

Schembera J., Leister R., Müller C., Scherließ R.

14<sup>th</sup> World Meeting on Pharmaceutics, Biopharmaceutics and Pharmaceutical Technology, Vienna, Austria (2024)



---

## Table of Contents

|        |  |    |
|--------|--|----|
| 1.     | Introduction .....                             | 1  |
| 2.     | Objectives .....                               | 3  |
| 3.     | Theoretical Background.....                    | 4  |
| 3.1.   | mRNA Therapeutics .....                        | 4  |
| 3.1.1. | Principle of Action of mRNA Therapeutics ..... | 4  |
| 3.1.2. | Delivery of mRNA Therapeutics .....            | 8  |
| 3.2.   | Respiratory Drug Delivery.....                 | 11 |
| 3.2.1. | Anatomy and Physiology of the Lungs .....      | 12 |
| 3.2.2. | Delivery to the Lungs .....                    | 13 |
| 3.3.   | Spray Drying.....                              | 16 |
| 4.     | Materials.....                                 | 18 |
| 4.1.   | Firefly Luciferase mRNA.....                   | 18 |
| 4.2.   | DOTAP and DOPE .....                           | 19 |
| 4.3.   | Matrix Materials .....                         | 20 |
| 4.3.1. | Mannitol .....                                 | 20 |
| 4.3.2. | Lactose .....                                  | 21 |
| 4.4.   | L-Leucine .....                                | 22 |
| 4.5.   | Cell Lines .....                               | 23 |
| 4.5.1. | Calu-3 Cells .....                             | 23 |
| 4.5.2. | A549 Cells.....                                | 23 |
| 5.     | Methods .....                                  | 24 |
| 5.1.   | Preparative Methods .....                      | 24 |
| 5.1.1. | Preparation of DOTAP:DOPE Liposomes.....       | 24 |
| 5.1.2. | Preparation of mRNA Lipoplexes .....           | 25 |
| 5.1.3. | Spray Drying .....                             | 26 |
| 5.1.4. | Preparation of Sweeper Crystal Blends.....     | 27 |
| 5.2.   | Characterisation Methods.....                  | 28 |
| 5.2.1. | Dynamic Light Scattering .....                 | 28 |

|  |     |
|--|-----|
| 5.2.2. Determination of the Zeta Potential .....   | 29  |
| 5.2.3. Fluorescence Displacement .....   | 29  |
| 5.2.4. Agarose Gel Electrophoresis .....   | 30  |
| 5.2.5. Particle Imaging .....  | 30  |
| 5.2.6. Water Content .....   | 31  |
| 5.2.7. Particle Size Distribution .....  | 31  |
| 5.2.8. Aerodynamic Characterisation .....  | 32  |
| 5.2.9. <i>In vitro</i> Cell Experiments.....   | 34  |
| 5.3. Statistical Methods .....   | 36  |
| 5.3.1. Box Plots.....  | 36  |
| 5.3.2. Significance Testing.....   | 36  |
| 6. Results and Discussion .....  | 37  |
| 6.1. Packaging mRNA for Efficient Transfection.....  | 37  |
| 6.1.1. Preparing DOTAP:DOPE Liposomes.....   | 38  |
| 6.1.2. Preparation of mRNA Lipoplexes.....   | 42  |
| 6.1.3. Conclusion on the Preparation of DOTAP:DOPE Liposomes and mRNA<br>Lipoplexes.....                 | 55  |
| 6.2. Formulation of mRNA Lipoplexes via Spray Drying: Process Optimisation<br>and Characterisation ..... | 57  |
| 6.2.1. Choosing Spray Dryer Model and Tubing Material .....  | 58  |
| 6.2.2. Mannitol and Lactose as a Matrix for Spray Drying mRNA Lipoplexes.....                            | 63  |
| 6.2.3. Spray Drying mRNA Lipoplexes in a Mannitol or Lactose Matrix .....                                | 67  |
| 6.2.4. Conclusion on Spray Drying mRNA Lipoplexes.....   | 81  |
| 6.3. Optimising the Aerodynamic Performance .....  | 83  |
| 6.3.1. Introduction of Sweeper Crystals.....   | 83  |
| 6.3.2. Increasing Particle Surface Hydrophobicity .....  | 90  |
| 6.3.3. Conclusion on Optimising the Aerodynamic Performance and Increasing<br>Detachment.....            | 105 |
| 7. Conclusion and Perspectives.....  | 107 |
| 8. Abstract .....  | 112 |

---

|       |                              |     |
|-------|------------------------------|-----|
| 9.    | Zusammenfassung.....         | 114 |
| 10.   | Appendix .....               | 116 |
| 10.1. | Abbreviations.....           | 116 |
| 10.2. | Substances .....             | 118 |
| 10.3. | Equipment and Software ..... | 121 |
| 11.   | References.....              | 124 |



---



## 1. Introduction

Since the approval of the first messenger RNA (mRNA) vaccine formulations against SARS-CoV-2 (severe acute respiratory syndrome coronavirus 2) by BioNTech/Pfizer and Moderna in 2021, mRNA therapeutics are on the rise with various application areas including cancer, viral infections, autoimmune diseases and metabolic disorders [1–4]. Through their ability to induce the production of a specific protein in the patients' own cells, mRNA therapeutics promise a powerful tool for preventive, curative and disease-modifying therapies.

mRNA can be synthesised through an *in vitro* transcription process, which is cost-effective and adaptable to various therapeutic applications. This method allows for the rapid production of mRNA, facilitating a swift response to emerging strains of pathogens or new therapeutic targets. This flexibility is particularly advantageous in the context of infectious diseases, where pathogens can evolve rapidly, necessitating timely adjustments to treatment strategies [5]. In 2022, this unique feature was particularly utilised to adapt the SARS-CoV-2 vaccines to the omicron variants of the virus [6, 7].

mRNA itself is a delicate, single-stranded molecule that is susceptible to degradation by nucleases and thermal or shear stress [8–10]. Effective delivery of mRNA to the target cells is key to therapeutic success because RNA itself cannot overcome the cell membrane. Thus, effective delivery of mRNA relies on encapsulating it within a vector. These vectors, whether lipids, polymer, or adapted viruses, offer protection and facilitate transfection into cells.

Administering mRNA therapeutics intravenously can expose the mRNA to harsh enzymatic conditions and leads to mRNA therapeutics inevitably ending up in the liver [11]. While intramuscular administration is the most common delivery route for vaccination, it often leads to a weak mucosal immune response and inadequate preparation of the actual entry point for infection [12].

An alternative and promising approach is delivering therapeutics by inhalation [2]. The lungs, with their enormous, highly vascularised surface area, especially enable the local treatment of diseases [13, 14]. This is particularly beneficial for respiratory ailments such as cystic fibrosis or lung cancer and vaccination against respiratory pathogens. By delivering the vaccine directly to the point of entry for many respiratory pathogens, specifically targeting the mucosal immune system becomes feasible, thereby inducing both local and systemic immune responses. Moreover, inhalation is a non-invasive administration method, eliminating the need for trained health personnel to prepare and administer doses and ultimately reducing barriers to access [15, 16]. This approach holds significant potential for improving the efficacy and convenience of mRNA therapeutics and vaccines.

A currently ongoing clinical trial investigates an mRNA therapeutic aimed to locally treat cystic fibrosis [17]. The drug was administered by nebulisation to the patients. During nebulisation, a liquid is required to be nebulised by an electronically powered nebuliser. The liquid has to be

reconstituted from a lyophilisate or comes as a solution or suspension. Those delivery forms necessitate stringent storage conditions like the liquid vaccines against SARS-CoV-2 [18]. Hence, a dry powder formulation is highly desirable due to its enhanced stability and properties, which can be tailored for efficient delivery. Moreover, dry powder inhalers offer advantages such as compactness, intuitive usage, and the possibility of pre-filled doses in a disposable inhaler.

In a world that can quickly be turned upside down by a pandemic, the need arose for a platform formulation that seamlessly combines the benefits of mRNA therapeutics with inhalation delivery, all while ensuring the protection of mRNA, efficient cellular delivery, and optimal aerodynamic performance. The endeavour to develop such a platform is the subject of the present work.

## 2. Objectives

The administration of mRNA to the lungs in a dry powder formulation combines the advantages of targeting the lungs for local and systemic drug delivery with an enhanced stability of powders compared to liquid formulations. Hence, the objective of this work is to develop an inhalable dry powder platform for mRNA therapeutics that facilitates high transfection efficiency while also possessing the necessary aerodynamic characteristics.

The formulation of mRNA into a dry powder for inhalation presents numerous challenges, as mRNA is prone to degradation from nucleases, as well as thermal or shear stress [8–10]. Furthermore, effective delivery of mRNA into the host cells is key to therapeutic success, as RNA alone cannot overcome the cell membrane. Therefore, effective delivery of mRNA relies on encapsulating it within a vector that provides protection and facilitates cellular delivery. Importantly, these mRNA-vector complexes must remain intact throughout downstream processing steps like spray drying.

Consequently, the first aim of this work is to encapsulate a model mRNA within a vector, in a composition that ensures the most efficient transfection. To focus on the development of the dry powder formulation, the combination of the lipids DOTAP and DOPE, which is a well-known, efficient and non-toxic transfection agent, is employed as a vector [19].

Once the most efficient lipoplex composition is determined, the second part of this work aims for the establishment of a spray drying process that maintains transfection efficiency while generating particles within the inhalable size range. As matrix materials for the spray dried formulation different excipients are being considered to explore their potential stabilising effects as excipients.

Spray dried formulations within the inhalable range often exhibit poor flowability and cohesiveness, posing challenges such as unfavourable low fine particle fractions or a high powder residue in the capsules used in the inhaler to deliver the formulation. Hence, the final aim of this work is to characterise and optimise the spray dried formulation and to overcome the challenges associated with the various process steps.

By developing the platform step by step, this work aims to show a proof of concept and to set the foundation for the enhancement of an inhalable dry powder platform for mRNA therapeutics with an excellent aerodynamic performance and high transfection efficiency.

## 3. Theoretical Background

### 3.1. mRNA Therapeutics

#### 3.1.1. Principle of Action of mRNA Therapeutics

Ribonucleic acid (RNA) therapy has demonstrated promising results in numerous preclinical and clinical studies for the treatment of a broad spectrum of diseases, spanning genetic disorders, viral infection, cancer, neurodegenerative conditions, and cardiovascular and cerebrovascular ailments. Various types of RNA are utilised to address diverse medical conditions. The two most common therapeutic RNAs currently in research are messenger and short interference RNA (mRNA and siRNA) [20].

The therapeutic potential of messenger ribonucleic acid (mRNA) holds unparalleled potential in the treatment of a broad range of partly incurable diseases, beyond its application as vaccine. mRNA-based therapeutics offer enhanced transfection efficiency compared to DNA and higher levels of intracellular proteins than protein drugs [2, 5].

mRNA itself is naturally created by transcription of DNA within the nucleus of a cell and subsequently released into the cytosol to be translated into a protein by a ribosome (Figure 3.1).

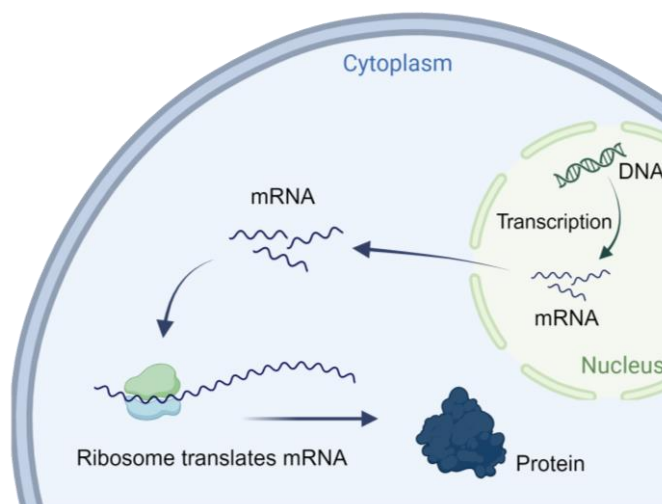


Figure 3.1: The processing of DNA and mRNA to produce a protein in a schematic, simplified representation. Created with BioRender.com

Protein expression is a tightly regulated process and pivotal for cellular functionality. A decisive parameter is the regulation of mRNA half-life to change the overall abundance of functional proteins or to eliminate aberrant mRNA, preventing the production of potentially toxic or misfolded proteins. mRNA decay is mediated by several types of ribonucleolytic enzymes that degrade mRNA through different mechanisms. The major mRNA decay pathways involve

exonucleases and endonucleases, which work tightly together with other enzymes and proteins in a highly regulated process in order to facilitate degradation [21–23].

This mechanism of protein expression and its regulation is a vital procedure to keep organisms functional, while at the same time presenting a promising tool in curative and disease-modifying therapies [24].

mRNA and DNA can be designed *in vitro* to produce a specific protein *in vivo*. In contrast to DNA, which is more commonly used in gene therapy, mRNA does not need to enter the nucleus to be processed and does not insert into the genome [5].

mRNA is typically a single-stranded molecule, including a cap structure at the 5' and a poly(A) tail at the 3' end (Figure 3.2) [25].

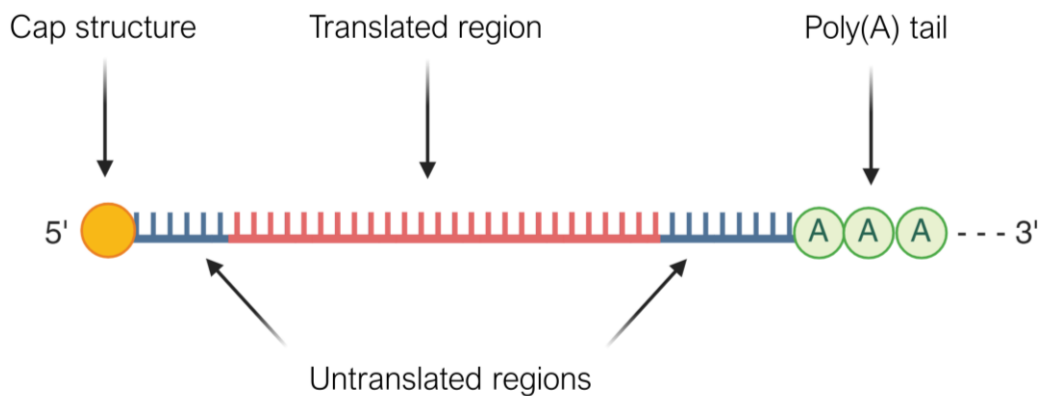


Figure 3.2: Schematic image of a mRNA molecule. Created with BioRender.com

In between these structures lies a long strand of nucleotides, which is composed of the actual encoding nucleotides framed by untranslated regions. Each of these mRNA components plays a pivotal role in translation and offers a potential modification site to enhance protein expression [2, 26]. Various strategies have been employed to optimise mRNA. For instance, maximising the guanine-cytosine content or prolonging the poly(A) tail can improve stability, while inducing global changes in mRNA secondary structure can enhance protein expression. Moreover, introducing modified uridines within the mRNA structure is currently the most efficient method to minimise cellular recognition of mRNA by RNA-binding proteins, which are key players in the innate immune reaction to foreign mRNA [2].

A remarkably interesting example for optimisation is the addition of the self-replicating basis of an RNA alphavirus to the strand of nucleotides. This virus is able to amplify RNA transcripts in the cytoplasm, thus increasing protein expression while requiring less initial mRNA [27–30].

Therapeutic mRNA can be synthesised through *in vitro* transcription, which involves the transcription of a deoxyribonucleic acid (DNA) template by an RNA polymerase, utilising nucleotides as substrates along with a cofactor. To prevent degradation, the mRNA must be capped at the 5' end, and a poly(A) tail must be added at the 3' end. The process is finalised with a purification step to obtain pure mRNA [31].

Those optimisations and the ease of syntheses facilitates rapid deployment across diverse therapeutics areas and serve various therapeutic strategies [32]. One approach involves the delivery of mRNA encoding functional proteins to directly replace a missing or downregulated endogenous protein or to provide functional foreign antibodies or proteins [32]. An example for this direct strategy is the mRNA-based treatment of cystic fibrosis. Cystic fibrosis is caused by a gene mutation of the cystic fibrosis transmembrane conductor regulator (CFTR). The CFTR, a membrane protein and anion channel, mainly functioning as a chloride channel, is involved in the production of sweat, digestive fluids, and mucus. Caused by the CFTR gene mutation the viscosity of these secretions increases, leading to difficulties in breathing, frequent lung and sinus infections, pancreatitis and infertility, for example [33]. One approach to deliver CFTR mRNA by inhalation to CFTR expressing epithelial cells started a phase 1/2 clinical trial in 2023 [17].

In addition to this direct strategy, mRNA can be applied as a vaccine against viruses, such as severe acute respiratory syndrome Coronavirus 2 (SARS-CoV-2) and potentially against the Influenza virus, Zika virus, or Human Immunodeficiency Virus (HIV) [32]. Comirnaty® and Spikevax®, developed by BioNTech/Pfizer and Moderna, respectively, are vaccines against the SARS-CoV-2 virus approved by the FDA in 2021 [3, 4]. They contain mRNA encoding the spike protein of the SARS-CoV-2 virus. After translation of this mRNA by the host cell, the spike protein is presented on the cell surface, providing the antigen target for B cells. Moreover, parts of the Spike proteins enter antigen presenting pathways, enabling T-cell recognition of antigens through MHC presentation of T-cell epitopes [1, 34].

mRNA-based cancer vaccines work by leveraging the body's immune system to recognise and neutralise cancer cells. Once in the body, the mRNA instructs cells to produce proteins that may stimulate an immune response against specific cancer antigens. These vaccines are personalised based on the molecular features of an individual's tumour and can be adapted to changes or modifications of the tumour. Numerous preclinical and clinical studies are ongoing in this field [26].

While mRNA is a useful tool to increase or correct target gene expression, another therapeutic strategy of RNA is to trigger gene inhibition. One example to inhibit gene expression is short interfering RNA (siRNA). siRNA mediates targeted mRNA degradation and thereby prevents the translation of these mRNAs into proteins. This process, known as RNA interference (RNAi), a natural defence mechanism for the invasion of exogenous genes, allows the selective silencing of disease-causing genes [35]. Onpattro®, an siRNA therapeutic formulated in lipid nanoparticles, was approved in 2018 for the treatment of the metabolic disease hereditary transthyretin amyloidosis [36]. This condition is characterised by the buildup of abnormal deposits of amyloids in organs or tissues. Onpattro® works by reducing the level of transthyretin protein, which helps to decrease the formation of amyloid deposits and ease the symptoms [37].

In order to use mRNA in a way that unlocks its full potential for treating difficult-to-treat diseases and for personalised medicine, mRNA requires a delivery system.

### 3.1.2. Delivery of mRNA Therapeutics

mRNA is susceptible to both degradation as well as physical instability. In addition to enzymatic degradation by nucleases, chemical degradation, particularly temperature-dependent hydrolysis, is a threat to mRNA integrity [38]. Despite the efforts to stabilise and optimise the mRNA itself, it requires a delivery system to protect it against degradation and to facilitate transfection, intracellular release and translation [2, 32]. Due to the negative potential across the cell surface, the negatively charged mRNA cannot overcome the membrane on its own [39]. However, the negative charge of mRNA can be exploited to form complexes with carrier molecules, commonly referred to as vectors.

In general, those carrier molecules can be categorised into non-viral and viral vectors. Owing to their high transfection efficiency viral vectors, such as genetically modified adenoviruses or alpha viruses, can be employed for mRNA delivery [40]. However, due to their high immunogenicity and complex and expensive preparation procedures, their clinical application is limited [26]. Hence, the non-viral vectors with slightly lower transfection efficiency, but improved safety profile, have emerged [41, 42]. As non-viral vectors, various technologies have already been and are still being developed [39]. Lipids and polymers have been extensively studied as non-viral vectors, with lipids being given priority following the approval of the lipid-based formulation Onpattro® in 2018, an siRNA treatment for hereditary transthyretin amyloidosis developed by Pieter Cullis and Alnylam [43]. Additionally, the mRNA vaccines against SARS-CoV-2 developed by BioNTech/Pfizer and Moderna in 2021 have also contributed to the increased interest in lipids as a vector system [1, 3, 4, 44].

These lipid-based formulations, schematically displayed in Figure 3.3, comprise an ionisable cationic lipid, a neutral lipid, cholesterol and a PEG-ylated lipid in varying molar ratios [1, 45].

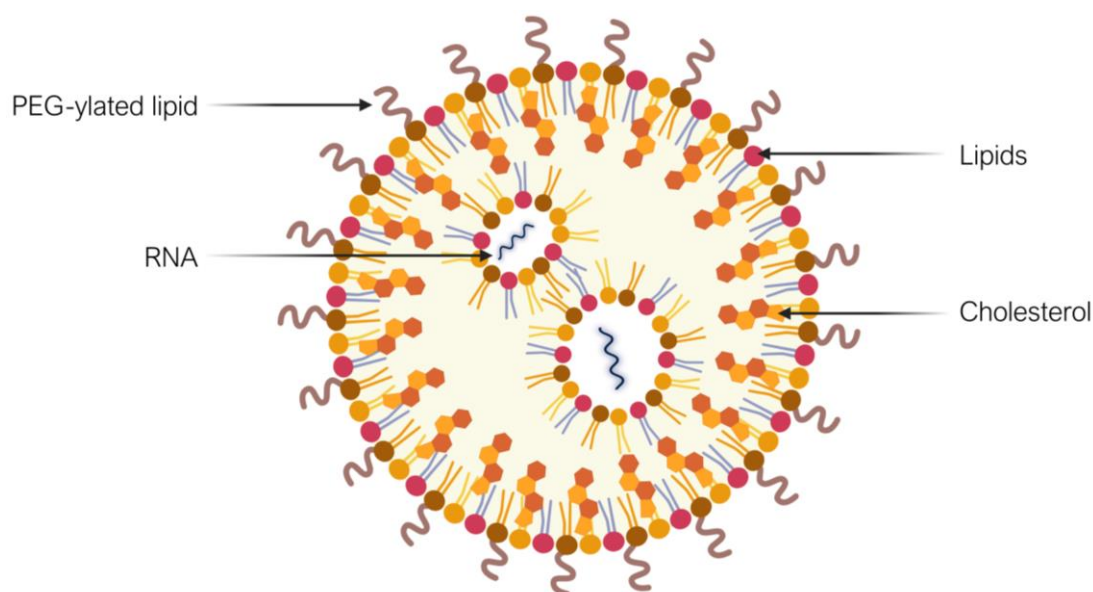


Figure 3.3: RNA complexed with lipids, stabilising PEG-ylated lipids and cholesterol. Created with BioRender.com

They all fulfil different functions, as cholesterol and the neutral lipid increase stability and the PEG-ylated lipid reduces immunogenicity as well as controls particle size and stability through steric hindrance [2, 46].

The principle of the ionisable lipids is that they remain neutral at physiological pH for safe systemic nucleic acid delivery, but become protonated in the acidic environment within the endosome, thereby enhancing endosomal escape [47]. Protonation is also the mechanism how the RNA is encapsulated. At a pH below the  $pK_a$  of the ionisable lipid, it forms complexes with the negatively charged RNA through electrostatic interactions [46]. These sophisticated lipids are based on amphiphilic cationic lipids, which are well-studied and known for their good transfection efficiency, such as DOTAP (1,2-dioleoyloxypropyl-N,N,N-trimethylammonium chloride). DOTAP in combination with the neutral helper lipid DOPE (1,2-dioleoyl-sn-glycero-3-phosphoethanolamine) builds stable cationic liposomes, which were previously used to complex DNA and RNA through electrostatic interactions [48]. The combination is safe for human administration and provided an efficient foundation for the formulation development of the inhalable dry powder platform for mRNA therapeutics in this work [49].

By preparing cationic lipoplexes from mRNA and an excess of cationic DOTAP:DOPE liposomes, the lipoplexes are attracted to the negatively charged cell membrane, thereby initiating transfection (Figure 3.4).

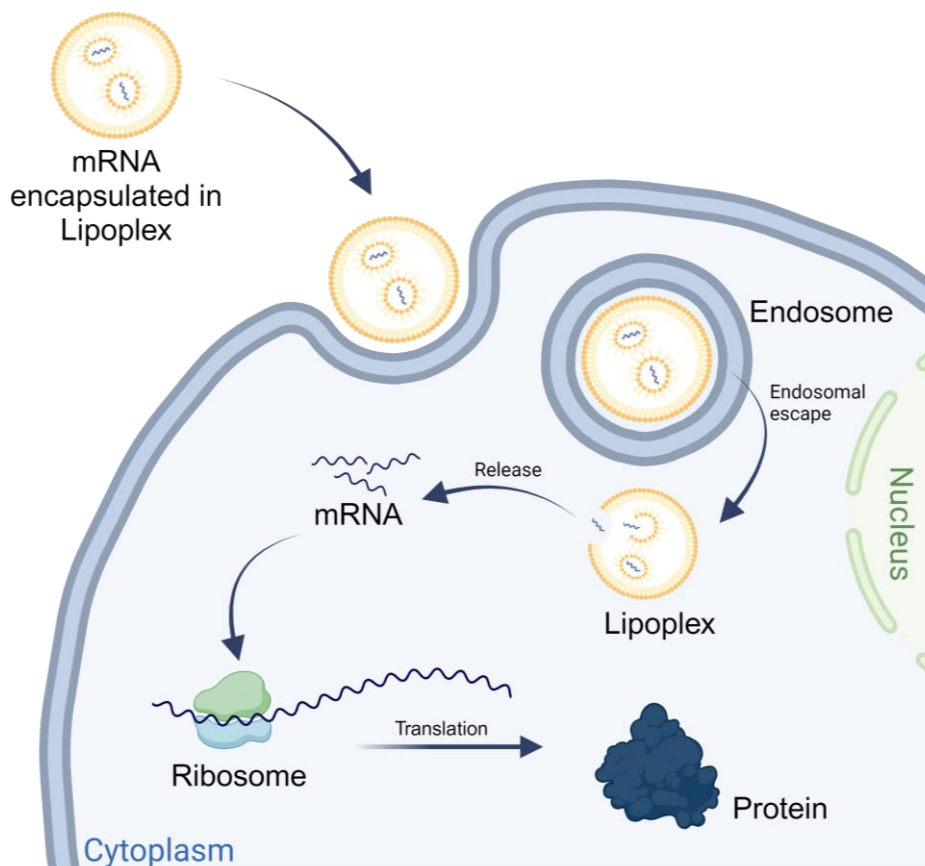


Figure 3.4: Cellular uptake and processing of mRNA lipoplexes. Created with BioRender.com

After uptake into the cells via endocytosis the lipoplex is enclosed in the endosome [50–53]. For endosomal escape, cationic lipids can form ion pairs with anionic phospholipids within the endosomal membrane, destabilising the membrane until the lipoplex can escape [53]. After reaching the cytosol, the mRNA is released from the lipoplex and available for translation by a ribosome to produce the encoded protein.

#### **3.1.2.1. Size Requirements and Preparations Methods for mRNA Therapeutics**

To design the lipoplexes as efficiently as possible, certain size requirements have to be met. Zhdanov et al. reported that a size in the lower nanometre range, between 70 and 200 nm, is suitable for efficient transfection [48]. This size ensures a balance between higher transfection levels *in vitro*, achieved by a larger size, and a preferable smaller particle size for a successful transfection *in vivo*. The lipid nanoparticle formulation in Comirnaty® (BioNTech/Pfizer) exhibits a hydrodynamic diameter of around 87 nm, while Spikevax® (Moderna) shows a z-average of approximately 217 nm [54, 55]. This demonstrates that the range set by Zhdanov et al. has no sharp borders and depends on the characteristics of the lipid nanoparticles.

In order to produce such small particles, various methods can be employed. There are two distinct preparation principles [56]. The first method is characterised by the *in situ* self-assembly of lipids and nucleic acids to lipid nanoparticles. This is achieved by mixing lipids, dissolved in ethanol, with an aqueous nucleic acid solution [46, 47]. While this principle of microfluidics allows large-scale production, it requires mixing and tubing systems. Although there have been advancements in the construction of those machines to reduce the dead volume and minimum required volume to produce lipid nanoparticles, there is still a significant amount of wasted material, especially in a laboratory setting [57].

The second strategy involves pre-forming liposomes in an aqueous solution as a first step. Those cationic liposomes are then mixed with anionic nucleic acids to build lipoplexes driven by electrostatic interactions. To obtain these liposomes in the first place, various methods are available [58]. The methods can be categorised in mechanical dispersion methods, such as sonication, and solvent dispersion methods, like ethanol injection [59]. Preparing liposomes by ethanol injection involves the rapid injection of an ethanolic lipid solution in an aqueous solution. Disadvantages of this method are a very high dilution of the liposomes, that the ethanol has to be removed and the heterogenous size of the particles obtained, likely making further homogenisation steps necessary [60]. Sonication, on the other hand, allows the production of small and uniform vesicles in a single step. However, particularly when using a probe-tip sonicator, the sample's temperature can rise locally, necessitating measures to control the temperature and to keep the homogenisation time as short as possible [59, 61].

### 3.1.2.2. Administration Routes and Stability of mRNA Therapeutics

Most of the RNA therapeutics in clinical trials and on the market, such as the mRNA vaccines against SARS-CoV-2 and the siRNA therapeutic Onpattro®, are typically delivered by intramuscular (i.m.) or intravenous (i.v.) injection or infusion. These administration routes require liquid formulations, which have to be stored under challenging storage conditions and usually necessitate dilution and aliquoting into the final dose. For example, the SARS-CoV-2 vaccine Comirnaty® needs to be stored frozen at - 75 °C for storage periods exceeding two weeks [18]. The maintenance of the storage conditions and the need for trained health personnel to prepare and administer the final drug can be difficult in areas with limited healthcare access. Therefore, a dry powder formulation would offer increased stability and shelf life as well as broader accessibility [16].

For targeting the liver, i.v. administration is the delivery route of choice for the lipid nanoparticle formulation Onpattro®. Lipid nanoparticles can easily pass through the fenestrated vasculature in the liver, enabling efficient hepatic expression of mRNA cargos [2]. On the other hand, in cases of targeting lung cancer or respiratory infections and diseases, a local administration of mRNA therapeutics directly to lungs may be more beneficial.

## 3.2. Respiratory Drug Delivery

Administering inhalable formulations to the lungs by using the patients' inspiration is a valuable tool in drug delivery and can achieve both local and systemic drug effects [62].

This approach is suitable for a wide range of substances, from small molecules like salbutamol or budesonide for the treatment of asthma, to very large oligonucleotides or proteins, such as Dornase alfa, which is used to treat cystic fibrosis. Respiratory delivery enables precise targeting of lung tissues, allowing for reduced drug doses compared to intravenous routes, thereby minimising systemic side effects [63]. Moreover, the lungs offer a vast, highly vascularised alveolar surface area of approximately 70 to 140 m<sup>2</sup>, whose epithelial cells serve as potential target cells for drugs such as RNA therapeutics. Pulmonary delivery is a promising approach for vaccination against respiratory pathogens and managing various lung disorders, ranging from cystic fibrosis to lung cancer [64].

### 3.2.1. Anatomy and Physiology of the Lungs

The lungs are responsible for the exchange of carbon dioxide, carried into the lungs in venous blood, with oxygen in the inhaled air. Inhaled air enters the lungs after passing the upper airways where it is heated to body temperature and humidified to a relative humidity of 99% [65]. As displayed in Figure 3.5, the lungs are divided into two lung lobes.

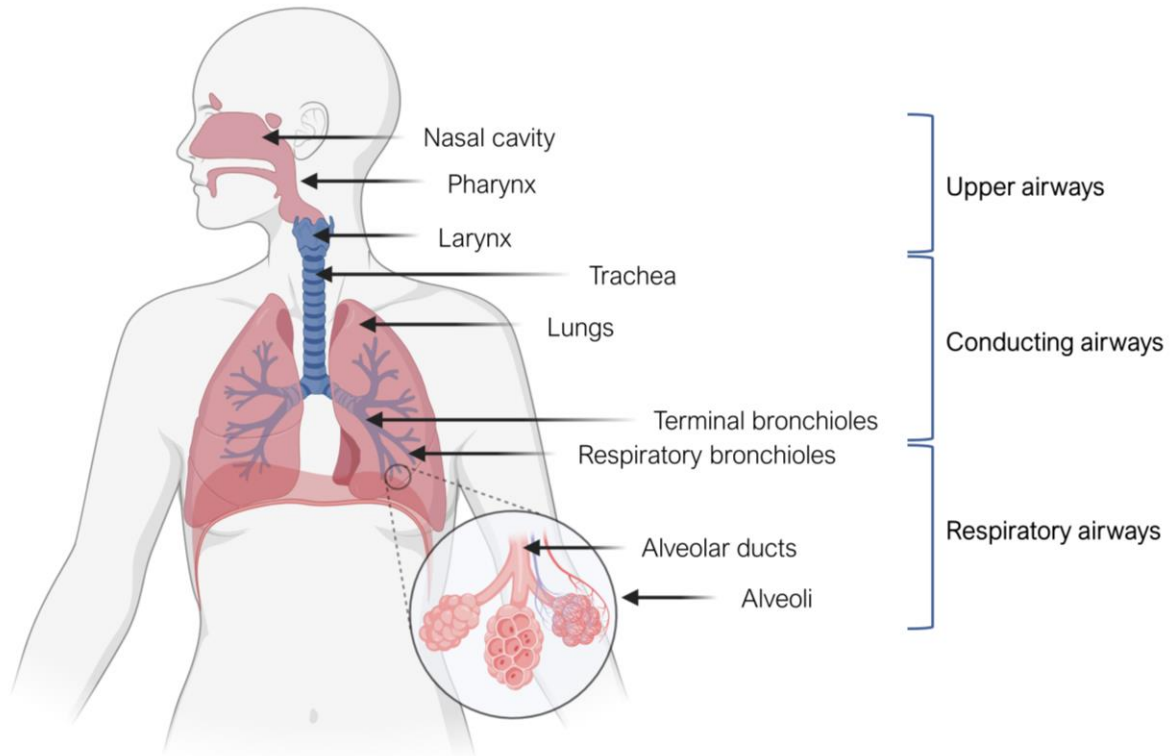


Figure 3.5: Anatomy of the respiratory tract. Created with BioRender.com

The airways are continuously bifurcating in a complex tubing system, which is comprised of two zones. The first zone of the lung entered by the air are the conducting airways, followed by the second zone the respiratory airways. The conducting airways are incapable of gas exchange and are guiding the air through the trachea, the bronchi and the bronchioles to the terminal bronchioles, which transfer the air into the respiratory airways. In the respiratory airways, which are equipped with all structures that participate in gas exchange, the branching of the airways continues until the alveoli are reached [66]. As the air stream travels through the airways, which decrease in diameter and increase in number, the velocity of the airflow decreases [65].

The respiratory tract is equipped with intrinsic defence mechanisms. Epithelial cells, provided with cilia and capable of mucus secretion, serve as primary clearance mechanisms in the upper and central regions of the lungs. The coordinated movement of cilia removes mucus, entrapping foreign particles, from the airways. In the peripheral lungs, the pulmonary surfactant layer assumes the predominant defence mechanism. Moreover, cellular components, such as macrophages, form intrinsic barriers against intruders [13, 67, 68].

### 3.2.2. Delivery to the Lungs

In order to efficiently deliver a drug particle to the lungs, it has to meet certain size requirements. To evaluate and compare different formulation strategies, the aerodynamic diameter was introduced. The aerodynamic diameter is defined as the diameter of a sphere with a density of  $1 \text{ g/cm}^3$  that has the same aerodynamic properties as the analysed particle. This definition allows the comparison between particles of differing shapes and densities on the basis of their aerodynamic properties [66]. Consequently, a porous particle with low density and a geometric diameter above  $5 \mu\text{m}$  may still have an aerodynamic diameter below  $5 \mu\text{m}$  [69]. The aerodynamic diameter can be assessed by cascade impaction (e.g. utilising the Next Generation Impactor (NGI)). An important result of this analysis is the fine particle fraction (FPF), which represents the percentage of the particles discharged from the device with an aerodynamic diameter smaller than  $5 \mu\text{m}$  [70].

There are three categories of how an aerosol particle can deposit onto the airway wall (Figure 3.6).

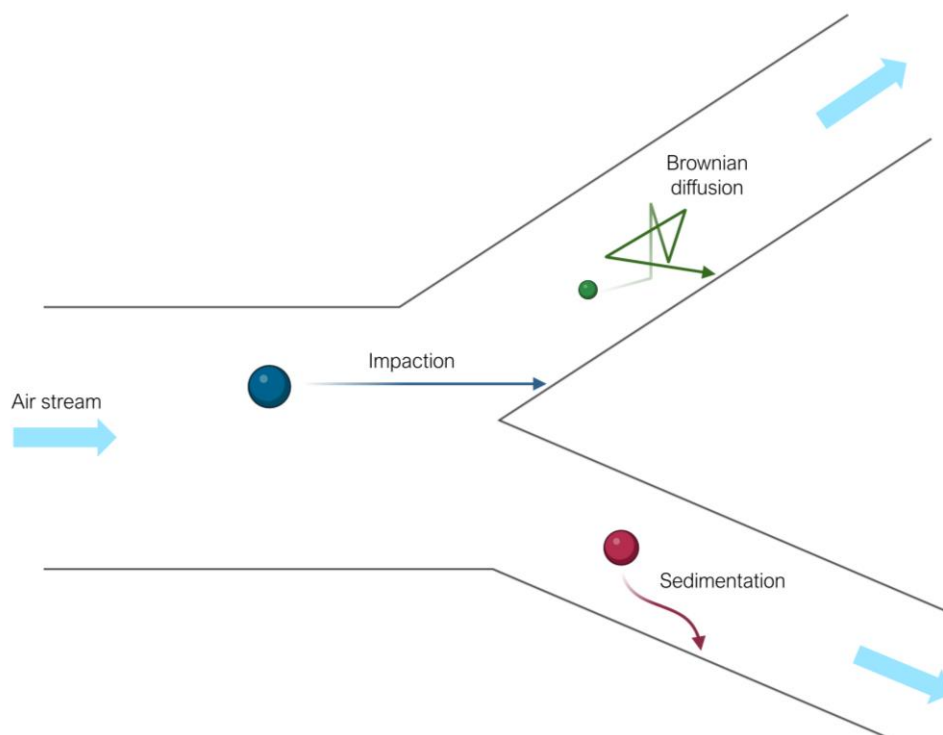


Figure 3.6: Schematic illustration of the three major deposition mechanisms for inhaled particles in the respiratory tract. Created with BioRender.com

While the mouth, pharynx and larynx constitute the major potential sites of aerosol deposition, particles also deposit at the branching points between the larger airways within the lungs. Since in these regions the airstream rapidly changes direction, a particle that has too much inertia (size range  $> 3 \mu\text{m}$ ) to follow the airstream impacts into the moist airway wall. Entering the small conducting airways and the respiratory zone, gravitational sedimentation is generally the dominant deposition process. Gravitational sedimentation of aerosol particles, occurring during

slow inhalation or breath holding, results in particles between 0.5 and 3  $\mu\text{m}$  descending under gravity and settling upon the airway surface. The third category of deposition is caused by Brownian diffusion of particles with diameters less than 0.5  $\mu\text{m}$  [65]. Particles with this aerodynamic particle size are likely to be exhaled [71, 72]. Hence, to reach an efficient deposition in the lungs particles of an aerodynamic diameter above 1  $\mu\text{m}$  and below 5  $\mu\text{m}$  are desirable, as those particles pave their way through the upper airways to deposit in the lungs due to impaction or sedimentation [66]. Furthermore, if the aerodynamic particle size measures less than 3  $\mu\text{m}$ , there is an 80% probability of reaching the lower airways, with a deposition likelihood in the alveoli from 50% to 60% [14].

#### **3.2.2.1. Inhalation Devices**

Developing a safe and effective inhalant therapy depends not only on the formulation, but also on the delivery system. Inhalation devices can be divided into three different categories: nebulisers, electrically powered systems in which a liquid formulation is nebulised by ultrasound or pressurised air, and two compact, portable devices, pressurised metered dose inhalers (pMDI) and dry powder inhalers (DPIs) [73].

pMDIs and DPIs are the two most used categories of inhalers for oral inhalation. pMDIs generally consist of a canister fitted into an actuator. This canister is filled with a solution, suspension, or emulsion of the active pharmaceutical ingredient dissolved or dispersed in a propellant [74].

DPIs come in various types, distinguished whether the powdered DPI product is pre-filled in a reservoir for multiple inhalations or individually packaged in capsules or blisters, from which the powder is released during inhalation. The application principle of most DPIs is based on the active inhalation by the patient, with which the dry powder formulation is carried out of the device and administered to the patient. This principle prevents miscoordination between aspiration and triggering the device. In addition to offering a more intuitive operating procedure, dry powder inhalers present cost advantages over nebulisers, as they do not need electricity and enable the administration of high doses at a shorter time frame [69].

In general, a dry product offers superior stability and longer shelf-life compared to liquids [75]. Dry powder inhalers can also be designed to protect the prefilled formulation from moisture and be made from lightweight materials, facilitating distribution in remote areas without the need for challenging storage conditions. In the case of vaccines, a single dose dry powder inhaler can also ensure the immunisation of people living in areas with limited health care access. Unlike intramuscular injection, no trained personnel is required for inhalation, thus simplifying the process and extending the vaccination reach [16].

### 3.2.2.2. Formulation Strategies for Inhalable Dry Powders

Formulating dry powders for inhalation addresses the challenge to deliver particles smaller than 5  $\mu\text{m}$  to the lungs. Particles in this micrometre range are characterised by poor flowability due to cohesiveness. Therefore, several strategies have been developed to successfully deliver those particles. One strategy, often used for low dose formulations, are adhesive mixtures. Adhesive mixtures comprise a micronised active pharmaceutical ingredient (API) attached to a coarse carrier particle in the size range of 60 to 250  $\mu\text{m}$  [13, 69]. During inhalation, it is crucial for the API to detach from the carrier and disperse into the airstream in order to reach the lungs. The interaction between the micronised drug and the carrier is highly complex, posing challenges in balancing attachment during blending and detachment during inhalation [69].

Micronised particles do not only attach to each other or to the carrier but can also attach to the device or capsule used for application. Consequently, sweeper crystals, which are coarse particles similar to the carriers, have been employed to clear the inner surface of the capsule or device free of any remaining powder, enabling it to follow the air stream [76, 77]. In contrast to adhesive mixtures, which typically contain an excessive amount of carrier with a drug load of only 5 to 10% (w/w), sweeper crystals are added in a small ratio and are not meant to be attached to by the API [69]. This principle has been applied to enhance the performance of soft pellet formulations, for example [78]. Soft pellets, or spheronised powder formulations, take advantage of the natural tendency of particles smaller than 5  $\mu\text{m}$  to aggregate, by forming spherical agglomerates with controlled size and density. However, it is essential for the agglomeration strength of the soft pellets to be low, to ensure that the agglomerates break up into the original inhalable particles during inhalation [69].

Another formulation strategy is particle engineering. Particle engineering allows the production of tailored particles with properties that enhance the dispersibility and aerodynamic performance. This strategy can minimise cohesion, improve dispersibility, enhance drug stability, increase wettability and the dissolution rate, control the drug release pattern or prolong the particles' residence time in the lungs [69]. One production method for engineered particles is spray drying. Spray drying enables the co-processing of the actual drug with excipients that, for example, alter the shape, size or morphology of the spray dried particles. These particles could be large porous particles, which were developed for high dose inhalation [69]. Large porous particles have a geometric diameter of 5 to 30  $\mu\text{m}$ . However, due to their low density, they exhibit an aerodynamic diameter of 1 to 5  $\mu\text{m}$ , which is optimal for lung deposition [65]. Another example for particle engineering is co-spray drying particles with L-leucine. L-leucine has the ability to alter the shape and decrease surface energy of the spray dried particles, thereby enhancing dispersibility and detachment, improving the aerodynamic performance. This technique was employed in the present work and is elaborated in detail in the next chapter.

### 3.3. Spray Drying

Spray drying is a common process of thermal drying, well established in the food and pharmaceutical industries [79]. Owing to its adaptability and relatively straightforward scalability, spray drying is the method of choice for designing powders with sophisticated characteristics [16]. In the pharmaceutical industry and research, it is frequently employed for particle engineering and the production of powders with low densities. Particles with specific shapes, including wrinkled particles or particles full of holes and low densities, are commonly used in inhalable dry powder formulations, produced by spray drying [80].

Moreover, spray drying is a widely acknowledged method for processing heat-sensitive materials [81]. In this technique, a solution, emulsion or dispersion containing a potentially heat sensitive material is atomised into fine droplets by a single-, two- or three-fluid nozzle, an ultrasonic nozzle, or an atomising disc. These liquid droplets undergo a remarkably brief interaction with hot air as they pass the drying chamber. During this short exposure, the solvent undergoes evaporation, inducing a cooling effect. Notably, this ensures that the product typically experiences the outlet temperature as its maximum temperature [81]. The brevity of contact time and the concurrent cooling time play a pivotal role in preventing thermal degradation of sensitive materials, making spray drying a promising drying technique for formulations comprising RNA, proteins and peptides [82].

The size of the spray dried particles can be tailored through adjustments in feed concentration, inlet and outlet temperature, and the atomisation process [80]. Particle morphology is influenced by the properties of the substances being spray dried and the process temperatures, with predictions aided by the Peclet Number. The Peclet Number describes the relationship between the velocity of mass transport from the droplet surface to its centre and the evaporation rate of the solvent [83]. A Peclet Number  $\leq 1$  indicates that the mass transport occurs as quickly as, or faster than, solvent evaporation. If the substance being dried has good solubility in the solvent, late crystallisation may occur, resulting in solid particles (Figure 3.7 A).

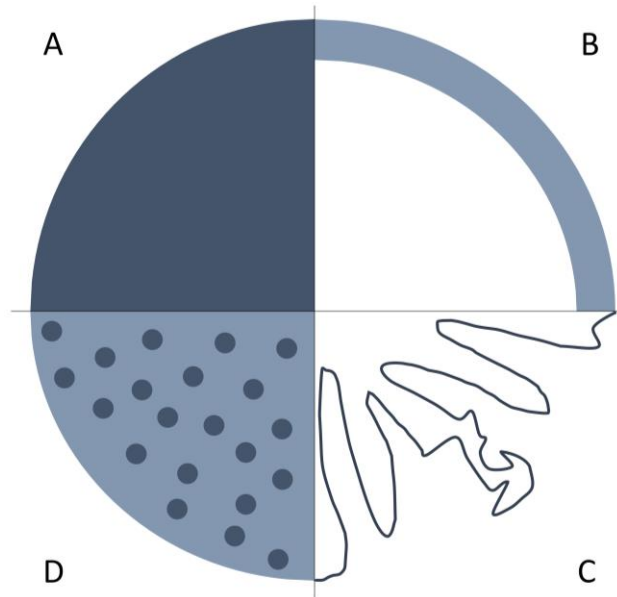


Figure 3.7: Schematic representation of particle morphologies: (A) solid particle, (B) hollow particle, (C) wrinkled particle, (D) nanoparticles embedded in a microparticle.

Conversely, a Peclet Number  $> 1$  signifies that the substance tends to concentrate on the droplet surface, leading to the formation of hollow particles (Figure 3.7 B). It is noteworthy that the specific properties of the substance being dried, such as its solubility, crystallisation behaviour and surface activity, significantly influence the observed particle morphology. Therefore, wrinkled particles can be obtained, for instance, by the addition of L-leucine, an amino acid which tends to accumulate on the droplet surface with its hydrophobic side chain oriented towards the air (Figure 3.7 C) [84]. In addition to solutions, emulsions containing different volatile phases can also be spray dried, resulting in porous particles with holes. Furthermore, dispersions encompassing nanoparticles can be spray dried to form hollow spheres, with the shell composed of nanoparticles, known as Trojan particles. Additionally, nanoparticles like lipoplexes can be embedded in a matrix microparticle (Figure 3.7 D) [62]. Spray drying can also be employed to spray dry microparticles within the inhalable range. Commonly used matrix excipients for this are mannitol and lactose, both approved for inhalation by the FDA [85]. Although mannitol and lactose are freely soluble in water, which is necessary to release their nanoparticle cargo readily after deposition in the lungs, spray drying can also enhance dissolution velocity. Poorly soluble substances can be converted into particles in the low micrometre range, which additionally are porous or amorphous, facilitating quicker dissolution. These various applications of spray drying illustrate the versatility and potential applications of spray drying in particle engineering.

As spray drying allows for the processing of sensitive materials, the production of inhalable particles and optimisation possibilities of the aerodynamic performance in one step, this technique was chosen to embed mRNA complexed with the lipids DOTAP and DOPE into a dry powder formulation in this work.

## 4. Materials

This work employed various materials, with this section offering a detailed description of the most relevant ones. A comprehensive list of all material used, along with their respective suppliers and supplier codes, is provided in Table 10.2 of the appendix.

### 4.1. Firefly Luciferase mRNA

The model messenger RNA (mRNA) used in this work encodes for the enzyme firefly luciferase, which generates luminescence through the conversion of the substrate luciferin. The mRNA is approximately 1680 nucleotides long, has a cap-1 structure on the 5' end and a 150 nucleotides comprising poly(A) tail (Figure 4.1).

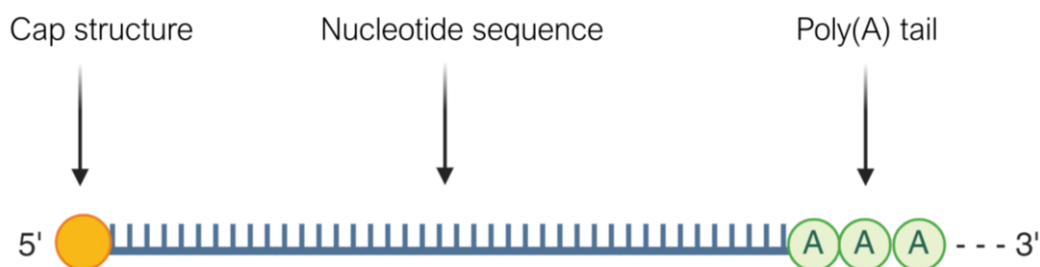


Figure 4.1: Schematic mRNA structure. Created with BioRender.com

It was purchased from RiboPro (Oss, the Netherlands). The cap structure at the 5' end of the mRNA is essential for the initiation of protein synthesis and functions as a protective group from nucleases [86]. The poly(A) tail is a string of adenosine monophosphate molecules added to the mRNA's 3' end. Its main purpose is to delay mRNA decay and to ensure efficient translation [25, 87]. All steps involving the handling of mRNA were conducted within a laminar air flow environment and utilising certified RNase-free disposables whenever feasible.

## 4.2. DOTAP and DOPE

The combination of the cationic lipid DOTAP (1,2-dioleoyloxypropyl-N,N,N-trimethylammonium chloride) and the neutral phospholipid DOPE (1,2-dioleoyl-sn-glycero-3-phosphoethanolamine) in equal weight ratios was chosen to complex the mRNA in this work (Figure 4.2 and Figure 4.3).

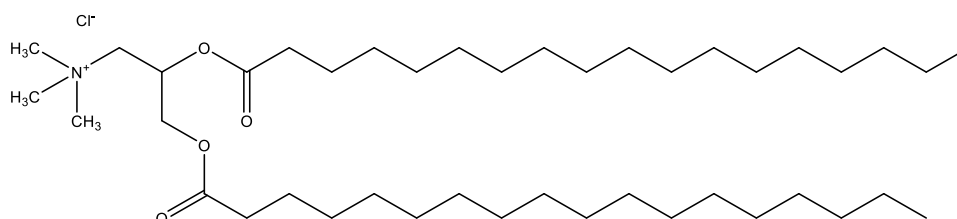


Figure 4.2: Chemical structure of DOTAP

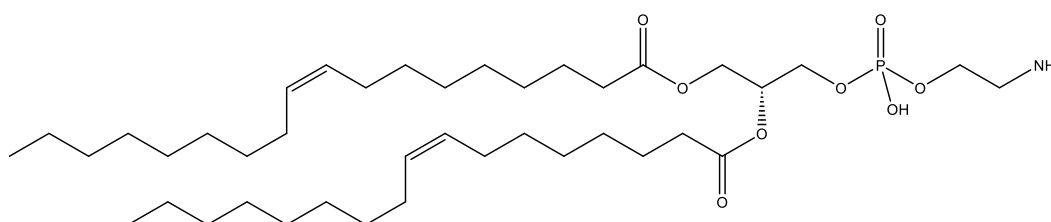


Figure 4.3: Chemical structure of DOPE

The role of the cationic lipid in the lipoplex formulation is to facilitate the formation of complexes with the negatively charged mRNA through electrostatic interactions. DOPE, the helper lipid, is employed to enhance the stability of the lipoplexes and to facilitate endosomal escape [53]. DOTAP:DOPE, a well-known transfection reagent, was previously used in humans and was purchased as “Transfection Reagent 1” from Avanti Polar Lipids (Birmingham, USA) [49, 58].

### 4.3. Matrix Materials

A dry powder formulation to deliver mRNA lipoplexes into the lungs requires a matrix to embed these nanoparticles in microparticles within the inhalable size range. For this purpose, lactose and mannitol were selected. Both excipients are approved for inhalation by the FDA and should release the mRNA lipoplexes, after readily dissolving in the lung fluid [14, 85]. Due to these properties, the two excipients have previously been used as matrices for nucleic acid formulations [67].

#### 4.3.1. Mannitol

Mannitol, a non-reducing sugar alcohol, is a widely used component in pharmaceutical formulations. Naturally occurring in marine algae, fungi and exudates from trees, it is industrially synthesised by hydrogenating hexoses like fructose and mannose [88]. The chemical structure of mannitol is displayed in Figure 4.4.

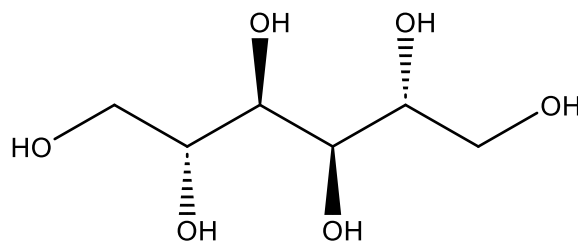


Figure 4.4: Chemical structure of mannitol.

Mannitol presents itself as a white or nearly white powder and is freely soluble in water [70, 89]. Crystallisation of mannitol results in three polymorphs ( $\alpha$ ,  $\beta$ ,  $\gamma$ ), with the  $\beta$ -polymorph being the most thermodynamical stable one [90]. In addition to its primary use as an inactive ingredient in pharmaceutical products like tablet formulations, mannitol is employed as active pharmaceutical ingredient [91]. For instance, it is inhaled to treat patients with cystic fibrosis. As a mucoactive hyperosmotic agent, mannitol is able to hydrate airway surface liquid thereby changing the viscoelastic properties of the mucus and increasing mucociliary clearance [92]. For this application, it is of advantage that mannitol can easily be formulated by particle engineering via spray drying. In this work, D-mannitol from Carl Roth (Karlsruhe, Germany) was used and is referred to as mannitol.

### 4.3.2. Lactose

Lactose, a reducing disaccharide composed of galactose and glucose, is a white to nearly white powder and freely soluble in water. The Ph. Eur. lists lactose in two forms: the anhydrous form with its  $\alpha$ - and  $\beta$ -anomer, and  $\alpha$ -lactose monohydrate, which is displayed in Figure 4.5 [70].

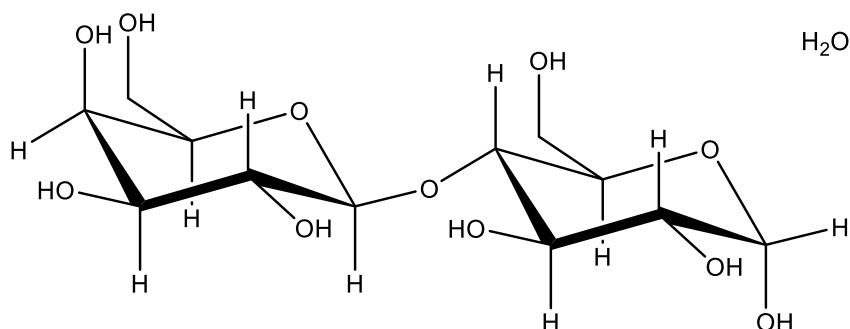


Figure 4.5: Chemical structure of  $\alpha$ -lactose monohydrate.

Lactose is primarily produced from milk and whey, a byproduct of cheese production. After cooling down a hot, supersaturated solution, lactose is crystallised. The crystals display a typical pyramid, prism or tomahawk shape. Depending on the crystallisation temperature, different modifications can be produced. Below 93 °C,  $\alpha$ -lactose monohydrate is obtained, which can be converted to  $\alpha$ -lactose at temperatures around 120 °C under vacuum. Above 93 °C, predominantly  $\beta$ -lactose is formed. In addition to its crystalline forms, amorphous lactose may be present, comprising both the  $\alpha$ - and  $\beta$ -forms in the same proportion as the original solution [93].

Similar to mannitol, lactose is a commonly used inactive ingredient in the production of pharmaceutical products, such as tablets, capsules and inhalable formulations. In inhalable formulations, it is primarily employed as a carrier for active pharmaceutical ingredients in adhesive mixtures [94].

Four different lactose qualities were utilised in this work. InhaLac 70, 120, 180 and 251 were provided by Meggle (Wasserburg am Inn, Germany) and employed as sweeper crystals in Chapter 6.3.1. For the lactose matrix in the spray drying experiments, InhaLac 251 was dissolved and referred to as lactose.

#### 4.4. L-Leucine

The essential proteinogenic amino acid L-leucine is characterised by its crystalline, white, shimmering platelet structure. Its four-carbon aliphatic nonpolar hydrophobic side chain gives L-leucine certain hydrophobic properties (Figure 4.6) and leads to a poor solubility in water of 24 g/L at 20 °C [95].

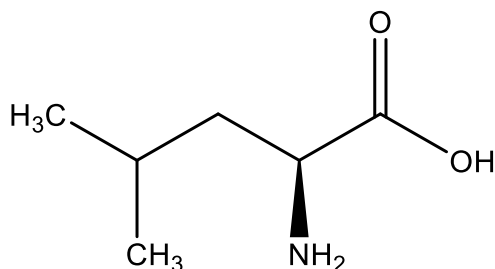


Figure 4.6: Chemical structure of L-leucine.

L-leucine is employed in inhalable formulations to minimise interparticle interactions and enhance powder dispersibility [84]. These formulations are often produced by co-spray drying with L-leucine. During spray drying L-leucine locates on the surface of the produced droplets and crystallises early due to its low solubility, forming an L-leucine enriched shell. This shell decreases the surface energy and is thus enhancing powder dispersibility by reducing the cohesive forces among the particles [96, 97].

In this work, L-leucine was purchased from Sigma Aldrich (Darmstadt, Germany).

## **4.5. Cell Lines**

The human lung carcinoma cell lines Calu-3 and A549 were selected as model cell lines for the *in vitro* cell experiments. These cell lines represent different areas of the respiratory tract and were purchased from the American Type Culture Collection (ATCC, Manassas, USA).

### **4.5.1. Calu-3 Cells**

The Calu-3 cell line was derived from the bronchial epithelium of a 25-year-old, Caucasian male patient with lung adenocarcinoma [98, 99]. This cell line is differentiated, builds tight monolayers in culture and produces mucus [100]. The presence of mucus can constitute an additional barrier to substances with which the cells are treated.

### **4.5.2. A549 Cells**

The A549 cell line was isolated from the alveolar epithelium of a 58-year-old, Caucasian male with lung adenocarcinoma [101]. A549 cells form confluent monolayers and are commonly used for transfection studies, as they are relatively easy to transfect and exhibit a strong protein expression after transfection [75, 102].

## 5. Methods

This section outlines the methods used in this work. In the appendix, Table 10.3 provides a comprehensive list of the equipment utilised, along with the respective manufacturers.

### 5.1. Preparative Methods

This work aimed to develop an inhalable dry powder platform for mRNA therapeutics. Since mRNA has to be packaged to guarantee stability and to facilitate transfection into the host cells, DOTAP:DOPE liposomes were produced to complex the mRNA into lipoplexes. All steps prior to the spray drying of the mRNA lipoplexes were conducted under aseptic conditions within a laminar air flow environment. In general, sterile and nuclease-free disposable materials were used whenever feasible.

These mRNA lipoplexes were then spray dried to yield a dry powder formulation. To tailor the physicochemical properties and the aerodynamic performance of the final formulation different strategies were evaluated, including various excipients during spray drying or the addition of sweeper crystals.

#### 5.1.1. Preparation of DOTAP:DOPE Liposomes

DOTAP:DOPE liposomes were prepared by dissolving an equal weight ratio of the cationic DOTAP (1,2-dioleoyloxypropyl-N,N,N-trimethylammonium chloride) and the neutral lipid DOPE (1,2-dioleoyl-sn-glycerol-3-phosphoethanolamine) in chloroform. The lipid solution was aliquoted, and the solvent was evaporated in a fume hood to create a lipid film. This film was stored below -20 °C until needed and then solubilised by adding water, resulting in a total lipid concentration of 1 µg/µL. In order to find a suitable homogenisation method, the solubilised lipids were placed in a sonication bath (Transsonic 460/H, Elma Schmidbauer GmbH, Singen, Germany) at 40 °C for 20 min, as described by Kim et al. [19]. As an alternative strategy, a probe-type sonicator (Sonoplus HD 4100, Bandelin GmbH & Co. KG, Berlin, Germany) was held into the dispersion, which was subjected to 30 s of homogenisation at 10%, 25% or 50% amplitude. As the formulation development proceeded beyond Chapter 6.1.1 the liposomes were prepared by sonication for 30 s using the probe-type sonicator at an amplitude of 25%.

### **5.1.2. Preparation of mRNA Lipoplexes**

In order to prepare mRNA lipoplexes, the mRNA stock solution was diluted to a concentration of 0.2  $\mu\text{g}/\mu\text{L}$ . The prepared DOTAP:DOPE liposomes were added to the mRNA solution in an equal volume and incubated for 2 h in a refrigerator. In Chapter 6.1.2, the concentration of the DOTAP:DOPE liposome dispersion was varied to achieve six increasing DOTAP:DOPE to mRNA weight ratios (1+1, 3+1, 5+1, 7+1, 9+1, 11+1) while keeping the amount of mRNA constant. After selecting the DOTAP:DOPE to mRNA weight ratio of 5+1 for further formulation development, the mRNA lipoplexes were prepared by mixing the mRNA dilution with a DOTAP:DOPE liposome dispersion with a concentration of 1  $\mu\text{g}/\mu\text{L}$ . The mRNA lipoplexes were incubated for 2 h, unless stated otherwise.

### 5.1.3. Spray Drying

For the spray drying dispersion with a solid concentration of 4% (w/w), a mannitol or lactose solution was mixed with the prepared mRNA lipoplexes to obtain a weight ratio of 1 part mRNA, 5 parts DOTAP:DOPE and 19,994 parts mannitol or lactose. To increase surface hydrophobicity in Chapter 6.3.2, 5% (w/w) L-leucine, calculated from the solid content, was added to the described spray drying dispersion.

Spray drying was conducted using a Mini Spray Dryer B-290 (Büchi Labortechnik GmbH, Flawil, Switzerland) equipped with a high-performance cyclone, a dehumidifier B-296 (Büchi Labortechnik GmbH, Flawil, Switzerland) and a two-fluid nozzle with an internal diameter of 0.7 mm and a nozzle cap with a diameter of 1.4 mm (Figure 5.1).

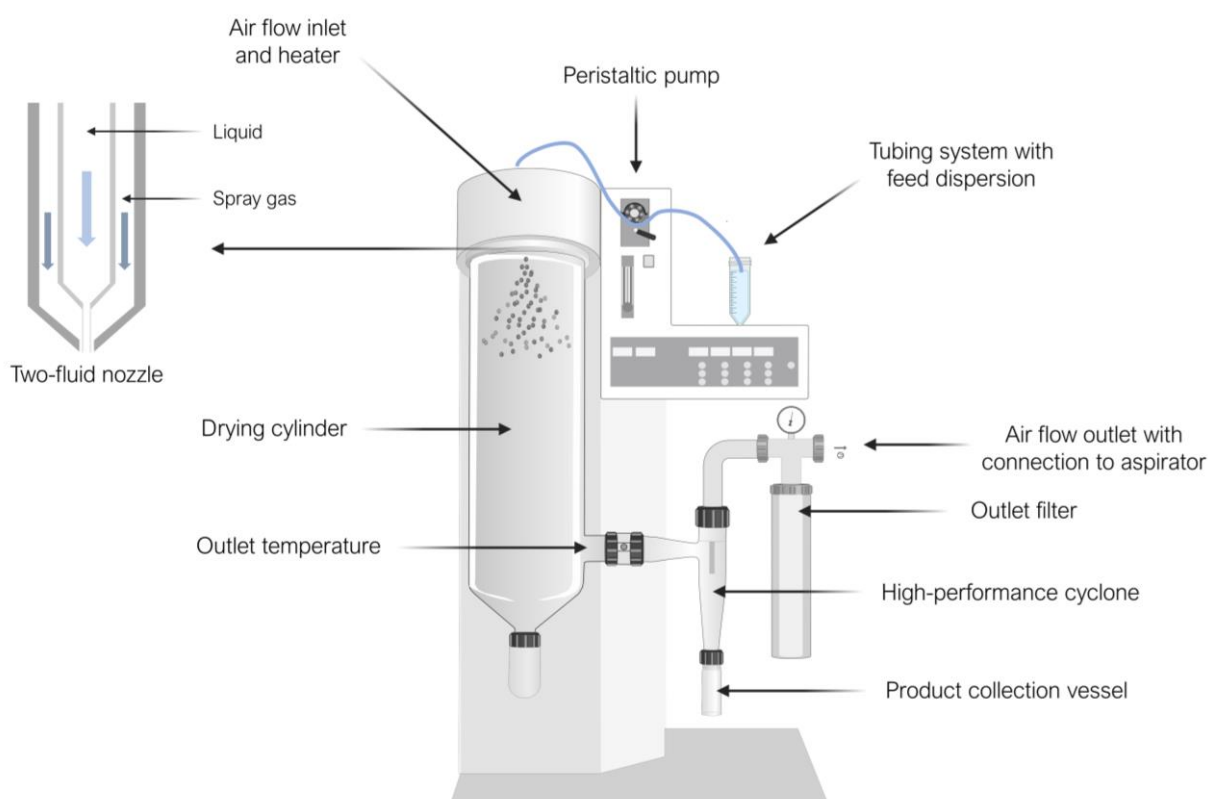


Figure 5.1: Schematic image of the utilised Spray Dryer B-290 and the used two-fluid nozzle. Created with BioRender.com

To initiate the process, the spray dryer was heated to an inlet temperature of 120 °C. The gas air flow was set to 601 l/h, the aspirator to 100% (corresponds to approximately 35 m<sup>3</sup>/h) and the pump rate of the feed was regulated accordingly to attain the desired outlet temperature of 50, 60 or 70 °C. After determining that the outlet temperature for the subsequent formulation development should be 50 °C, the spray drying dispersions with L-leucine were spray dried at an outlet temperature of 50 °C.

The yield of each spray drying run was determined by the powder recovered from the collecting vessel.

#### **5.1.4. Preparation of Sweeper Crystal Blends**

In order to reduce the amount of powder remaining in the capsules and to increase the FPF (in Chapter 6.3.1), the mRNA lipoplexes in mannitol matrix, spray dried at an outlet temperature of 50 °C, were blended with 4 different lactose qualities: InhaLac 70, InhaLac 120, InhaLac 180 and InhaLac 251, respectively. These lactose qualities served as sweeper crystals in the blends, which comprised 1.2 g powder and were weighted using the sandwich method with a weight ratio of 2 parts spray dried powder and 1 part lactose, respectively. The blends were mixed in cylindrical glass vessel, with its volume filled to one third with powder, using a Turbula Blender (Willy A. Bachofen AG, Muttenz, Switzerland) with 42 rpm for 10 min, subsequently sieved with a 300 µm sieve and then mixed again for 10 min. These blends were spread out on a large sheet of paper and 5 samples were randomly picked and checked for homogeneity. For this purpose the samples were dispersed in Tris-acetate EDTA (TAE) buffer and the fluorescence dye SYBR Gold was added to a concentration of 1X. The fluorescence intensity of the samples was measured at an emission wavelength of 560 nm (10 nm) (excitation wavelength: 495 nm (10 nm)) with a Tecan Spark plate reader (Tecan Group Ltd., Männedorf, Switzerland).

## 5.2. Characterisation Methods

### 5.2.1. Dynamic Light Scattering

The prepared mRNA lipoplexes exhibited a particle size in the nanometre range. Nanoparticles show a distinct behaviour, they move randomly in dispersion. This Brownian motion is measured by dynamic light scattering (DLS), also known as photon correlation spectroscopy. When illuminating the particles with a laser, each particle scatters the light in all directions. DLS analyses the intensity fluctuations in the scattered light and relates it to the size of the particles. In fact, the Brownian motion of small particles is quicker than that of larger particles. This relationship is defined by the Stokes-Einstein equation [103, 104]. For this equation (Equation 5.1), the dynamic viscosity ( $\eta$ ) is an important factor, as particles in a low viscosity dispersion move faster than in a dispersion of high viscosity [105].

*Equation 5.1: Stokes-Einstein equation.  $D_h$  represents the hydrodynamic diameter,  $k$  the Boltzmann's constant,  $T$  the absolute temperature,  $\eta$  the dynamic viscosity and  $D$  the translational diffusion coefficient.*

$$D_h = \frac{k * T}{3\pi * \eta * D}$$

Hence, to calculate the dynamic viscosity according to Equation 5.2 the kinematic viscosity was measured using an SV-10 Vibro-Viscosimeter (A&D Company Ltd., Tokio, Japan). Additionally, the density of the samples was determined with a density meter DMA 48 (Anton Paar Germany GmbH, Ostfildern, Germany).

*Equation 5.2: Equation to calculate the dynamic viscosity  $\eta$  by multiplying the kinematic viscosity  $\nu$  by the density  $\rho$ .*

$$\eta = \nu * \rho$$

Subsequently, a Zetasizer ZS Nano (Malvern Panalytical GmbH, Kassel, Germany) measured the rate of the intensity fluctuation and calculated the particles size, given as z-average. The z-average is the normalised intensity weighted mean hydrodynamic size of the measured particles.

The z-average measurement run, which consists of approximately 10 to 15 single measurements, automatically determined by the Zetasizer Nano software (Malvern Panalytical GmbH, Kassel, Germany), includes the assessment of the polydispersity index (PDI). The PDI is an important parameter for the interpretation of the z-average, providing information about the reliability of the z-average measurement. A PDI of  $\leq 0.1$  is typically considered an indication of highly monodisperse particles, while values between 0.1 and 0.4 are generally regarded as moderately polydisperse, and those  $> 0.4$  are considered to indicate highly polydisperse

particles [106]. If the PDI is higher than 0.5, it is not recommended to rely on the z-average mean. In this study, aiming to produce uniform liposomes and lipoplexes, a PDI of < 0.4 was targeted. To conduct the measurements in triplicate, three independently prepared samples were measured, unless stated otherwise. The lipoplexes were measured at an mRNA concentration of 0.0005 µg/µL. The spray dried powder was reconstituted in water prior to measurement.

### 5.2.2. Determination of the Zeta Potential

The zeta potential offers valuable insight into the stability of nanoparticles. There exists a potential difference between the particle surface and the surrounding liquid. This potential varies depending on the distance from the particle surface. Close to the particle, oppositely charged ions from the solution are tightly bound, and as the distance increases, the potential gradually diminishes. The reduction in potential follows a gentle slope until the slipping plane is reached, beyond which the potential experiences an exponential decrease. The potential at the slipping plane is termed the zeta potential [103, 106]. The zeta potential determines whether the particles within a liquid will exhibit repulsion or attraction towards each. The typical dividing line distinguishing stable from unstable suspensions is set at +30 mV or -30 mV. Hence, particles exhibiting a zeta potential exceeding +30 mV or falling below -30 mV are generally considered stable [103]. In this study, a cationic and a neutral lipid were utilised, leading to an expectation of a positive zeta potential for the liposomes. The lipoplexes were anticipated to show a lower zeta potential depending on the mRNA content. The zeta potential was determined in water in triplicates, unless stated otherwise, using a Zetasizer ZS Nano (Malvern Panalytical GmbH, Kassel, Germany).

### 5.2.3. Fluorescence Displacement

Two strategies were adapted from Qiu et al. and performed to investigate the mRNA binding affinity of DOTAP:DOPE [107]. Both are kinds of fluorescence displacement assays, which are based on the property of the fluorescence dye SYBR Gold to exhibit more than a 1000-fold signal magnification when bound to free RNA. The first method was the titration of DOTAP:DOPE to a previously prepared mRNA/SYBR Gold mixture to observe the incremental replacement of SYBR Gold by DOTAP:DOPE. After every titration step, the fluorescence intensity was measured at an emission wavelength of 560 nm (10 nm) (excitation wavelength: 495 nm (10 nm)) with a Tecan Spark plate reader (Tecan Group Ltd., Männedorf, Switzerland). The fluorescence intensity was then plotted as the percentage of the fluorescence intensity of mRNA/SYBR Gold against the DOTAP:DOPE to mRNA weight ratio upon titration.

The second approach began by complexing DOTAP:DOPE and mRNA in a 5+1 weight ratio. After a 2 h incubation at 4 °C, SYBR Gold was added to the lipoplexes. Subsequently, heparin

was titrated to the lipoplexes to dissociate the complexes and release the mRNA in order to assess the mRNA binding affinity of DOTAP:DOPE. The fluorescence intensity was plotted as the percentage of the fluorescence intensity of mRNA/SYBR Gold without DOTAP:DOPE against the amount of heparin upon titration. The data was fit to a four-parameter logistic sigmoidal curve, and the half-maximal effective concentration (EC<sub>50</sub>) and hill slope were calculated using GraphPad Prism 10.2. (GraphPad Software, Boston, USA).

#### **5.2.4. Agarose Gel Electrophoresis**

Agarose gel electrophoresis was carried out to assess the free mRNA after complexation with DOTAP:DOPE. mRNA lipoplexes were prepared in six increasing DOTAP:DOPE to mRNA weight ratios (1+1, 2+1, 3+1, 4+1, 5+1, 6+1), whereby the amount of mRNA was kept constant at 0.25 µg per lane. For complexation, the components were incubated in water for 2 h at 4 °C. The lipoplexes were then diluted with 1X Tris-acetate EDTA (TAE) buffer to 13.5 µL, before 1.5 µL DNA gel loading dye (6X) were added. The agarose gel was prepared by suspending 0.45 g of agarose in 30 mL of TAE buffer and heating the suspension to 100 °C until the agarose was completely dissolved. The agarose solution was quickly poured into the gel tray, immediately followed by putting the well comb in place. The gel was allowed to solidify at 20 °C for 30 min before 5 µL of the lipoplex samples were loaded into the 1.5% (w/v) agarose gel and the electrophoresis was run in TAE buffer at 120 V for 30 min. The gel was stained in a 1X SYBR Gold solution in TAE buffer for 20 min. Subsequently, the gel was visualised using blue light in an ChemoStar 21 TS imager (INTAS Science Imaging Instruments GmbH, Göttingen, Germany).

#### **5.2.5. Particle Imaging**

##### **5.2.5.1. Transmission Electron Microscopy**

The mRNA lipoplexes were prepared in water at a mRNA concentration of 0.002 µg/µL and incubated for 2 h in a refrigerator. A continuous carbon grid was negative-glow discharged at 25 mA for 30 s using a Quorum SC 7620 Sputter Coater (Quorum Technologies Ltd, Laughton, UK). Subsequently, the sample was transferred to the carbon grid and stained with a half-saturated solution of uranyl acetate. The grid was air dried and then transferred into a JEOL-1400-Plus-Transelectron microscope (TEM) (JEOL Germany, Munich, Germany) operating at 100 kV. The images were generated using an integrated TemCam-F416 camera (TVIPS, Munic, Germany). This procedure was adapted from Arnold et al. [108]. TEM images were taken at the Department of Anatomy at Kiel University with the kind support of Frank Lichte.

### 5.2.5.2. Scanning Electron Microscopy

The spray dried formulations and sweeper crystals were visualised using scanning electron microscopy. In a first step, the samples were attached to an aluminium stub with double-sided carbon tapes and then coated with a thin gold layer using a sputter coater (BAL-Tec SCP 050, Leica Microsystems, Wetzlar, Germany) for 40 s. Subsequently, the samples were visualised with the scanning electron microscope (Phenom World XL, Thermo Fisher Scientific Inc., Waltham, USA) using an acceleration voltage of 10 kV and a vacuum of 10 Pa.

### 5.2.6. Water Content

The water contents of the spray dried formulations were determined by a Karl-Fischer Titrator V20 (Mettler Toledo AG, Analytical, Greifensee, Switzerland). A 1% water standard was used to calibrate the titrator prior to every set of measurements. Approximately 100 mg of powder was required for a sufficient measurement. Therefore, assuming that the small amount of mRNA has no effect on the water content, spray dried formulations were assessed in triplicates, containing DOTAP:DOPE and the respective excipient.

### 5.2.7. Particle Size Distribution

A laser diffractometer (Helium Laser Optical System, HELOS, Sympatec GmbH, Clausthal-Zellerfeld, Germany) was used to determine the particle size distributions of the spray dried formulations and sweeper crystals.

The RODOS module was employed to disperse the powders in air at a pressure of 3 bar and inject them into a laser light beam. A detector records the diffraction patterns produced by the particles at various angles. The evaluation was conducted in accordance with the Fraunhofer theory by the PAQXOS 5.2.1 software (Sympatec GmbH, Clausthal-Zellerfeld, Germany), resulting in a volume-based particle size distribution. In case of non-spherical particle shapes, a size distribution equivalent to spherical particles was obtained. The characteristic values  $x_{10}$ ,  $x_{50}$ ,  $x_{90}$  and the span value were determined to compare the spray dried formulation and sweeper crystals. The  $x_{10}$ ,  $x_{50}$  and  $x_{90}$  values represent the diameters of particles in a given sample where a certain percentage (10%, 50%, and 90%) of the particles are smaller than the specified diameter. The span value (Equation 5.3) signifies the width of the distribution, the smaller the span value the narrower the particle size distribution. The measurements were performed in triplicates.

*Equation 5.3: Calculation of the span value.*

$$span = \frac{x_{90} - x_{10}}{x_{50}}$$

### 5.2.8. Aerodynamic Characterisation

A clear distinction exists between the geometric particle size and the aerodynamic diameter. The aerodynamic diameter describes the diameter of a sphere with a density of  $1 \text{ g/cm}^3$  that has the same aerodynamic properties as the analysed particle. This allows the comparison between particles of differing shapes and densities on the basis of their aerodynamic properties [66]. Consequently, a porous particle with low density with a geometric diameter above  $5 \mu\text{m}$  may still have an aerodynamic diameter below  $5 \mu\text{m}$  [69].

The aerodynamic characterisation was carried out using the Next Generation Impactor (NGI, Copley Scientific, Nottingham, UK), also known as the apparatus E in the European Pharmacopoeia (Ph. Eur.) 2.9.18: "Preparations for inhalation: aerodynamic assessment of fine particles" [70].

The NGI, displayed in Figure 5.2, is a cascade impactor comprising seven horizontally arranged stages and a micro-orifice collector (MOC) with decreasing orifice diameter.

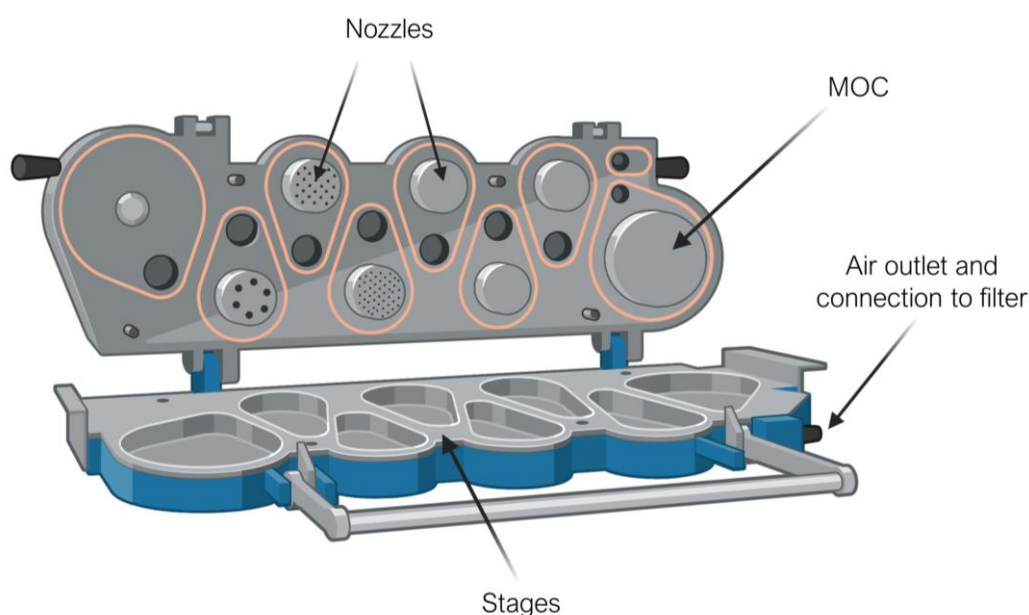


Figure 5.2: Schematic picture of an open NGI. Created with BioRender.com

The distance between the orifices and the impact plates is reduced with decreasing orifice diameter. Hence, the speed of the air flow through the NGI increases from stage to stage. A filter was placed behind the MOC to catch the ultrafine particles, which did not deposit in the MOC. The NGI was used in combination with a preseparator, a throat and a mouthpiece. To reduce particle bounce, each stage was coated with a thin layer of a solution containing Brij 35, Ethanol and Glycerol (15%, 51%, 34% w/w) prior to each run. For each run assessing the spray dried powders, 5 hydroxypropyl methylcellulose capsules (Vcaps Plus, Capsugel, Lonza Inc., Morristown, USA) were loaded with 20 mg each (weighed accurately) and placed in an RS01 dry powder inhaler with a low resistance (Plastiaple/Berry Global Inc., Evansville, USA). For the sweeper crystal blends, 5 capsules filled with 30 mg each (weighed accurately) were

used. Each capsule was hole-punched and then discharged with a flow rate of 80 l/min for a duration of 3 s. All experiments were performed in triplicates and at constant environmental conditions (45% relative humidity, 21 °C). All samples, including the capsules, the device, the mouthpiece, the throat, all parts of the NGI and the filter, were collected by rinsing with a particular volume of water, as displayed in Table 5.1. mRNA quantification was performed by adding the fluorescence dye SYBR Gold in TAE buffer to achieve a dye and buffer concentration of 1X.

Table 5.1: Volumes used to rinse the various parts of the setup for the aerodynamic characterisation.

|              | Volume, mL |
|--------------|------------|
| Capsules     | 5          |
| Device       | 5          |
| Mouthpiece   | 5          |
| Throat       | 10         |
| Preseparator | 10         |
| Stage 1      | 5          |
| Stage 2      | 2.5        |
| Stage 3      | 2.5        |
| Stage 4      | 2.5        |
| Stage 5      | 2.5        |
| Stage 6      | 2.5        |
| Stage 7      | 2.5        |
| MOC          | 5          |
| Filter       | 5          |

The fluorescence signal was measured at an emission wavelength of 560 nm (10 nm) (excitation wavelength: 495 nm (10 nm)) with a Tecan Spark plate reader (Tecan Group Ltd., Männedorf, Switzerland). The recovered dose, defined as the sum of the mRNA powder mass assayed on inhaler and all NGI stages in one run, was standardised to represent 100% of the applied mRNA powder. Subsequently, all recovered fractions were calculated as a proportion of the recovered dose. The CITDAS Software V3.1 (Copley Scientific, Nottingham, UK) was used to calculate the aerodynamic characteristics of the powder: emitted dose (ED), fine particle dose (FPD), fine particle fraction (FPF) and mass median aerodynamic diameter (MMAD). The ED is the mass of mRNA which was discharged from the device and the FPD is the mass with an aerodynamic diameter lower than 5 µm. The FPF relates the FPD to the ED. The MMAD represents a threshold particle size, indicating that 50% of the aerosol mass is smaller than this value, while the remaining 50% is larger than the specified parameter [72].

## 5.2.9. *In vitro* Cell Experiments

### 5.2.9.1. Cell Culture

In this study, Calu-3 cells and A549 cells were used as model cell lines and cultured in a humidified atmosphere containing 5% CO<sub>2</sub> at 37 °C. Calu-3 cells were cultivated in supplemented Minimum Essential Medium Eagle (EMEM), while A549 grew in supplemented Ham's F-12 K medium (F-12K). Table 5.2 displays the detailed composition of the cell culture media. The respective culture medium above the cells was changed every two to three days. Once the cells reached about 80% confluence, the cells were washed with phosphate buffered saline (PBS), detached through trypsin/EDTA treatment, and then transferred and reseeded into new cell culture flasks. To preclude mycoplasma infections, regular testing was conducted to ensure the absence of this contamination.

Table 5.2: Composition of cell culture media.

| Cell line | Abbreviation | Base medium  | Supplements                  |
|-----------|--------------|--|------------------------------|
| Calu-3    | EMEM         | Minimum Essential Medium Eagle, with Earle's salts, L-glutamine and sodium bicarbonate | 10% Fetal bovine serum (FBS) |
|           |              |  | 1% Sodium pyruvate           |
|           |              |  | 1% Non-essential amino acids |
|           |              |  | 1% Penicillin/streptomycin   |
| A549      | F-12 K       | Ham's F-12 K medium  | 10% FBS                      |
|           |              |  | 1% Penicillin/streptomycin   |

### 5.2.9.2. Transfection Efficiency

In order to confirm the integrity of the mRNA lipoplexes, *in vitro* transfection was carried out. To compare the transfection efficiency of the samples, the amount of mRNA in each sample was kept constant within one experiment. The amount of mRNA was set to 100 ng per well for studying the DOTAP:DOPE to mRNA ratios in Chapter 6.1.2.2 and to 50 µg for all the other transfection experiments. To obtain the desired concentrations, the prepared mRNA lipoplexes were diluted with Opti-MEM and the spray dried samples were dissolved in Opti-MEM.

1.6 x 10<sup>4</sup> Calu-3 or A549 cells per well were seeded in 100 µL culture medium onto a transparent 96-well plate. After 24 h incubation under culture conditions, the medium was

removed and replaced by serum reduced medium (0.2% FBS), as transfection was found to be more successful in a medium with reduced serum. In each well, 10  $\mu\text{L}$  sample was added to the cells. After 5 h of transfection time under culture conditions, the medium was replaced with culture medium. 24 h after transfection the medium was removed, the cells were washed with 50  $\mu\text{L}$  PBS and 50  $\mu\text{L}$  of 1.5 X lysis buffer were added to each well. After the plate was shaken for 45 min, the luciferase activity was measured using the Bright-Glo Luciferase Assay System according to the manufacturer's protocol and luminescence was measured in a white 96-well plate with a Tecan Spark plate reader (Tecan Group Ltd., Männedorf, Switzerland). The luminescence signals were normalised to the protein content of the wells after performing the Pierce Coomassie (Bradford) Protein-Assay-Kit with the remaining lysate according to the manufacturer's instructions.

### 5.2.9.3. Cell Viability

The toxicity of substances was assessed utilising the CellTiter-Glo Luminescent Cell Viability Assay. This assay is based on measuring the ATP concentration, which is directly proportional to the number of viable cells in the culture [109, 110]. Calu-3 and A549 cells were seeded and treated analogously to the transfection assay, to investigate the influence on cell viability under transfection conditions.  $0.32 \times 10^4$  cells per well were seeded in 20  $\mu\text{L}$  culture medium onto a white 384-well plate. After 24 h under culturing conditions, the medium was removed and replaced by serum reduced medium (0.2% FBS). 30  $\mu\text{L}$  of the samples, dissolved in Opti-MEM, were added to the cells and incubated for 5 h under culturing conditions. For the negative (0% viability) and positive control (100% viability) pure Opti-MEM was added to the cells. 15 min before the end of the incubation time, the medium in the wells for the negative control was replaced by Triton-X (1% in PBS). After the incubation period, the serum reduced medium including the samples was replaced by cell culture medium and the cells were incubated for an additional 19 h. Subsequently, the medium above the cells was removed and the CellTiter-Glo Luminescent Cell Viability Assay was performed according to manufacturer's instructions and measured with a Tecan Spark plate reader (Tecan Group Ltd., Männedorf, Switzerland) [109]. The viability of the cells after treatment was calculated by relating the measured luminescence to the positive and negative control.

### 5.3. Statistical Methods

All calculations in this work were conducted with Microsoft Excel for Microsoft 365 (Microsoft Corporation, Redmond WA, USA). The results presented in this work represent the mean value and standard deviation of multiple determinations, unless stated otherwise. Except for the presentation in box plots, the standard deviation is depicted as error bars. The mean value and standard deviation were calculated using Equation 5.3 and Equation 5.4, respectively.

Equation 5.4: Calculation of the mean value.

$$\bar{x} = \frac{1}{n} \sum_{i=1}^n x_i$$

Equation 5.5: Calculation of the standard deviation.

$$s = \sqrt{\frac{\sum_{i=1}^n (x_i - \bar{x})^2}{n - 1}}$$

#### 5.3.1. Box Plots

In box plots, error bars show the 10 - 90% interval, the box represents the 25 - 75% interval, the median is exhibited by “—” and “+” displays the mean.

#### 5.3.2. Significance Testing

A two-tailed t-test was employed to test statistical significance. Prior to this, an F-test was conducted to determine if the variances of the samples were significantly different. If the variances were not significantly different, a homoscedastic t-test was applied. For samples with significantly different variances, a t-test with Welch’s correction was conducted. The resulting significance value p was categorised as displayed in Table 5.3. The statistical tests in this work were performed with GraphPad Prism 10.2. (GraphPad Software, Boston, USA).

Table 5.3: Classification of the significance value p.

| Significance value p | Classification     | Symbol |
|----------------------|--------------------|--------|
| > 0.05               | Not significant    | ns     |
| 0.01 < p < 0.05      | Significant        | *      |
| 0.001 < p < 0.01     | Very significant   | **     |
| ≤ 0.001              | Highly significant | ***    |

## 6. Results and Discussion

### 6.1. Packaging mRNA for Efficient Transfection

The formulation of mRNA into a dry powder for inhalation presents numerous challenges, as mRNA is a delicate, single-stranded molecule that is susceptible to degradation from nucleases and thermal or shear stresses [8–10]. Given its susceptibility, effective delivery of mRNA is key to therapeutic success, as RNA itself cannot overcome the cell membrane. Thus, effective delivery of mRNA relies on encapsulating it within a vector that provides protection and facilitates transfection into cells.

Among non-viral vectors, lipid nanoparticles have emerged as a promising delivery strategy due to their capability of efficient and scalable synthesis, their ability to protect mRNA against degradation and to facilitate endosomal escape [16, 111]. Especially, positively charged lipids are used for delivering mRNA in a lipoplex, as they enable the formation of complexes with negatively charged mRNA by electrostatic interactions [53]. While their positive charge facilitates locating the lipoplex at the negatively charged cell membrane, it also carries the risk of cell toxicity [10, 112–114]. Therefore, it was essential to choose lipids that were previously tested and have proven safe for the use in humans. The combination of the cationic lipid DOTAP (1,2-dioleoyloxypropyl-N,N,N-trimethylammonium chloride) and the neutral helper lipid DOPE (1,2-dioleoyl-sn-glycero-3-phosphoethanolamine) is a safe transfection agent for human administration and was chosen for this study [49]. As a first step, a preparation method for DOTAP:DOPE liposomes was established and the concentration depended toxicity on the lung cancer cell lines Calu-3 and A549 was assessed. Subsequently, a model mRNA was complexed with DOTAP:DOPE in six different weight ratios. These six ratios were characterised physicochemically and *in vitro* to determine the optimal lipoplex composition.

### 6.1.1. Preparing DOTAP:DOPE Liposomes

There are various methods to prepare liposomes from phospholipids like DOTAP and DOPE [115]. The aim of these first experiments was to find a preparation method for DOTAP:DOPE liposomes, which requires only a small amount of material and reliably forms liposomes within the desired hydrodynamic particle size range of a z-average between 70 to 200 nm, allowing efficient transfection [48]. This method was also intended to generate monodisperse to moderately polydisperse and stable liposomes. As outlined in Chapters 5.2.1 and 5.2.2, a polydispersity index (PDI) of  $< 0.4$  ensures moderately polydisperse liposomes, and a zeta potential higher than  $+ 30$  mV or below  $- 30$  mV signifies stable liposomes.

To obtain liposomes matching these properties, the lipids DOTAP:DOPE were dissolved in chloroform, which was subsequently evaporated to form a thin lipid film. Water was then added to the lipid film, allowing the lipids to rehydrate overnight at a temperature of  $4$  °C. Subsequently, this dispersion was homogenised using two different strategies of sonication. The first strategy was adapted from Kim et al. and included homogenisation in a sonication bath at  $40$  °C for 20 min [19]. For the second strategy, a probe-type sonicator was held into the solubilised dispersion, which was then homogenised with an intensity of 10, 25 or 50% for 30 s. Table 6.1. summarises the homogenisation energy applied to the liposomes at the three different intensities.

Table 6.1: Homogenisation energy the liposomes were subjected to during homogenisation with the sonicator.  $n \geq 3$ , mean  $\pm$  standard deviation.

| Intensity, % | Time, s | Energy, J    |
|--------------|---------|--------------|
| 10           | 30      | $457 \pm 6$  |
| 25           | 30      | $544 \pm 8$  |
| 50           | 30      | $754 \pm 13$ |

After homogenisation, the z-average, PDI and zeta potential of the prepared liposomes were measured. The sonication bath subjects the samples to less homogenisation forces than the probe-type sonicator, which was held directly into the samples. Therefore, larger liposomes combined with a higher PDI value were expected for the sonication bath. Within the probe-type sonicator samples, a higher intensity of homogenisation should produce smaller z-averages and more monodisperse liposomes. Regarding the zeta potential, all samples should exhibit a positive value, as the liposomes comprised a cationic and a neutral lipid.

All samples showed a z-average within the desired range following the expected trend (Figure 6.1).

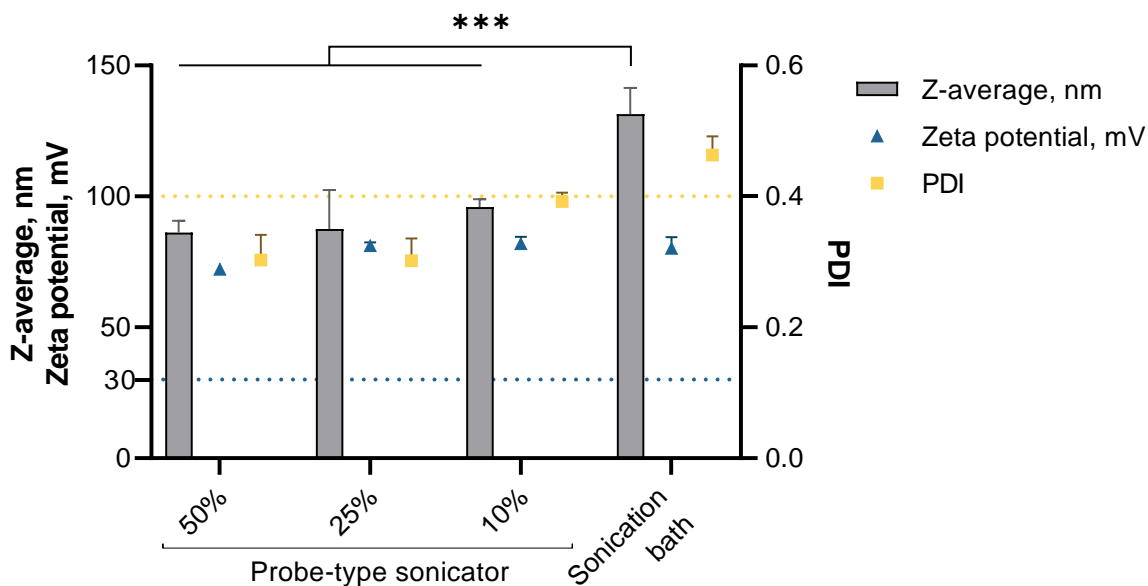


Figure 6.1: Assessment of z-average, zeta potential and PDI of DOTAP:DOPE liposomes after homogenisation using the probe-type sonicator with different intensities and the sonication bath. The blue line indicates the lower end of the desired zeta potential range, while the yellow line displays the upper limit for a favourable PDI.  $n \geq 3$ , bars show mean, error bars show standard deviation, \*\*\* $p < 0.001$

The largest liposomes were produced using the sonication bath with a z-average of  $131 \pm 10$  nm, while the z-average of the probe-type sonicator samples decreased with increasing intensity. Thus, the smallest liposomes with  $86 \pm 5$  nm were produced sonicating with an intensity of 50%. This z-average was not significantly different ( $p > 0.05$ ) to the sonication at 25% intensity, which formed particles of  $88 \pm 15$  nm. Sonication at intensities of both 50% and 25% generated significantly smaller particles ( $p < 0.001$ ) than at an intensity of 10%, which resulted in nanoparticles of  $96 \pm 3$  nm. In contrast to all samples produced by the probe-type sonicator, a PDI of  $> 0.4$  was measured for the sonication bath sample (0.46). This also matched with the expectation that a higher homogenisation intensity produces less polydisperse liposomes. A similar particle z-average of approximately 110 nm and a PDI of around 0.4 was measured by Taetz et al. using ethanol injection as preparation method [60]. They injected an ethanolic lipid solution rapidly into water while stirring it with a magnetic bar. This suggests that not only the shear forces, to which the liposomes are subjected, are the main influencing factor for particle size, but that the size is also highly dependent on the preparation method.

Upon examining the zeta potential, all analysed samples showed a positive zeta potential far above the minimum requirement of 30 mV. All samples produced with the probe-type sonicator met the targeted z-average, PDI and zeta potential. However, sonicating with an intensity of 50% was challenging when using small volumes, as the dispersion often spouted out of the

tube. And as one aim was to find a preparation method, which only requires small amounts of lipids, probe-type sonication with an intensity of 50% was excluded as potential method. This was also the case for the sonication bath and probe-type sonication with an intensity of 10%, as the PDI values were above and very close to 0.4, respectively. In comparison, the probe-type sonicator method with an intensity of 25% produced particles with a PDI value significantly lower ( $p < 0.001$ ) than 0.4 and a z-average in the desired range. Hence, homogenising with the probe-type sonicator at an intensity of 25% was chosen for the further formulation development. The next steps involved the evaluation of toxicity and transfection efficiency to demonstrate that liposomes, aligning with the desired particle size range, PDI and zeta potential, also function safely *in vitro*.

### 6.1.1.1. Cytotoxicity of DOTAP:DOPE Liposomes

Transfection efficiency is generally tightly connected with cytotoxicity [10, 116]. After finding a suitable production method for DOTAP:DOPE liposomes the dose depended cytotoxicity of DOTAP:DOPE liposomes was assessed. Although DOTAP:DOPE was found to be safe for human administration after intravenous application, cytotoxicity was analysed on Calu-3 and A549 cells to investigate the influence of DOTAP:DOPE on cell viability of lung cancer cells [49]. Calu-3 and A549 cells were treated with four increasing concentrations of DOTAP:DOPE liposomes within the range of 0.0005 and 0.057  $\mu\text{g}/\mu\text{L}$ . To study concentration dependent cell viability, the CellTiter-Glo assay was conducted, an assay system that is based on measuring ATP, which is directly proportional to the number of viable cells in the culture [109, 110].

The cell viability of Calu-3 cells was found to be unaffected by any DOTAP:DOPE concentration within the investigated range, while A549 cells showed a decrease in viability to 78% and 42% for DOTAP:DOPE concentrations of 0.011 and 0.057  $\mu\text{g}/\mu\text{L}$ , respectively (Figure 6.2).

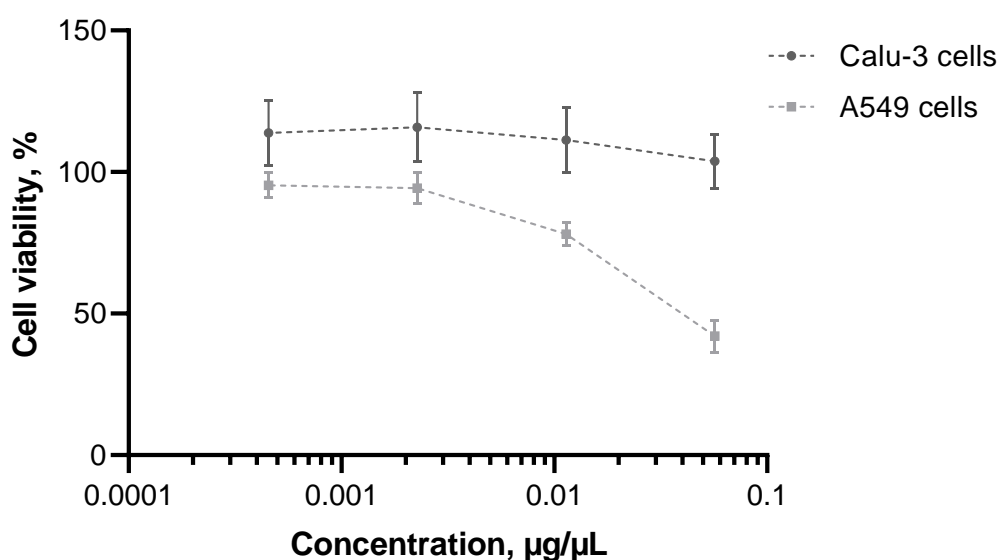


Figure 6.2: Concentration-dependent cytotoxicity of DOTAP:DOPE on Calu-3 and A549 cells after treatment for 5 h determined by CellTiter-Glo assay.  $n = 3$ , symbols show mean, error bars show standard deviation.

Comparable concentration-dependent cytotoxicity and a similar difference between the two cell lines was observed by Taetz et al., although the used assay system and conditions were slightly different. This indicates that the A549 cells are more sensitive than Calu-3 cells, which is probably caused by the production of mucus by Calu-3 cells, acting as a protective layer [60, 100]. In conclusion, DOTAP:DOPE did not alter the cell viability in Calu-3 cells over the investigated concentration range and in A549 cells in concentrations lower than 0.011  $\mu\text{g}/\mu\text{L}$ . Hence, DOTAP:DOPE was applied below this concentration in the transfection assays for further formulation development.

### 6.1.2. Preparation of mRNA Lipoplexes

Therapeutic messenger RNA is translated by host cells to produce the desired protein, which is ultimately responsible for the pharmacologic effect [111, 117]. In this study, firefly luciferase mRNA acted as a model mRNA to investigate the influence of every formulation step. This model mRNA encodes the enzyme firefly luciferase, whose activity can readily be measured in a microplate format to functionally demonstrate the intact condition of both the mRNA and its lipoplex. The successful expression of luciferase in the *in vitro* experiments is dependent on the integrity of both components, as their combined functionality is required for successful transfection and translation. After preparing DOTAP:DOPE liposomes of a favourable size for transfection, the complex formation with mRNA followed as the subsequent step. DOTAP:DOPE has been commonly used as a transfection agent for plasmid DNA and RNA in various lipid to nucleic acid ratios [19, 58, 118, 119]. Thus, to find the optimal ratio for the setup of this study, six mRNA to lipids ratios were prepared, physicochemically characterised and tested on Calu-3 and A549 cells. As the first step to form lipoplexes, DOTAP:DOPE liposomes were produced following the previously developed procedure (Chapter 6.1.1). Thereafter, the mRNA was added to the liposomes. The amount of liposomes was chosen to prepare six increasing DOTAP:DOPE to mRNA weight ratios (1+1, 3+1, 5+1, 7+1, 9+1, 11+1) while the amount of mRNA was kept constant.

### 6.1.2.1. Physicochemical Characterisation of mRNA Lipoplexes

The physicochemical characterisation involved the assessment of the z-average, PDI and zeta potential of the prepared mRNA lipoplexes with increasing DOTAP:DOPE to mRNA weight ratios. Non-complexing liposomes (11+0) were used as a reference (Figure 6.3).

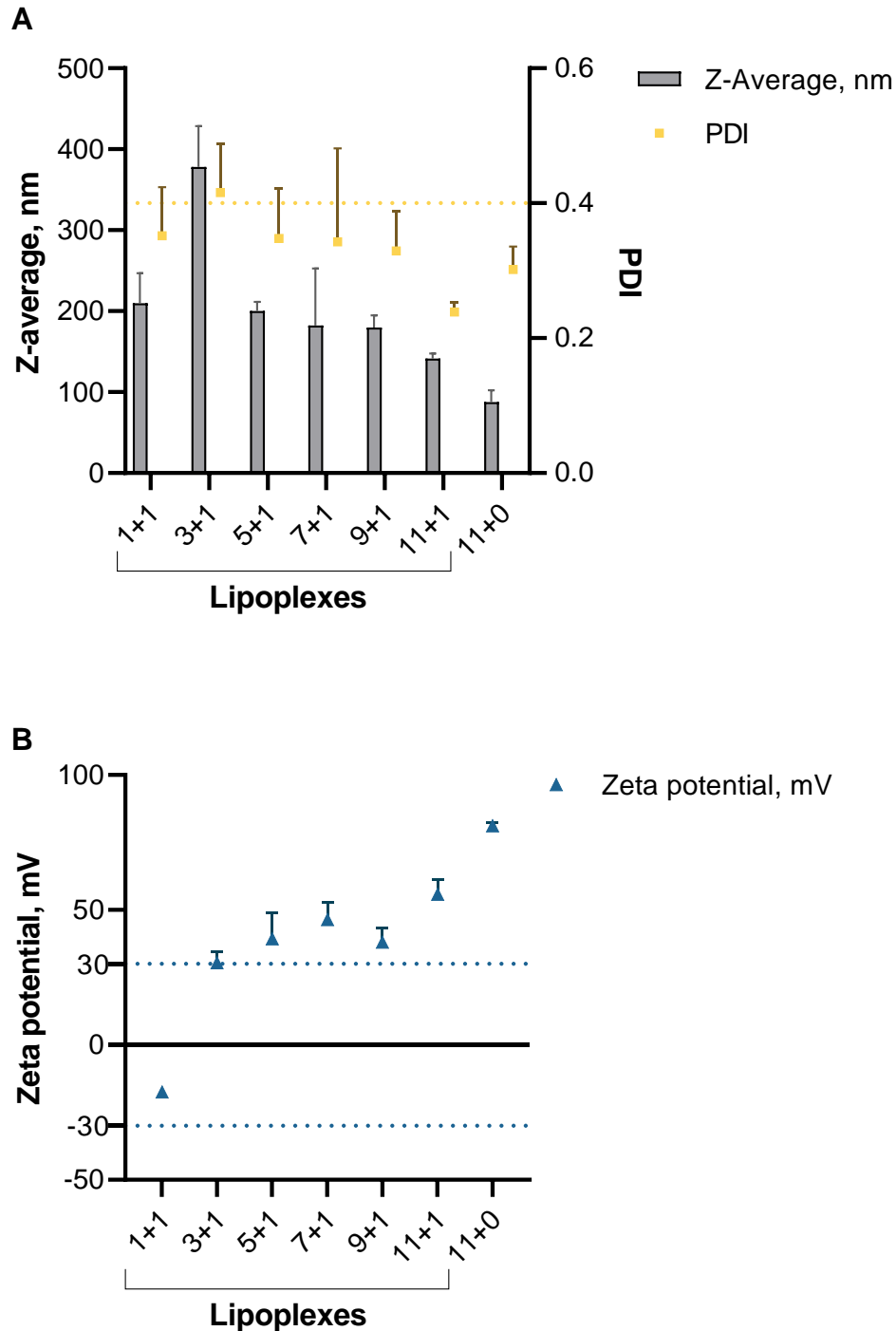


Figure 6.3: Z-average, PDI (A) and zeta potential (B) of the mRNA lipoplexes with increasing DOTAP:DOPE to mRNA weight ratio (1+1, 3+1, 5+1, 7+1, 9+1, 11+1) and DOTAP:DOPE liposomes (11+0) as control. The dotted yellow line represents the upper limit for a favourable PDI, while the upper and lower dotted blue lines display the lower and upper ends, respectively, of a favourable zeta potential.  $n \geq 3$ , bars and symbols show mean, error bars show standard deviation.

The targeted z-average, PDI and zeta potential were set in accordance with those employed for the preparation of empty DOTAP:DOPE liposomes. The target hydrodynamic particle size range was set at 70 to 200 nm to facilitate transfection. The PDI should be below 0.4 and the zeta potential higher than 30 mV or lower than -30 mV [48, 103]. Starting at a liposome size of around 88 nm for the empty liposomes, a slight increase of particle size was anticipated for the lipoplexes due to the additional mRNA molecules. How the increasing DOTAP:DOPE to mRNA ratio influences the z-average was not easy to predict, as the effects of the ratio differs in literature [15, 19, 120]. Regarding the zeta potential the highest value was expected for the pure liposomes, as negatively charged mRNA was absent. Hence, the highest DOTAP:DOPE to mRNA ratio of 11+1 was expected to show the next highest zeta potential. Considering this expectation, the zeta potential should further decrease with increasing negatively charged mRNA portion within the lipoplex as also reported by Pires et al. [121]. For the PDI, a slight increase in comparison to the pure liposome was expected, as an additional particle building component was added to the dispersion.

As anticipated, all prepared mRNA lipoplexes exhibited significantly larger ( $p < 0.001$ ) z-averages compared to the pure liposomes with a minimum increase of 54 nm for the ratio 11+1 and a maximum increase of 291 nm for the 3+1 ratio. The ratio 3+1 was not only the sample with the largest z-average of  $378 \pm 50$  nm, but also depicted a PDI above 0.4. Both parameters placed the ratio 3+1 outside of the desired range, although its zeta potential indicated stable nanoparticles. The next ratios in line of z-average were 1+1 with  $210 \pm 37$  nm, 5+1 with  $200 \pm 11$  nm and both 7+1 and 9+1 with a z-average around 180 nm ( $182 \pm 70$  nm and  $180 \pm 15$  nm, respectively). The PDI of all those samples was found to be lower than 0.4 by mean, but the ratio 7+1 showed a large standard deviation of the PDI of 0.138. However, the standard deviations of the z-averages were considerably high for all ratios apart from 5+1 (11 nm) and 11+1 (6 nm), indicating more reproducible lipoplex formation for these ratios. The ratio 11+1 displayed the smallest z-average with  $142 \pm 6$  nm, a PDI of 0.239 and a zeta potential of 56 mV. The further ratios revealed the expected trend of decreasing zeta potential with decreasing DOTAP:DOPE to mRNA ratio, up to a negative zeta potential of -17 mV for the ratio 1+1. While this zeta potential indicated unstable nanoparticles, all higher ratios exhibited a zeta potential of at least 30 mV, placing them within the range of stable nanoparticles. These measured zeta potentials were higher than the zeta potential of the lipid nanoparticles (LNPs) of Zimmerman et al. and Qiu et al. [14, 15].

In conclusion, the mRNA lipoplexes exhibited z-averages aligning with those for the LNPs produced by Zimmermann et al. [14]. In contrast, the PEG<sub>12</sub>KL4/mRNA complexes formulated by Qiu et al. were more than twice the size and the LNPs prepared by Sheperd et al. were at least 42 nm smaller than the mRNA lipoplexes in the present study [14, 15, 24].

Assessing the physicochemical properties of lipoplexes plays an important role in understanding the different factors influencing the transfection capabilities of lipoplexes. However, the actual impact particle size has on transfection varies between applied model systems and is overall difficult to predict [19, 122]. Hence, transfection efficiency measurements were conducted to determine the optimal ratio of DOTAP:DOPE to mRNA. This optimal ratio was then selected for the further formulation development of the inhalable dry powder platform for mRNA therapeutics.

#### **6.1.2.2. Determining the Optimal DOTAP:DOPE to mRNA Ratio for Transfection**

Since the particle size alone does not adequately predict the functionality of lipoplexes *in vitro*, transfection experiments were performed to determine the optimal weight ratio of lipids (DOTAP:DOPE) to mRNA for the subsequent formulation steps. Identifying the ideal weight ratio is critical because an excessive amount of cationic liposomes could overly bind the mRNA, potentially impeding its release from the liposome after endosomal escape. Conversely, an insufficient amount of liposome might not adequately protect the mRNA and compromise effective transfection and endosomal escape [53].

A549 and Calu-3 cells served as model cell lines in this study. These two cell lines are human lung carcinoma cell lines representing different areas of the respiratory tract. The Calu-3 cell line was derived from human bronchial epithelium, while A549 cells are alveolar epithelial cells [98–101]. Analogously to the assessment of z-average, PDI and zeta potential, six distinct ratios were prepared (1+1, 3+1, 5+1, 7+1, 9+1, 11+1), while maintaining a constant amount of mRNA. As a negative control, naked mRNA and DOTAP:DOPE without mRNA were tested, while mRNA transfected with Lipofectamine 2000 served as a positive control. Lipofectamine 2000 is a multivalent cationic lipid that is commonly used as transfection reagent in *in vitro* cell experiments and is specifically designed for high transfection efficiency. While the transfection is very reliable, the multivalent cationic lipid is much more toxic than monovalent cationic lipids such as DOTAP [123]. This high toxicity is the reason why Lipofectamine 2000 is commonly used *in vitro* but not *in vivo*. However, Lipofectamine 2000 is a widely used standard to compare different transfection agents and was thus included in these experiments as a control. Figure 6.4 displays the transfection efficiency of all investigated samples on Calu-3 and A549 cells.

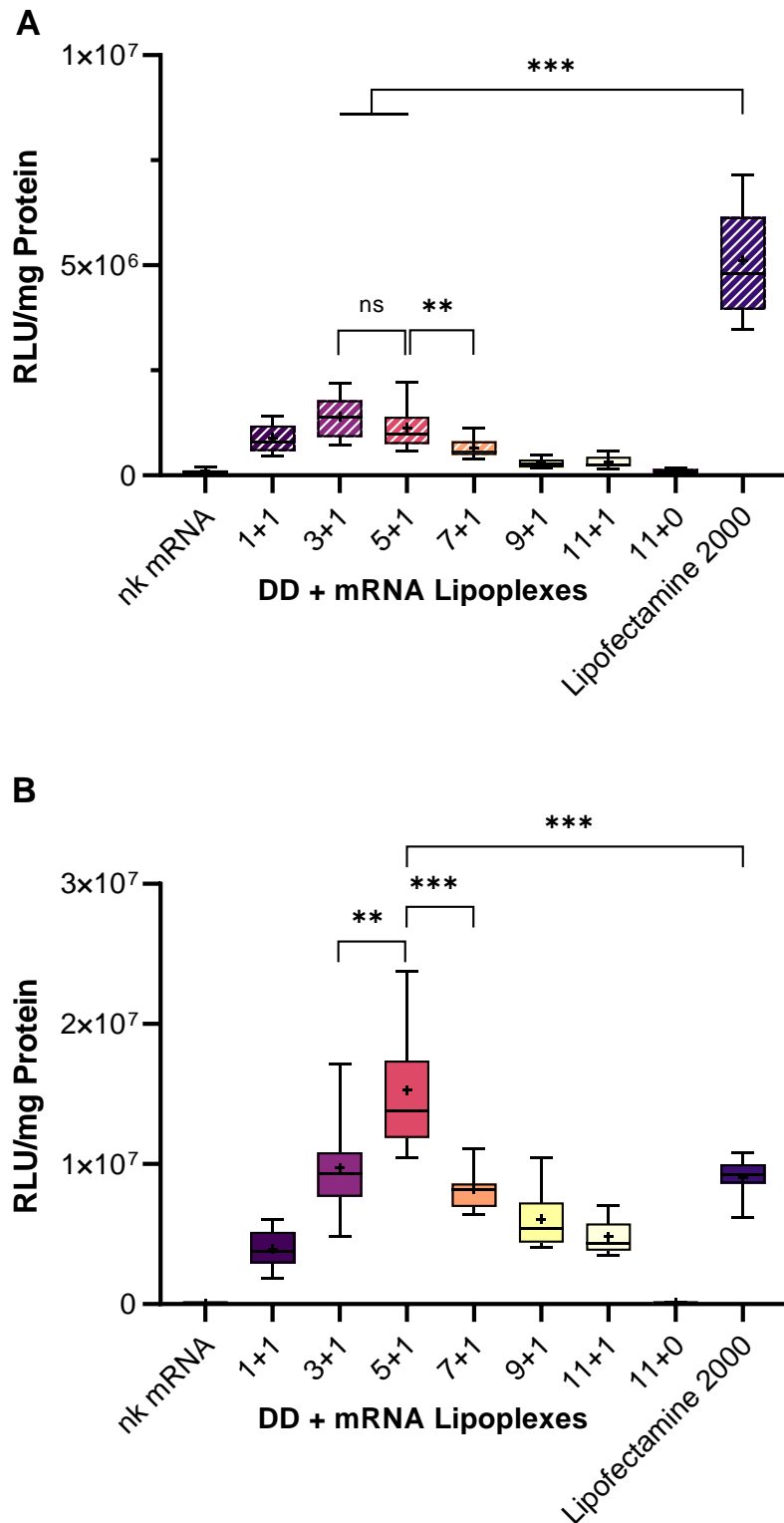


Figure 6.4: Luciferase mRNA transfection on Calu-3 cells (A) and A549 cells (B). 6 different lipoplex compositions were transfected. A composition of 5+1 represents the weight ratio of DOTAP:DOPE (DD) to mRNA. Naked mRNA (nk), DD without mRNA (11+0) and Lipofectamine 2000 served as controls. Transfection efficiency was expressed as relative light units normalised to the protein concentration.  $n = 3$ , for description of box plots see chapter methods, ns = not significant, \*\* $p < 0.01$ ; \*\*\* $p < 0.001$ .

Upon comparing both cell lines, the overall signals of the A549 cells are approximately one decimal power higher than the signals of the Calu-3 cell line. This was expected, as the Calu-3 cells have the ability to form a monolayer of cells and establish tight junctions, as well as secrete mucus [100]. This mucus secretion provides an additional barrier to gene delivery and is the reason why Calu-3 have been shown to be more difficult to transfect [60, 107, 124, 125]. While the negative controls, including naked mRNA and DOTAP:DOPE samples without mRNA, exhibited signals close to the blank in both cell lines, Lipofectamine 2000 displayed a luminescence signal of  $5 \cdot 10^6$  RLU/mg in Calu-3 cells.

This signal was significantly higher ( $p < 0.001$ ) than the strongest signal observed among the DOTAP:DOPE lipoplexes in Calu-3 cells, which was  $1.1 \cdot 10^6$  RLU/mg measured for the ratio 3+1. In contrast, in A549 cells the luminescence signal of the Lipofectamine 2000 sample was significantly lower ( $p < 0.001$ ) than the signal of the lipoplexes with a ratio of 5+1, which displayed a signal of  $1.5 \cdot 10^7$  RLU/mg, the highest of all the lipoplex samples on A549 cells. The disparity in transfection efficiency may be attributed to the higher sensitivity of A549 cells, to both transfection and cytotoxic agents such as Lipofectamine 2000, compared to Calu-3 cells. This interplay between sensitivity and cytotoxicity may lead to a lower transfection efficiency for Lipofectamine 2000 compared to DOTAP:DOPE, as DOTAP:DOPE is less toxic [60]. Moreover, the circumstance that the DOTAP:DOPE to mRNA ratio of 5+1 resulted in an even higher signal than Lipofectamine 2000 on A549 cells underlined the potential of these lipids. Qiu et al. reported an equal transfection efficiency to Lipofectamine 2000 for their PEG<sub>12</sub>KL4/mRNA complexes [117]. When comparing the ratios within the same cell line, it was observed that the signal of the ratio 5+1 in A549 cells was also significantly stronger than the signal of 3+1 with  $9.6 \cdot 10^6$  RLU/mg ( $p = 0.002$ ) and 7+1 with  $8.2 \cdot 10^6$  RLU/mg ( $p < 0.001$ ), respectively. Transfecting those lipoplex ratios into Calu-3 cells did not result in a significant difference ( $p > 0.05$ ) between the ratios 3+1 and 5+1 ( $1.4 \cdot 10^6$  and  $1.1 \cdot 10^6$  RLU/mg), but the 5+1 ratio showed a very significant difference ( $p = 0.001$ ) to the ratio 7+1 ( $6.6 \cdot 10^5$  RLU/mg). The ratios 9+1 and 11+1 exhibited a significantly lower ( $p < 0.001$ ) signal compared to 5+1 in both cell lines, while the ratio 1+1 was significantly lower ( $p < 0.001$ ) in A549 cells and not significantly different ( $p > 0.05$ ) in Calu-3 cells. Interestingly, the physicochemically assessment of the ratio 11+1 revealed in theory the best properties for transfection with a z-average of 142 nm, a PDI of 0.239 and a zeta potential of 56 mV. As a zeta potential above 30 mV indicates stable particles, a mRNA lipoplex with a zeta potential of 56 mV might have a too high surface charge and might be too stable to sufficiently dissociate in the cytosol [48]. Conclusively, these results demonstrated a favourable transfection efficiency for the ratio 3+1 and 5+1 on Calu-3 cells. However, the considerable advantage of the ratio 5+1 on A549 cells led to the decision to proceed with the formulation development of the inhalable dry powder platform using a DOTAP:DOPE to mRNA ratio of 5+1.

### 6.1.2.3. Assessment of Free mRNA, Complexation and Lipoplex Properties

#### 6.1.2.3.1. Assessment of Free mRNA

Agarose gel electrophoresis is often employed to verify the size of an RNA molecule and to assess the stability of RNA complexes [117, 126]. The principle of separating samples based on their charge and molecular weight is useful for analysing mRNA lipoplexes. In this experiment, the agarose gel was run and the free mRNA was subsequently stained with SYBR Gold. SYBR Gold exhibits a signal magnification of more than 1000-fold when bound to nucleic acids. Therefore, when mRNA is freed of its lipoplex and SYBR Gold can intercalate into the molecule, the mRNA is visible as a band in the gel electrophoresis. This analysis provides insight into the complexation of mRNA by the lipids. With an increasing amount of DOTAP:DOPE, the mRNA band is expected to fade, as DOTAP:DOPE complexes mRNA more thoroughly. To visualise the progress of complexing mRNA, six mRNA lipoplexes with increasing amount of DOTAP:DOPE (1+1, 2+1, 3+1, 4+1, 5+1, 6+1) were analysed (Figure 6.5).

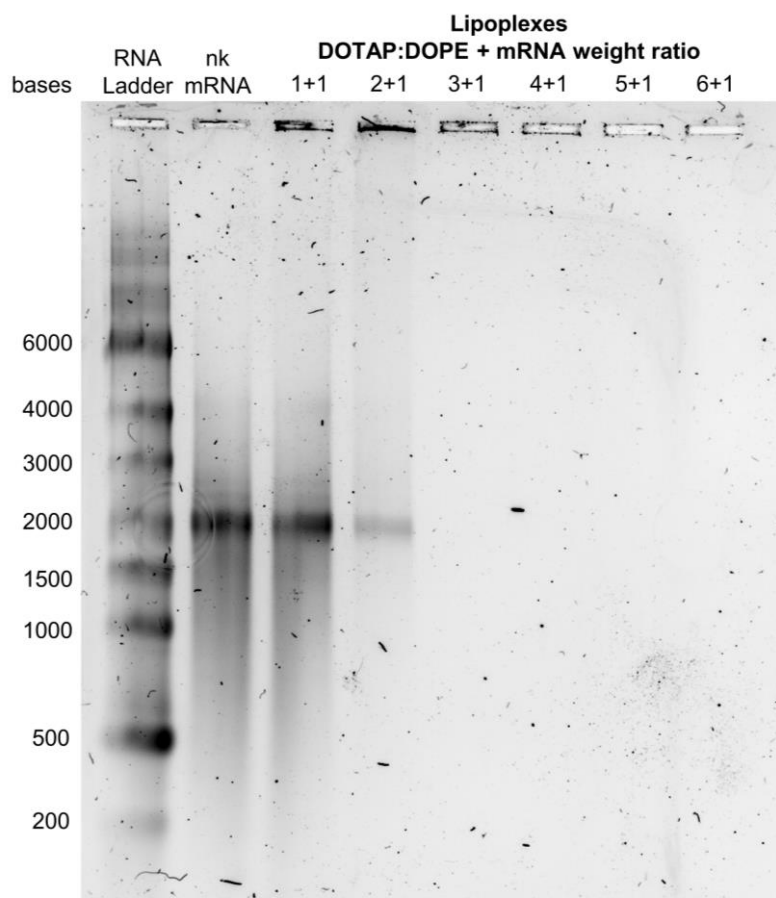


Figure 6.5: Representative image of an agarose gel with six weight ratios of DOTAP:DOPE and mRNA with the amount of mRNA held constant. A ratio of 5+1 represents a weight ratio of DOTAP:DOPE to mRNA of 5 to 1. An RNA Ladder and naked mRNA (nk mRNA) were included as controls.

An RNA ladder and naked mRNA were included as controls. The naked mRNA showed its band around 2000 bases. This was expected as the mRNA comprises approximately 1680 nucleotides with a cap structure at the beginning and a 150-nucleotides poly-A tail. Upon examining the bands of the mRNA lipoplexes, a band for naked mRNA was observed for the ratios 1+1 and 2+1. The band intensity decreased with increasing amount of DOTAP:DOPE. For the ratio of 2+1 a pale band is still visible, while for 3+1 no band is visible anymore. The reason for this observation was that more complexing lipids are available, increasing the ionic interactions with the negatively charged mRNA. Hence, mRNA is not free to be bound by SYBR Gold to display a band. This procedure was adapted from Qiu et al. and their small interfering RNA (siRNA) binding studies of KL4/siRNA complexes [15, 117]. These findings align with the results of the transfection efficiency study, as the weight ratios 3+1 and 5+1 yielded higher luminescence signals than 1+1, where the mRNA was not yet completely complexed. Lipoplexes with a proportion of lipids higher than 5+1 also did not show a visible band, however, they previously exhibited a lower transfection efficiency. This can be explained by an excess of lipid perturbing proper mRNA release and thus hindering translation [48].

### 6.1.2.3.2. Influence of Complexation Period

The time given the complexes to form from lipids and mRNA depends on the system and preparation methods. For instance, Qiu et al. waited 30 min, Taetz et al. 15 min and the manufacturer's protocol for Lipofectamine 2000 recommends an complexation time of 5 to 20 min after mixing the transfection reagent with RNA [60, 117, 127]. The first transfection experiments of this study with DOTAP:DOPE as transfection agent were also performed after an complexation time of 20 min. However, in subsequent experiments, it was recognised that a longer complexation time led to stronger luminescence signals and a complexation time of 120 mins was established. After determining the optimal DOTAP:DOPE to mRNA ratio to be 5+1, the incubation time was thoroughly assessed. Since Calu-3 cells are more critical, as they are less sensitive to transfection, the different complexation periods were tested on Calu-3 cells. The transfection of mRNA lipoplexes increased generally with increasing time of complexation, as previously recognised (Figure 6.6).

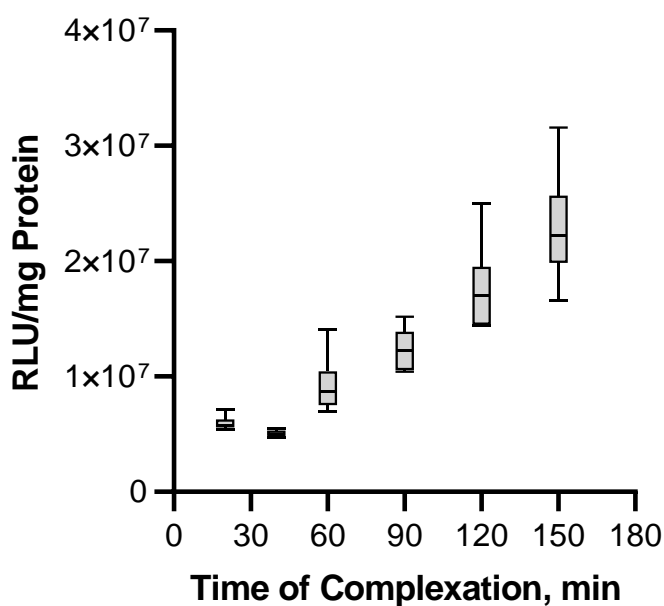


Figure 6.6: Assessment of luciferase mRNA transfection on Calu-3 cells after increasing time of complexation of mRNA with DOTAP:DOPE.  $n = 2$ , for description of box plots see chapter methods.

Nevertheless, the transfection efficiency of a complexation period of 120 and 150 min showed a considerable overlap, indicating the initiation of a plateau. With convincing results obtained from a complexation time of 120 min for A549 cells as well, the subsequent experiments were conducted, allowing the formation of lipoplexes over a 120-minute period.

#### 6.1.2.3.3. *Assessing Complex Binding Affinity via Fluorescence Displacement*

The complexation between mRNA and DOTAP:DOPE is driven by electrostatic interactions. mRNA, being negatively charged, forms complexes with the positively charged lipid DOTAP and the neutral lipid DOPE. With the aim of producing an inhalable dry powder formulation in mind, these interactions, holding mRNA and DOTAP:DOPE together, have to withstand shear and thermal stress during the spray drying process. In the quest to characterise the stability of DOTAP:DOPE lipoplexes, a fluorescence displacement assay, as described by Qiu et al., was applied [107]. Qiu et al. pursued two strategies based on SYBR Gold's properties. Firstly, they evaluated the amount of complexing agent, their modified KL4 peptides, required to displace SYBR Gold from bound siRNA. For this, the complexing peptides were titrated to the siRNA/SYBR Gold mixture. The fluorescence intensity sharply decreased as peptides were added, indicating displacement. However, when applying the same approach to DOTAP:DOPE lipoplexes and mRNA, the fluorescence intensity exhibited a reduction of 5.8% following the initial addition of DOTAP:DOPE and only marginally decreased during subsequent addition, reaching a maximum decrease of 17.7% at a weight ratio of 83+1 (Figure 6.7 A).

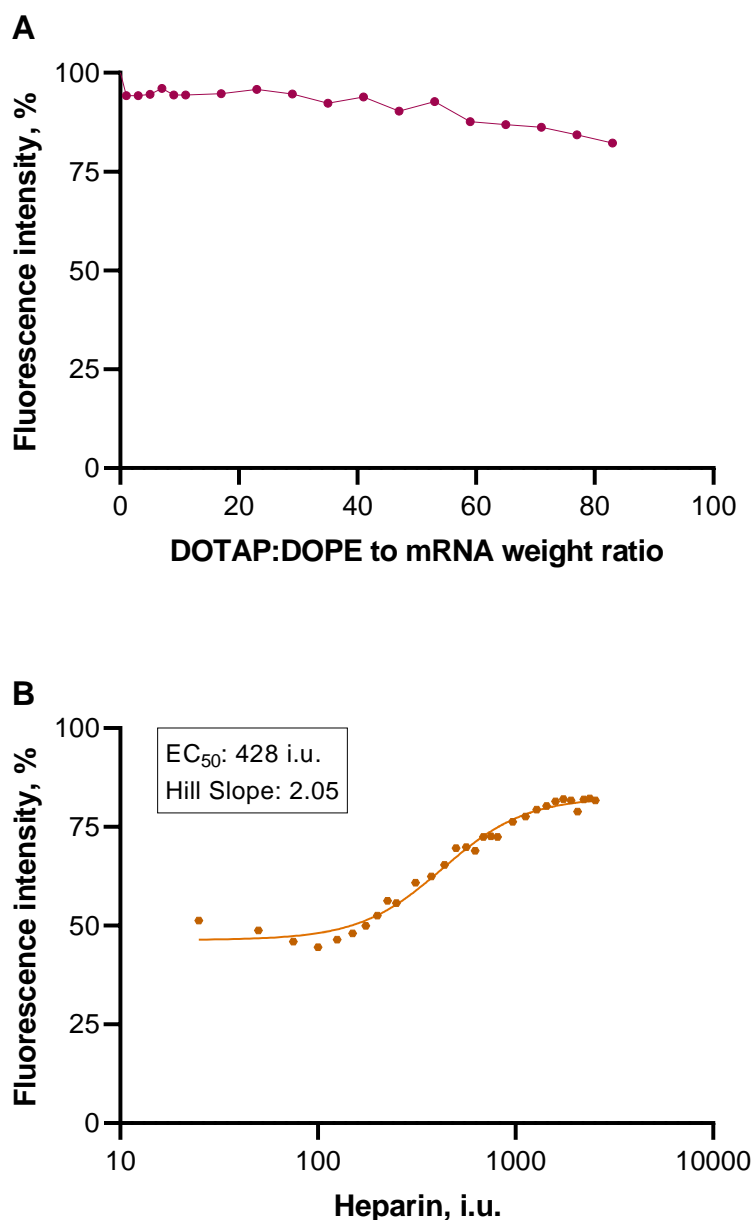


Figure 6.7: Assessment of mRNA binding affinity of DOTAP:DOPE (DD) using the fluorescence displacement assay. (A) DD was titrated to the mRNA/SYBR Gold mixture. Fluorescence intensity was plotted as the percentage of the fluorescence intensity of mRNA/SYBR Gold against DD to mRNA weight ratio upon titration.  $n = 1$ . (B) DD/mRNA lipoplexes were complexed in presence of SYBR Gold and titrated with heparin to dissociate the complexes. Fluorescence intensity was plotted as the percentage of the fluorescence intensity of mRNA/SYBR Gold without DD against the amount of heparin upon titration. The data was fit to a four-parameter logistic sigmoidal curve, and the half-maximal effective concentration ( $EC_{50}$ ) and hill slope were calculated.  $n = 1$ .

Potential reasons for this plain curve include higher binding affinity of SYBR Gold to mRNA compared to the siRNA used by Qiu et al., given that siRNAs are typically 20 to 30 nucleotides long, whereas the used mRNA is around 1680 nucleotide long [120, 128]. This longer mRNA can provide more binding sites for SYBR Gold per molecule than siRNA. Alternatively, the results could be attributed to a lower binding affinity of DOTAP:DOPE to mRNA compared to the KL4 peptides' affinity to siRNA.

An increased binding affinity could offer more protection from degradation through nucleases and other stress factors, but it could also deteriorate the release in the cytosol prior to translation. Nevertheless, the transfection efficiency assessment demonstrated satisfactory results for lipoplexes with a DOTAP:DOPE to mRNA weight ratio of 5+1. Therefore, the outcome of this experiment did not alter the choice of DOTAP:DOPE to mRNA weight ratio.

The second strategy Qiu et al. pursued was to reverse the set up. For this, in the first step, complexes of DOTAP:DOPE and mRNA were prebuilt in presence of SYBR Gold. Then heparin was titrated to the complexes and, as before, the fluorescence intensity was measured. The strongly negative charged heparin was intended to dissociate the complexes and release the siRNA while building complexes with the cationic KL4 peptides. Free siRNA was then available for SYBR Gold, and the fluorescence intensity increased. The  $EC_{50}$  (half-maximal effective concentration) and hill slope were calculated to assess binding affinity. The  $EC_{50}$  was the concentration of heparin that caused a 50% increase in fluorescence intensity. The hills slope investigated the steepness of the curve and thus how readily siRNA was released from the peptides. This assay was performed with the mRNA lipoplexes of this study to contextualise the binding affinity. Transferring this analysis method to the mRNA lipoplexes of this study, mRNA was complexed with DOTAP:DOPE in a weight ratio of 5+1 prior to titration with heparin. Fluorescence intensity was measured and, in analogy to Qiu et al., both the  $EC_{50}$  and hill slope were calculated (Figure 6.7 B). The  $EC_{50}$  was found to be at 428 i.u. heparin, indicating a slightly lower binding affinity between mRNA and DOTAP:DOPE in comparison to Qiu et al.'s siRNA/PEG<sub>12</sub>KL4 complex. Interestingly, the hill slope appeared to be slightly lower at 2.05 than the hill slope of siRNA/KL4PEG<sub>12</sub>, displaying a less readily released mRNA from DOTAP:DOPE. After the results of titrating DOTAP:DOPE, this heparin titration made it possible to contextualise the binding affinity of mRNA lipoplexes in the current study alongside with the complexes studied by Qiu et al.. However, whether the binding affinity is sufficient to protect the mRNA and hold the lipoplex together during spray drying is yet to be determined in Chapter 6.2.

#### 6.1.2.4. Visualising DOTAP:DOPE Lipoplexes

The physicochemical and *in vitro* assessment of mRNA lipoplexes revealed the DOTAP:DOPE to mRNA weight ratio of 5+1 to form stable and functional nanoparticles with a size of  $200 \pm 11$  nm. In addition to this important characterising information, transmission electron microscopy was used to generate insights of the lipoplex shape and visually confirm the size of the formulated lipoplexes. The images were taken of mRNA lipoplexes with a DOTAP:DOPE to mRNA weight ratio of 5+1 and displayed relatively round complexes of a size between 200 and 300 nm (Figure 6.8). With most particles being slightly above 200 nm, these results were consistent with the z-average of  $200 \pm 11$  nm measured with the Zetasizer for the 5+1 mRNA lipoplexes.

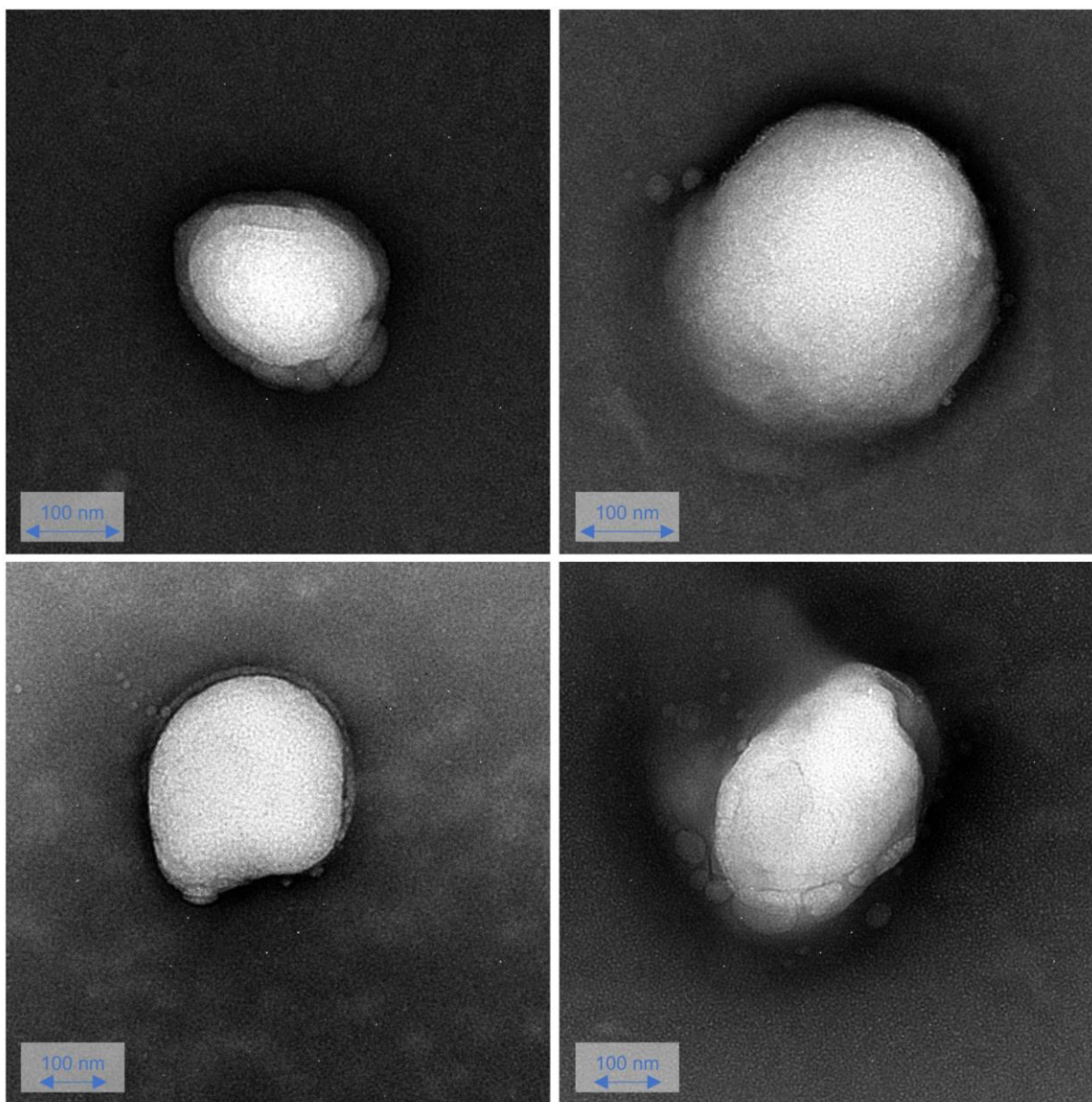


Figure 6.8: Representative transmission electron microscope images of four different mRNA lipoplexes in a DOTAP:DOPE to mRNA weight ratio of 5+1.

### 6.1.3. Conclusion on the Preparation of DOTAP:DOPE Liposomes and mRNA Lipoplexes

In conclusion, this section of the study focused on the crucial steps involved in preparing mRNA lipoplexes for efficient transfection, particularly emphasising the use of DOTAP:DOPE as a delivery system. The chosen lipids were carefully selected for their safety in human administration and demonstrated efficient transfection in previous studies [19, 49]. The investigation covered the preparation of liposomes, cytotoxicity assessment, determination of optimal lipid-to-mRNA ratios, stability analysis, and visual assessment of lipoplexes.

The preparation of DOTAP:DOPE liposomes involved careful consideration of various parameters, such as z-average, polydispersity index (PDI), and zeta potential, to ensure the formation of stable and relatively monodisperse liposomes. Preparation methods including homogenisation using a probe-type sonicator and a bath sonicator were evaluated, resulting in the development of a robust method for the production of liposomes with the desired properties using the probe-type sonicator.

Cytotoxicity assessment on Calu-3 and A549 cells evaluated the safety of DOTAP:DOPE, with a non-affecting concentration range below 0.04  $\mu\text{g}/\mu\text{L}$ . Then the study delved into the formulation development of mRNA lipoplexes using firefly luciferase mRNA as a model, with six different DOTAP:DOPE to mRNA weight ratios. The physicochemical characterisation revealed variations in z-average, PDI, and zeta potential with changing ratios, providing insights into the optimal lipoplex composition. Notably, the 5+1 ratio demonstrated favourable characteristics, with stable nanoparticles of about 200 nm, aligning with the requirements for efficient transfection [48]. The transfection efficiency of the 5+1 ratio, along with the 3+1 ratio, was the highest on Calu-3 cells and significantly surpassed all other ratios on A549 cells, even outperforming Lipofectamine 2000. Following this, the complexation of the mRNA in lipoplexes was further assessed through agarose gel electrophoresis, demonstrating a reduced intensity of the mRNA band with increasing DOTAP:DOPE ratio. This result correlated with the protective complexation of mRNA within lipoplexes, preventing its interaction with the SYBR Gold dye in which the gel was incubated. The mRNA band was not visible anymore exceeding a DOTAP:DOPE to mRNA weight ratio of 3+1, indicating satisfactory mRNA complexation for the ratio 5+1.

Additional investigations, including the assessment of free mRNA, determination of the optimal complexation period and complexation affinity via fluorescence displacement, provided valuable insights to optimise the mRNA lipoplex formation. An incubation time of 120 min was established as effective for complexation. The analysis of the ratios for free mRNA and the fluorescence displacement assay indicated a favourable complexation between DOTAP:DOPE and mRNA, further supporting the choice of the 5+1 weight ratio. Transmission electron

microscope images displayed spherical mRNA lipoplexes with a size range consistent with the Zetasizer measurements, providing a visual confirmation of the successful formulation.

Overall, the comprehensive approach in this study successfully developed and characterised DOTAP:DOPE liposomes for mRNA delivery, identified an optimal weight ratio of mRNA lipoplexes (5+1), and demonstrated their transfection efficiency. These findings laid the foundation for the formulation development of an inhalable dry powder platform for mRNA therapeutics and contributed valuable insights into the design and optimisation of mRNA delivery systems for therapeutic applications.

## 6.2. Formulation of mRNA Lipoplexes via Spray Drying: Process Optimisation and Characterisation

Liquid mRNA therapeutics encounter stability issues at ambient temperatures, which make tightly controlled cold-chain infrastructure indispensable, as exemplified by the vaccines against SARS-CoV-2, elaborated in Chapter 3.1.2.2 [16]. This project aims to increase stability and produce a formulation that does not need challenging storage conditions by using a dry and solid formulation. In order to produce a dry powder formulation a drying step is required. Spray drying is a common drying method, well established in the food and pharmaceutical industries [79]. Owing to its adaptability and relatively straightforward scalability, spray drying is the method of choice for designing powders with sophisticated characteristics [16, 69]. In the pharmaceutical industry including research and development it is also frequently employed for particle engineering and the production of powders with low densities for high dose inhalation [80]. Particles with low densities have a small aerodynamic size, in spite of a larger geometric size, which can achieve higher drug loads [69].

Moreover, spray drying is a widely acknowledged method for processing heat-sensitive materials like proteins [81]. The brief period the product is subjected to heat and the concurrent cooling during spray drying, play a pivotal role in preventing thermal degradation of the sensitive material. Henceforth, the method of choice to convert mRNA complexed within the lipids DOTAP and DOPE into a dry powder formulation suitable for inhalation was determined to be spray drying.

However, to produce particles by spray drying within the inhalable size range, which is considered to be between 1 and 5  $\mu\text{m}$ , the mRNA lipoplexes had to be embedded into a matrix particle [69, 79, 129]. Spray drying mRNA lipoplexes without a matrix material, if possible, would require a large amount of costly mRNA lipoplexes. For example, to produce 200 mg spray dried powder, the minimum quantity found feasible in this work, about 33 mg mRNA and 167 mg DOTAP:DOPE would have been required. This would have created costs in the five-figure range for the mRNA alone. Beside the economic reasons, spray drying lipid nanoparticles and lipoplexes without a matrix can lead to agglomeration and aggregation of the complexes [130]. Moreover, spray drying lipoplexes in a matrix material like mannitol or lactose, enables the production of spherical particles within the inhalable size range [14]. Therefore, this section aimed to establish a spray drying process to embed the mRNA lipoplexes within suitable matrix particles.

### 6.2.1. Choosing Spray Dryer Model and Tubing Material

During early development the availability of starting material can often be a limiting factor. This is especially true for mRNA and its complexing lipids, due to their high cost. Thus, a process requiring minimal amounts of sample while maintaining a high yield was of utmost importance. As the drying process was determined to be spray drying in this project two spray dryer models were available: the Büchi Nano Spray Dryer B-90 and the Büchi Mini Spray Dryer B-290 (Figure 6.9).

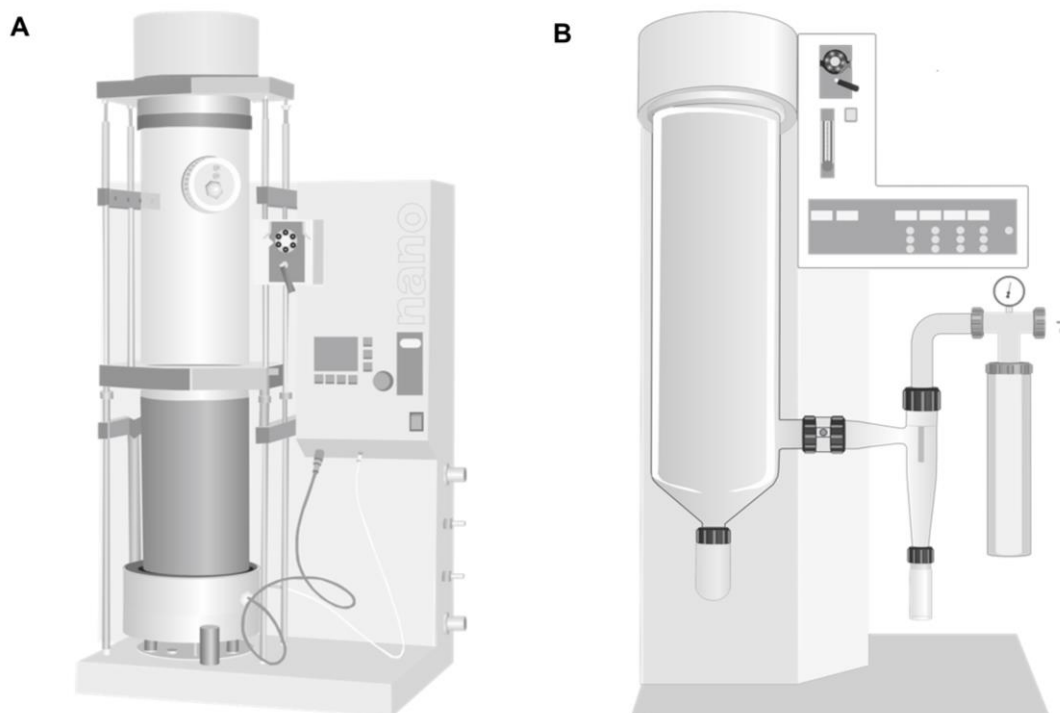


Figure 6.9: Büchi Nano Spray Dryer B-90 (A) and Büchi Mini Spray Dryer B-290 (B)

The Büchi Mini Spray Dryer B-290 is a widely established laboratory size spray dryer. It can be equipped with various traditional nozzles like the two-fluid nozzle and can typically produce particles ranging from 2 to 60  $\mu\text{m}$  with a yield between 50 and 70% [131]. In contrast, the Büchi Nano Spray Dryer B-90 is using piezoelectric driven nebulizer to atomise the spray drying dispersion, achieving a particle size of 0.2 to 5  $\mu\text{m}$  with a yield up to 90% [131]. Therefore, handling a valuable material like mRNA lipoplexes and aiming to produce a powder within the inhalable range, the first attempt was to develop a method to spray dry mRNA lipoplexes using the Büchi Nano Spray Dryer B-90. Due to the small particle sizes claimed to be producible by the Büchi Nano Spray Dryer B-90, the particles are collected in a specially designed particle collector (Figure 6.10).



*Figure 6.10: Particle collector of the Büchi Nano Spray Dryer B-90 comprising the cylindrical shaped collecting electrode in the centre of which a pile of star-shaped foils is located. The particles are intended to attach to the inner surface of the cylindrical shaped collecting electrode [79].*

The cylindrical-shaped particle collector comprises a pile of star-shaped foils located at the centre of a cylindrical collecting electrode. An electrical field is generated between the star-shaped electrode and the collecting electrode, creating negative gas ions that are attracted towards the collecting electrode. As the ions travel, they attach to the suspended particles in the drying gas, negatively charging them. The charged particles are then deflected towards the collecting electrode, where they attach and form a layer of particles [132]. These particles are intended to be recovered by scraping the particles from the collecting electrode onto a sheet of anti-electrostatic paper. However, during initial experiments, it was found that a considerable number of particles attached to the pile of star-shaped foils, and the particles on the inner surface of the cylindrical-shaped electrode were not easily recoverable. Even with considerable effort, the maximum yield of spray drying a mannitol-based lipoplex dispersion remained around 10%. Furthermore, the sophisticated spray head, equipped with a piezoelectric-driven mesh, presented difficulties with non-conductible solutions. Specifically, a 4% mannitol solution caused droplets to drip from the spray head, resulting in the wetting redissolution of previously dried and collected particles as the droplets fell from the spray head to the particle collector. Considering these challenges, experiments to establish a method using the Büchi Mini Spray Dryer B-290 were performed (Figure 6.11).

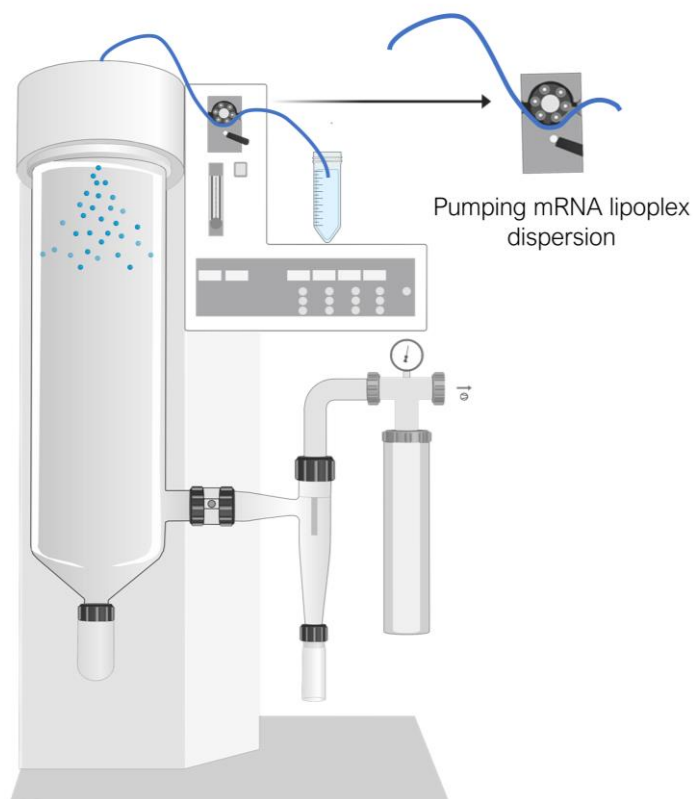


Figure 6.11: For the pumping experiments the peristaltic pump of the Büchi Mini Spray Dryer B-290 was used. The mRNA lipoplex dispersion was collected after pumping through different tubes and its transfection efficiency in the firefly luciferase reporter assay was compared to the not pumped sample.

In order to achieve a particle size of less than  $5\ \mu\text{m}$ , various concentrations of the feed solution and two different diameters of two-fluid nozzles were tested using pure lactose and mannitol solutions. Following the establishment of a stable spray drying procedure using the Büchi Mini Spray Dryer, which resulted in particles within the desired size range and a satisfactory yield, experiments with the actual product, mRNA lipoplexes in a mannitol or lactose matrix, were initiated.

The quality of the final product is influenced by a range of factors during the spray drying process. At the very beginning of the process, there is a built-in peristaltic pump that feeds the fluid through tubing and into the nozzle. The potential stress of the pumping step on the liquid feed is governed by shear forces during the pumping itself and the properties of the tubing material. The tubing material that is most frequently utilised in the production of biopharmaceuticals is silicone, as it is inert, non-adhesive for many substances and readily accessible [133].

To evaluate the influence of the tubing and pumping on the mRNA lipoplexes, in a first attempt, 1.5 mL of a mRNA lipoplex dispersion (conc. 0.002  $\mu\text{g}/\mu\text{L}$ ) was pumped through the silicone tubing and subsequently assessed in the firefly luciferase reporter gene assay. However, the *in vitro* cell experiments showed that using silicone tubing significantly reduced ( $p < 0.001$ ) the transfection efficiency to approximately 43% (Figure 6.12).

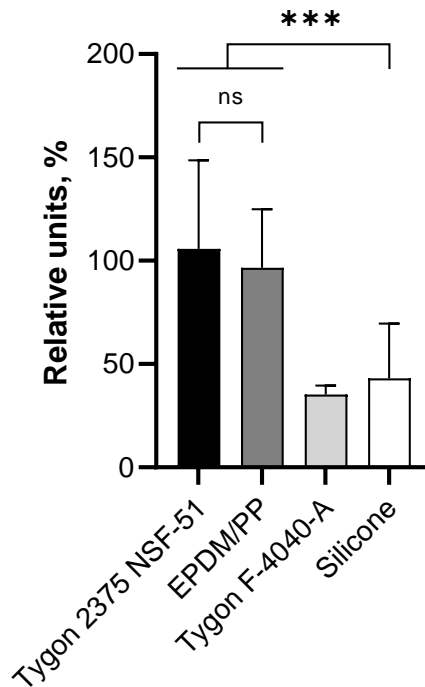


Figure 6.12: Transfection efficiency of mRNA lipoplexes after being pumped through the indicated tubing material: Tygon 2375 NSF-51, EPDM/PP (RCT 333647), Tygon F-4040-A or silicone tubing. Relative units were calculated from the luminescence/mg protein of sample normalised to the signal of not pumped lipoplexes. A value of 100% indicates a transfection efficiency as high as the control before pumping.  $n = 3$ , bars show mean, error bars show standard deviation, ns = not significant, \*\*\* $p < 0.001$ .

The same observation was made by Keil et al. using a polyplex formulation made of DNA and polyethyleneimine (PEI) [133]. Similar to the mRNA lipoplexes in the present study, the DNA/PEI polyplexes were positively charged and adsorbed to the inner tubing wall. This was also confirmed by experiments in the present study which measured the transfection efficiency of differently treated mRNA lipoplexes. On one hand, prebuilt mRNA lipoplexes were pumped through the tube, and on the other hand, naked mRNA was pumped through the tube. After being pumped through the tube, the naked mRNA was complexed with lipids, and both mRNA lipoplex samples were then transfected into Calu-3 cells. The transfection efficiency of the mRNA lipoplexes containing the naked pumped mRNA was considerably higher than that of the prebuilt mRNA lipoplexes. These results lead to the conclusion that only the lipids, and potentially some strongly encapsulated mRNA, adsorb to the tubing material, resulting in a loss of the transfecting lipids for the prebuilt lipoplexes. In order to address this issue, three alternative commercially available tubing materials were screened.

Two Tygon tubes were supplied with the spray dryer for spray drying organic solvents. In a first attempt those two tubing materials the Tygon 2375 NSF-51 and Tygon F4040-A were tested. The Tygon 2375 NSF-51 is made of thermoplastic polyolefins and is considered an ultra-chemical resistant tubing that is unaffected by acids, bases, ketones, salts and alcohols [134]. Furthermore, it is listed in the FDA's Code of Federal Regulations §177.1520 as a substance intended for use in contact with food [135]. The Tygon F4040-A on the other hand is made of thermoplastic elastomers and has its main field of application in fuels and industrial lubricants [136]. Both tubes have a very smooth and antiadhesive inner surface to prevent adsorption. To determine the most compatible tubing material, 1.5 mL of a mRNA lipoplex dispersion (mRNA conc. 0.002 µg/µL) was pumped through the respective tubes. The results, displayed in Figure 6.12, showed that the mRNA lipoplexes pumped through the Tygon 2375 NSF-51 achieved a transfection efficiency of approximately 106%. This is very close to the control sample which was set to a value of 100% as it was not pumped through any tubing material. On the other hand, mRNA lipoplexes collected after being pumped through the Tygon F-4040-A tubing exhibited a transfection efficiency of approximately 35%. Such a low value might be due to the surface that adsorbs either the mRNA itself or the lipids similar to the silicone tubing. These results indicated that Tygon 2375 NSF-51 tubing material is most suited for pumping the mRNA lipoplexes in this study. Nevertheless, it is also crucial for the tubing material to be robust enough to withstand shear forces that occur during pumping in a peristaltic pump. If the tubing material is too hard, the peristaltic pump may need to be adjusted very tightly to pump the fluid, potentially leading to the tubing being torn apart. In subsequent experiments, the Tygon 2375 NSF-51 tubing material was stretched and ultimately torn apart by the peristaltic pump. Hence, it became imperative to identify a tubing material possessing characteristics comparable to Tygon 2375 NSF-51, but which is characterised by either a softer composition or greater resistance to peristaltic pump-induced damage. As an alternative, the suitability of an EPDM/PP (ethylene-propylene-diene/polypropylene) pump and chemical tubing (RCT 333647), listed in the FDA's Code of Federal Regulations §177.2600 as a substance intended for repeated use in production and manufacturing of food, was investigated in accordance with the previously described testing protocol [135]. Notably, the transfection efficiency demonstrated no statistically significant deviation ( $p < 0.05$ ) from that observed of mRNA lipoplexes conveyed through Tygon 2375 NSF-51 tubing. Consequently, for subsequent experiments, the decision to use EPDM/PP tubing was made. After the spray dryer model had been selected to establish a stable process and the tubing material had been identified to preserve the mRNA lipoplexes' integrity during pumping, the formulation development using spray drying could proceed.

## 6.2.2. Mannitol and Lactose as a Matrix for Spray Drying mRNA Lipoplexes

When spray drying mRNA lipoplexes, these lipoplexes require a matrix for protection from degradation and to build dry powder particles with the desired properties. Lactose and mannitol are approved for inhalation by the FDA and readily dissolve upon contact with the lung fluid, releasing their cargo [14, 85]. Both lactose and mannitol were previously used in other studies to formulate RNA nanoparticles [67]. For example, Qiu et al. spray dried PEG<sub>12</sub>KL4/mRNA complexes in a mannitol matrix and Zimmermann et al. used lactose and mannitol as matrices for siRNA lipid nanoparticles [14, 117]. Hence, using lactose and mannitol was expected to produce a stable formulation with the desired properties.

### 6.2.2.1. Cytotoxicity of Mannitol and Lactose

Lactose and mannitol are approved for inhalation by the FDA [85]. However, to make sure, that both excipients do not have any unspecific effects on the model cells, which could negatively influence the transfection experiments, the concentration dependent cell viability of Calu-3 and A549 cells was analysed. Prior to performing the CellTiter-Glo assay, the Calu-3 and A549 cells were treated analogously to the incubation periods and media during the transfection assay. At first glance, both excipients seem to have a slightly higher negative effect on A549 cells than on Calu-3 cells (Figure 6.13).

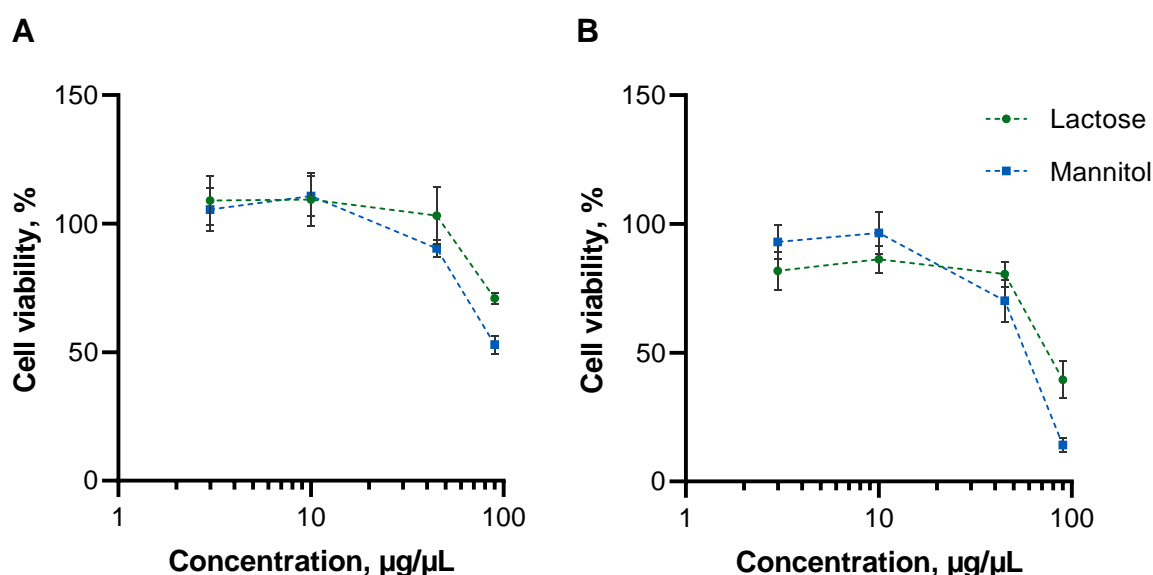


Figure 6.13: Concentration dependent cytotoxicity of lactose and mannitol on Calu-3 (A) and A549 cells (B) after treatment for 5 h, using the CellTiter-Glo assay.  $n = 3$ , symbols show mean, error bars show standard deviation.

This indicates a higher sensitivity of A549 in comparison to Calu-3 cells, which was also found for DOTAP:DOPE liposomes (Chapter 6.1.1.1) and can be explained by the fact that Calu-3 cells produce mucus, which acts as a protective layer [60, 100]. In general, it appeared that mannitol impacted cell viability slightly more than lactose for both cell lines. This observation was also made by Trenkel who performed a slug mucosal irritation assays using both excipients [137]. This assay bases on the correlation between the irritative effects of excipients on slugs and the human mucosa. Therefore, it is a different approach to assess the influence of excipient on human cells but leads to transferable results. For the Calu-3 cells Scherließ found an LC50 value of 190 µg/µL after treatment with lactose for 4 h [138]. This aligns well with the results of the present experiment as the highest used concentration, 100 µg/µL, still shows a cell viability above 50%.

Overall, in the range below 10 µg/µL, both excipients did not show any negative impact on the cell viability of Calu-3 and A549 cells. Moreover, Lactose concentrations below 45 µg/µL did not reduce cell viability significantly ( $p > 0.05$ ) for both cell lines. In contrast, mannitol caused a highly significant reduction ( $p < 0.001$ ) in cell viability when mannitol concentration exceeded 10 µg/µL for both cell lines, but the cell viability did not decrease below 50%. For optimal performance of the transfection assay, it was concluded to keep the concentrations of lactose and mannitol below 10 µg/µL.

### 6.2.2.2. Physicochemical Characterisation of mRNA Lipoplexes in the Presence of a Matrix Material

Inhalable particles of both excipients dissolve readily and release their cargo [14]. In this study, the cargo of those microparticles were incorporated mRNA lipoplexes of a particle size in the nanometre range. In Chapter 6.1.2 mRNA lipoplexes were successfully developed with a z-average around 200 nm and a satisfactory transfection efficiency. In this section of the study, the z-average, PDI and zeta potential were characterised after the addition of lactose or mannitol. As lactose and mannitol should be fully dissolved and have no influence on the lipoplexes, no differences in z-average, PDI and zeta potential were expected. As anticipated, the PDI did not change significantly ( $p > 0.05$ ) after the addition of lactose or mannitol (Figure 6.14).

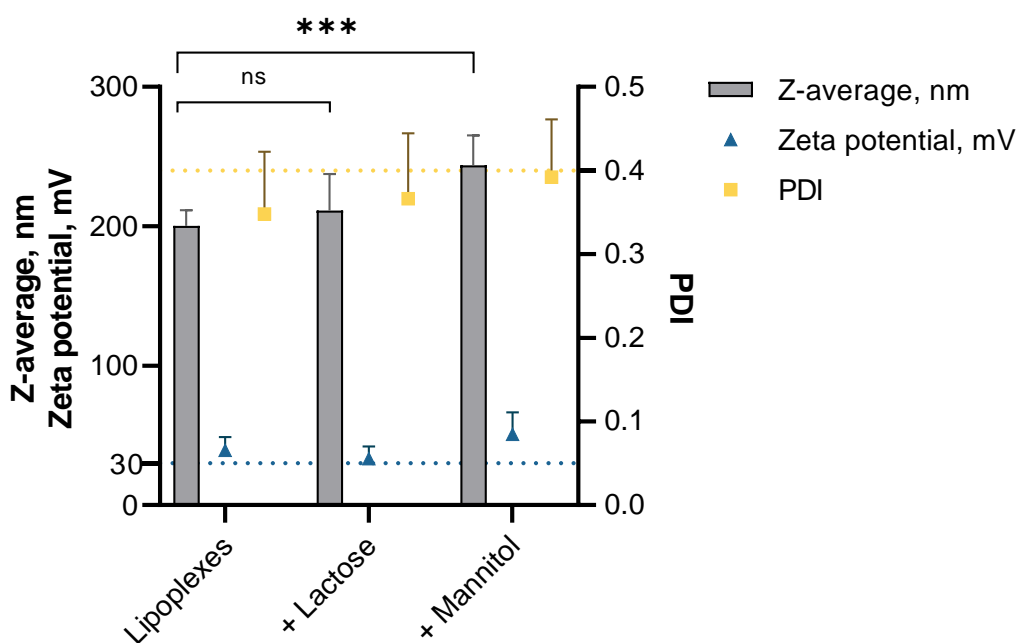


Figure 6.14: Z-average, PDI and zeta potential of lipoplexes with and without added lactose or mannitol. The blue line indicates the lower end of the desired zeta potential range, while the yellow line displays the upper limit for a favourable PDI.  $n = 3$ , bars or symbols show mean, error bars show standard deviation, *ns* = not significant,  $***p < 0.001$ .

The zeta potential increased slightly after the addition of mannitol, while lactose did not cause any change in zeta potential. However, a significant ( $p < 0.001$ ) increase in z-average from  $200 \pm 11$  nm to  $243 \pm 21$  nm was detected for the lipoplexes after adding mannitol. An increase in z-average by about 40 nm was also observed by Carrillo et al., after introducing mannitol to their plasmid DNA LNPs [139]. In contrast, the difference in the z-average after the addition of lactose was not significant ( $p > 0.05$ ). Nevertheless, mannitol molecules lead to a z-average above the range desired to facilitate transfection of 70 to 200 nm, set by Zhdanov et al. [48]. The transfection efficiency of the mRNA lipoplexes in presence of a matrix was subsequently determined in *in vitro* cell experiments.

### 6.2.2.3. Transfection Efficiency in the Presence of Matrix Material

*In vitro* transfection experiments were conducted to prove that the presence of lactose and mannitol has no negative effect on transfection efficiency. Both, A549 and Calu-3 cells revealed an increase of transfection efficiency in the presence of lactose or mannitol, as depicted in Figure 6.15.

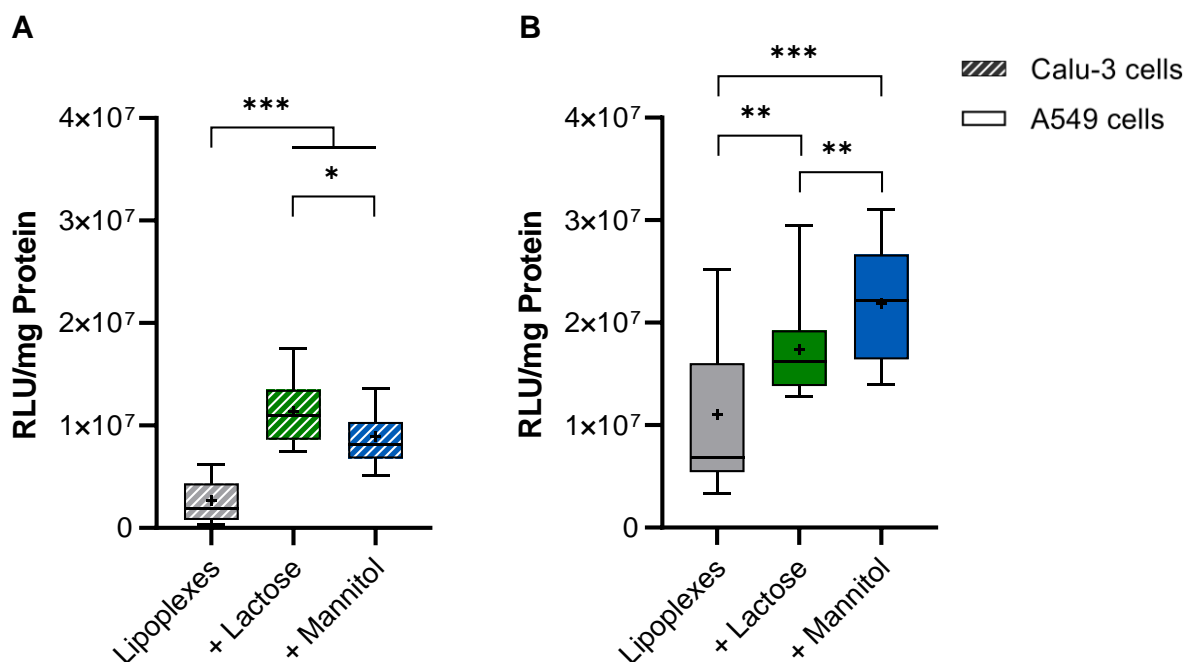


Figure 6.15: Luciferase mRNA transfection on Calu-3 cells (A) and A549 cells (B) of lipoplexes with and without lactose or mannitol.  $n = 3$ , for description of box plots see chapter methods, \* $p < 0.05$ ; \*\* $p < 0.01$ ; \*\*\* $p < 0.001$ .

In more detail, in Calu-3 cells the increase in transfection efficiency was highly significant ( $p < 0.001$ ) by both excipients, whereas in A549 cells lactose led to a very ( $p = 0.003$ ) and mannitol to a highly significant ( $p < 0.001$ ) improvement in transfection efficiency. Hence, mannitol caused a very significant increase ( $p = 0.008$ ) in transfection efficiency in comparison to lactose in A549 cells. In contrast, in Calu-3 cells, the presence of lactose resulted in a significantly higher ( $p = 0.017$ ) transfection efficiency than the addition of mannitol. Mannitol and lactose were previously used to formulate mRNA and siRNA, thus no negative impact was expected [14, 15]. In the present study, the transfection experiments revealed an improving effect, which was not mentioned in the referenced literature. The observed improvement in transfection efficiency in the presence of mannitol and lactose may be attributed to enhanced transfection into the cells or a change in culturing conditions that induced the cells to produce more protein. However, during spray drying, the mRNA lipoplexes undergo an interplay of factors, such as thermal stress and shear forces. The influence of these factors, depending on the matrix material, required investigation in spray drying experiments to determine the optimal matrix for the inhalable platform for mRNA therapeutics among the analysed matrices.

### 6.2.3. Spray Drying mRNA Lipoplexes in a Mannitol or Lactose Matrix

During spray drying, the interplay of two temperatures directly influences the product. The inlet temperature is set by the operator, while the outlet temperature depends on the amount of water that needs to be removed in a given time in the drying chamber and is therefore directly controlled by the pump rate. During drying, the product is cooled by the evaporating solvent. Since the outlet temperature is the maximum temperature a spray dried product is subjected to during the spray drying process, three outlet temperatures (50, 60, 70 °C) were tested to find the optimal one. The optimal temperature should maintain mRNA and lipoplex integrity, while producing a satisfactory yield of the spray dried powder. However, not only the outlet temperature has an influence on the integrity of mRNA and its lipoplex, but the matrix material as well. A matrix material that embeds the mRNA lipoplexes is necessary to both protect the mRNA lipoplexes and to ensure the generation of a manageable quantity of powder. In the previous chapter, the cytotoxicity, the physicochemical properties, and the transfection efficiency of mRNA lipoplexes in the presence of mannitol or lactose were tested. Moreover, pre-experimental screenings assessed the feasibility of various inlet and outlet temperatures to produce particles within the inhalable range of 1 to 5 µm. Those particles were successfully obtained with a total solid concentration of 4% in the spray drying dispersion, as described in detail in Chapter 5.1.3, using a two-fluid nozzle with a diameter of 1.4 mm, an inlet temperature of 120 °C, a drying air flow of 601 l/h and setting the aspirator to 100% (35 m<sup>3</sup>/h). This approach was adapted from Jüptner and Hellfritzsch [140, 141]. However, an unforeseen challenge arose during spray drying the lactose dispersion at an outlet temperature of 50°C. The resulting powder exhibited the immediate formation of sticky visible crystals on the walls of the collecting vessel, rendering it irrecoverable due to adhesion. The reason for this might be to high water content of the produced lactose powder. Therefore, only five of the spray dried formulation were available for characterisation.

To evaluate the spray dried formulations, the yield and properties of the spray dried powders were assessed. Utilising laser diffraction, the particle size distribution was analysed, while scanning electron microscopy was employed to examine the morphology. Moreover, the spray dried powder was dissolved to determine the particle size distribution and stability of the mRNA lipoplexes using dynamic light scattering. Importantly, the integrity of the mRNA and its lipoplexes was functionally verified through *in vitro* cell experiments. As a final step in this chapter, the Next Generation Impactor (NGI) was used to assess the aerodynamic performance of the powder. These experiments aimed to demonstrate a first proof of concept for the development of an inhalable dry powder platform for mRNA therapeutics.

### **6.2.3.1. Particle Morphology, Water Content and Particle Size Distribution**

Spray drying enables the production of particles with diverse shapes and sizes. The morphology of individual particles provides valuable insights into the properties of particle ensembles, like particle size distribution, shape, surface roughness and porosity. Analysing particle shape and morphology contributes to a deeper understanding of the characteristics exhibited by the bulk of particles. In this study, scanning electron microscopy was employed to visualise the size, shape and surface morphology of all five spray dried formulations. As displayed in Figure 6.16, the particles of all five spray dried formulations appeared as perfect spheres.

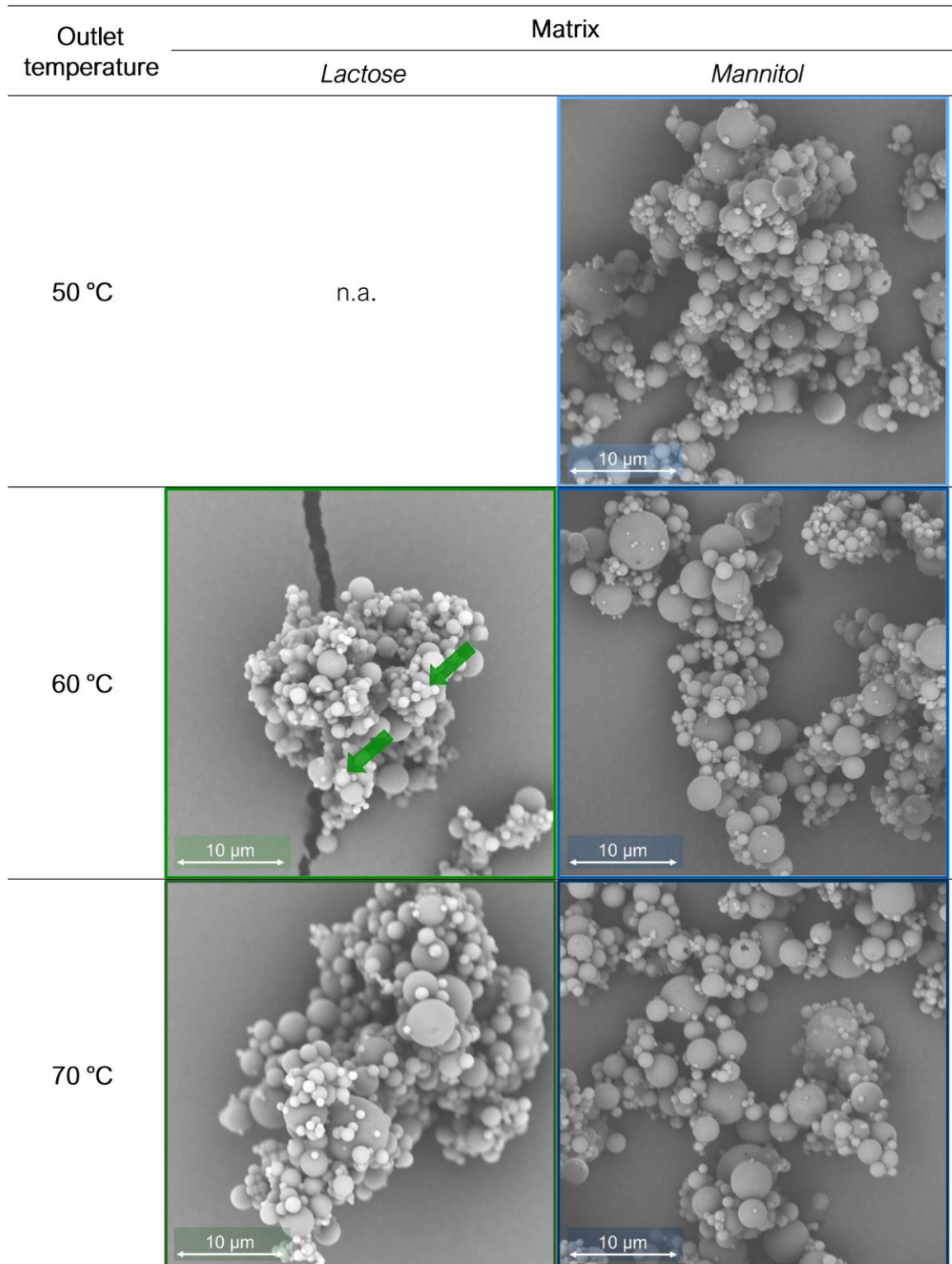


Figure 6.16: Representative scanning electron microscope images of all spray dried formulations (7500x magnification). The spray dried mRNA lipoplexes in lactose (left) and mannitol (right) matrix are shown from top to bottom with increasing outlet temperature. The green arrows mark solid bridges between particles.

Spherical shapes were anticipated, given that spray drying, in absence of shape-altering excipients, typically results in the formation of spheres [142]. However, the lactose-based formulation that was spray dried with an outlet temperature of 60 °C showed some particles which built solid bridges with one another. Those bridges are likely the result of high water content and recrystallisation after spray drying. High water content levels are known for amorphous sugars such as lactose and might also be the reason why it was not possible to recover any sample from the collecting vessel when spray drying lactose at an outlet temperature of 50 °C [143]. When spray dried at 60 °C and 70 °C outlet temperature, water contents of  $6.21 \pm 0.18\%$  and  $5.3 \pm 0.42\%$  were measured using a Karl-Fischer Titrator, respectively. These relatively high water content levels were expected as lactose is known to exhibit higher residual moisture levels after spray drying than mannitol. In fact, crystalline excipients such as mannitol can be spray dried with a water content below 0.5% [14, 67]. In this study, the water content of the mannitol samples was in the range of 0.5 to 1% and decreased with higher outlet temperature (Table 6.2).

Table 6.2: Water content and yield of all spray dried mRNA lipoplex formulations in lactose or mannitol matrix.  $n \geq 3$ , mean  $\pm$  standard deviation.

| Sample   |                  | Water content, % | Yield, %          |
|----------|------------------|------------------|-------------------|
| Matrix   | Outlet temp., °C |                  |                   |
| Mannitol | 50               | $0.98 \pm 0.11$  | $52.58 \pm 11.60$ |
|          | 60               | $0.62 \pm 0.06$  | $58.27 \pm 5.25$  |
|          | 70               | $0.59 \pm 0.03$  | $47.97 \pm 0.68$  |
| Lactose  | 60               | $6.21 \pm 0.18$  | $37.54 \pm 16.92$ |
|          | 70               | $5.30 \pm 0.42$  | $18.47 \pm 7.83$  |

The observation that low outlet temperatures correspond with an increase in water content is in agreement with current literature [144]. When handling costly materials, the yield plays a pivotal role for a production process and was expected to fall within the typical yield range between 50 and 70%, as specified by the manufacturer [131]. As displayed in Table 6.2, only two samples provided a yield over 50%. The highest yield,  $58.27 \pm 5.25\%$ , was achieved by spray drying the mannitol-based formulation at an outlet temperature of 60 °C.

For the other mannitol samples, an outlet temperature of 50 °C resulted in a yield of  $52.58 \pm 11.60\%$ , while at 70 °C, only  $47.97 \pm 0.68\%$  was recovered. Interestingly, spray drying the lactose-based formulation, an outlet temperature of 70 °C, produced the smallest yield of  $18.47 \pm 7.83\%$ , whereas at 60 °C  $37.54 \pm 16.92\%$  was recoverable. Zimmermann et al. spray dried their siRNA LNPs in lactose matrix at an inlet temperature of 100 °C and an outlet temperature of 62 °C [14]. They aimed for a water content level below 5% and achieved yields around 65% with a water content between 3.5 and 4.9%. The difference between the results of Zimmermann et al. and the present study may be attributed to the concentration of lipids in the spray drying solution. They used a lipid concentration over 100-fold higher, leading to a higher hydrophobicity of the produced particles. In the present study, it was observed for lactose that, in contrast the mannitol samples, more powder persisted in the cyclone, possibly due to the high water content of the lactose samples. In general, it was expected that decreasing water content would lead to less sticky particles and consequently to a diminished amount of remaining powder in the cyclone and a higher recoverable amount from the collecting vessel. However, it became apparent that the powders spray dried at 70 °C outlet temperature not only generated the smallest yields with the lowest water content, but also produced the smallest particles with x50 values of  $1.65 \pm 0.02 \mu\text{m}$  for the mannitol-based and  $1.32 \pm 0.17 \mu\text{m}$  for the lactose-based sample (Table 6.3, Figure 6.17 B, D).

Table 6.3: Characteristic values of particle size distributions of all spray dried mRNA lipoplex formulations in lactose or mannitol matrix assessed using laser diffraction.  $n = 3$ , mean  $\pm$  standard deviation.

| Matrix   | Sample           | x10, $\mu\text{m}$ | x50, $\mu\text{m}$ | x90, $\mu\text{m}$ | Span            |
|----------|------------------|--------------------|--------------------|--------------------|-----------------|
|          | Outlet temp., °C |                    |                    |                    |                 |
| Mannitol | 50               | $0.59 \pm 0.02$    | $1.79 \pm 0.13$    | $4.7 \pm 0.33$     | $2.30 \pm 0.05$ |
|          | 60               | $0.54 \pm 0.03$    | $1.76 \pm 0.12$    | $4.33 \pm 0.27$    | $2.16 \pm 0.08$ |
|          | 70               | $0.52 \pm 0.01$    | $1.65 \pm 0.02$    | $3.89 \pm 0.15$    | $2.04 \pm 0.07$ |
| Lactose  | 60               | $0.48 \pm 0.03$    | $1.88 \pm 0.23$    | $4.48 \pm 0.36$    | $2.16 \pm 0.34$ |
|          | 70               | $0.42 \pm 0.02$    | $1.32 \pm 0.17$    | $2.89 \pm 0.41$    | $1.87 \pm 0.10$ |

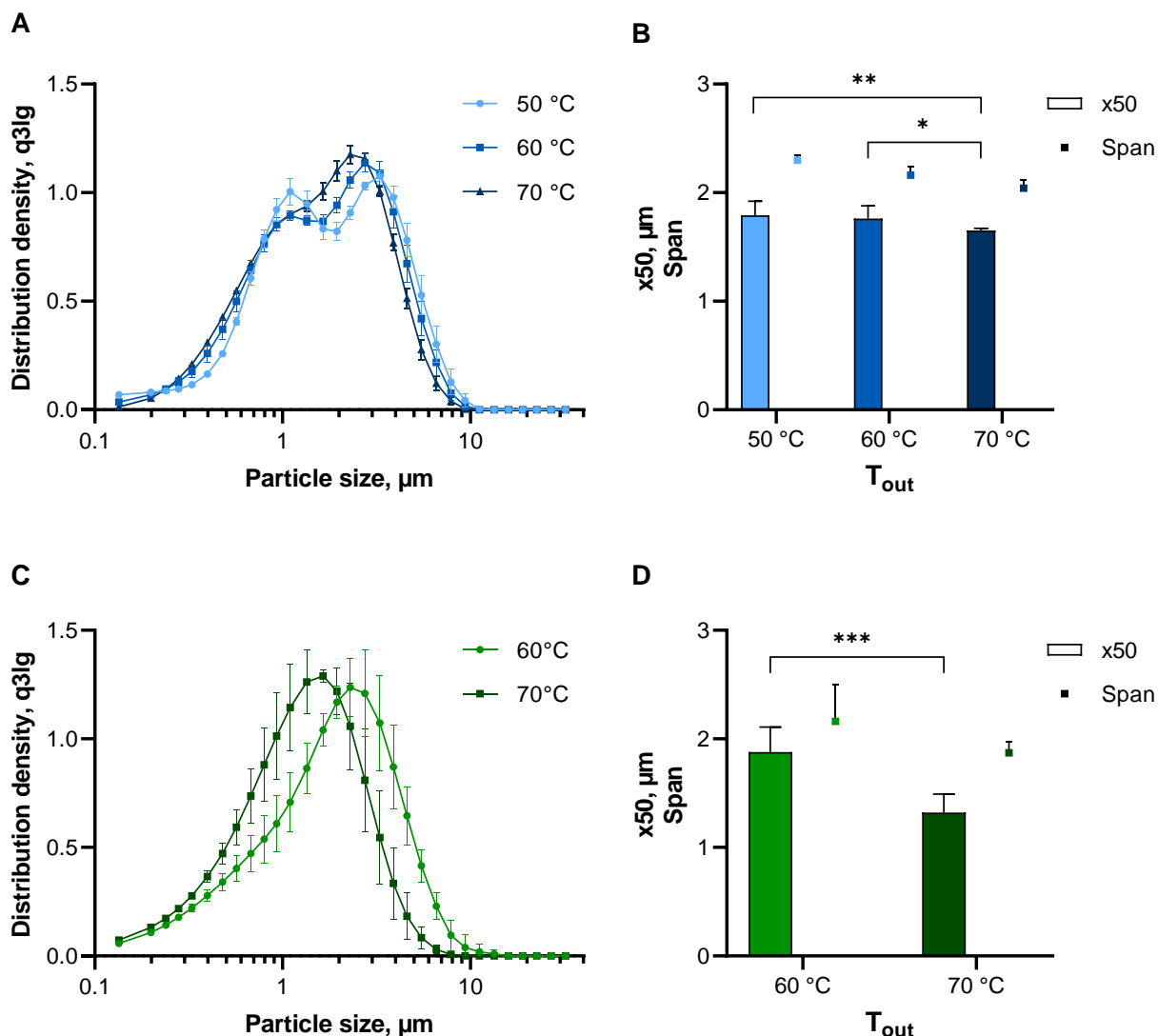


Figure 6.17: A, C: Particle size distributions of spray dried mRNA lipoplexes in lactose (A) and mannitol (C) matrix assessed using laser diffraction. B, D: x50 and span values of spray dried mRNA lipoplexes in lactose (B) and mannitol (D) matrix.  $n = 3$ , error bars show standard deviation. \* $p < 0.05$ ; \*\* $p < 0.01$ ; \*\*\* $p < 0.001$ .

These x50 values were significantly smaller than those of the powder spray dried at an outlet temperature of 60 °C (mannitol:  $p = 0.018$ , lactose:  $p < 0.001$ ) moving closer to the lower end of the inhalable size range.

These small particles might not have been sufficiently collected in the collecting vessel or were more electrostatic, impeding recovery. In agreement with the yield, the particle size of the spray dried powders was anticipated to increase with increasing outlet temperatures. During the spray drying process, droplets are sprayed into the drying chamber and exposed to heat. As described in more detail in Chapter 3.3, these droplets begin to dry on their surface, leading to diffusion of the dried material toward the inside of the particle. Once the solvent is completely evaporated, the shape and size of the particle are determined. The rate of this process increases with a higher drying temperature. Consequently, as the droplets are exposed to more heat, the materials in the droplet solidify sooner along their diffusion path, resulting in larger

particles [145]. Examining the particle size distributions closer, the lactose-based samples exhibit a monomodal pattern, with the sample dried at an outlet temperature of 70 °C displaying a lower span value than those dried at 60 °C (Figure 6.17 C, D; Table 6.3). A similar trend is observed for the mannitol-based samples, as the lowest outlet temperature resulted in the highest span value (Figure 6.17 B). The span value signifies the width of the distribution, the smaller the span value the narrower the particle size distribution.

Interestingly, the span values of the samples of both excipients are the same for an outlet temperature of 60 °C. For 70°C, however, the span value of the lactose-based samples is smaller than that of the mannitol-based sample indicating a broader particle size distribution for mannitol. Moreover, in contrast to the lactose-based samples, the mannitol-based samples exhibited a small shoulder, indicating a less monomodal particle size distribution (Figure 6.17 A).

Conclusively, particles with a geometric diameter of less than 5 µm with similar span values were successfully generated using both matrices. This diameter was targeted because particles intended for lung delivery must be able to pass through the respiratory system [69]. However, it is important to note that the geometric diameter and aerodynamic diameter are two distinct measures. Therefore, in a subsequent step, the aerodynamic performance of the spray dried powder had to be evaluated in Chapter 6.2.3.4.

### 6.2.3.2. Physicochemical Characterisation of Spray Dried mRNA Lipoplexes

A dry powder formulation that deposits in the lungs has to dissolve rapidly to release its cargo. In this study, mRNA lipoplexes are the load that is transported by a lactose or mannitol matrix. To mimic the process, the spray dried powder was reconstituted. While the mannitol or lactose matrix dissolved completely and was not detectable using DLS, the mRNA lipoplexes solubilised and were characterised for their z-average and zeta potential. After solubilisation the aim z-average was set to 70 to 200 nm, which allows efficient transfection [48]. As previously described, when measuring the z-average of nanoparticles, the polydispersity index (PDI) is an important parameter and was aimed to be  $< 0.4$ . Considering the spray drying subjects the mRNA lipoplexes to several stress factors, it was crucial to determine how the particle size and zeta potential of the mRNA lipoplexes changed after spray drying and reconstitution. Thus, the spray dried samples were compared to the not spray dried control samples. The not spray dried dispersions exhibited a z-average of 211 nm for the lactose and 244 nm mannitol mRNA lipoplex dispersion (Figure 6.18).

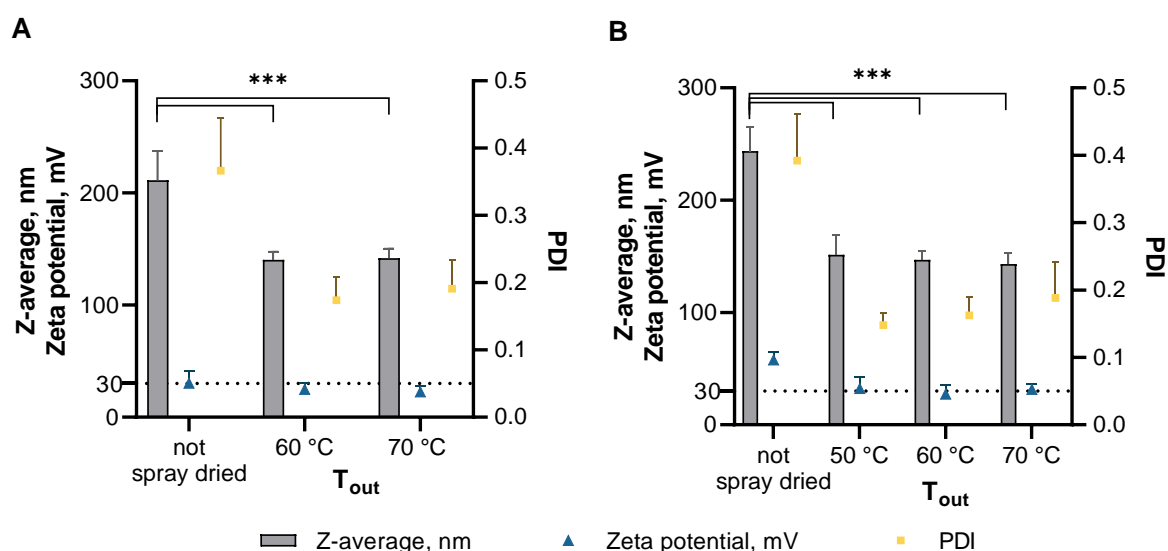


Figure 6.18: Z-average, zetapotential and PDI of not spray dried RNA lipoplexes and spray dried mRNA lipoplexes in lactose (A) or mannitol (B) matrix at the respective outlet temperatures ( $T_{out}$ ) after redispersion in water.  $n = 3$ , bars or symbols show mean, error bars show standard deviation, \*\*\* $p < 0.001$ .

The zeta potential of 30.4 mV for the lactose and 57.9 mV for the mannitol formulation suggested highly stable nanoparticles [106]. For all redispersed spray dried mRNA lipoplexes a z-average between 140 and 150 nm was measured. This measured z-average was significantly lower (all  $p < 0.001$ ) than the z-averages of both not spray dried dispersions. The PDI was measured to be lower than 0.4 for the not spray dried samples and lower than 0.3 for the reconstituted samples, indicating moderately polydisperse samples [106]. Qiu et al. also observed a slight reduction in hydrodynamic diameter after reconstitution of their PEG<sub>12</sub>KL4/mRNA complexes [117]. The significant differences in z-average between the not

spray dried and the spray dried samples of about 70 nm for lipoplexes in lactose matrix and 90 nm in mannitol matrix might be due to the shorter rehydration time after redispersion compared to the not spray dried control.

In further experiments measuring the z-average in the time after reconstitution, a trend of increasing z-average was observed with an increasing time frame after reconstitution. As depicted in Figure 6.19, both matrices spray dried at an outlet temperature of 60 °C exhibited a significant difference ( $p < 0.001$ ) 8 h after reconstitution.

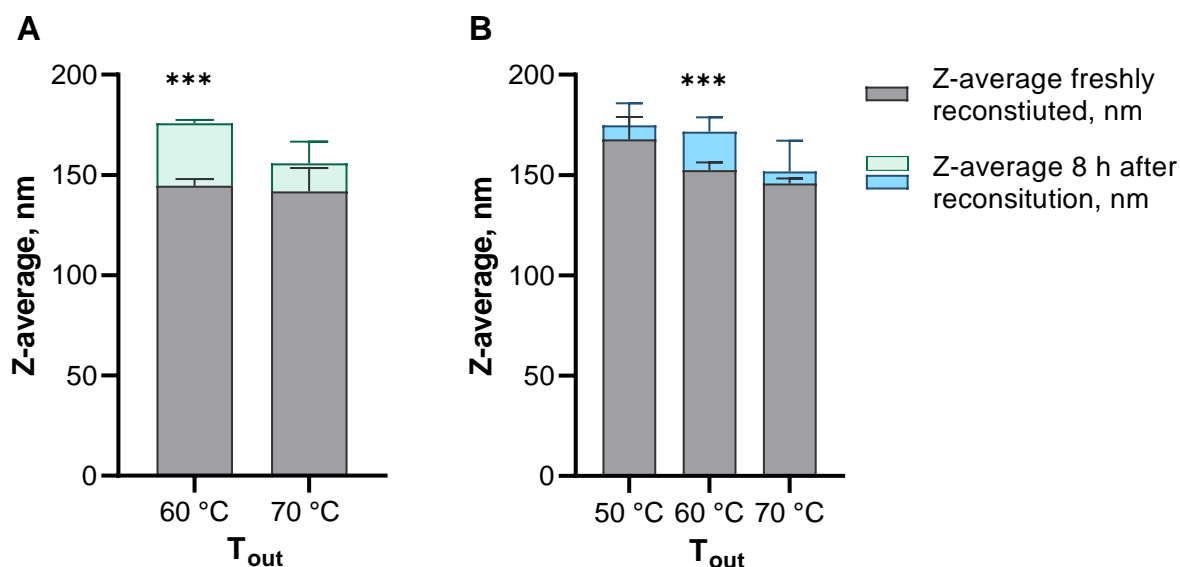


Figure 6.19: Z-average of spray dried mRNA lipoplexes in lactose (A) and mannitol (B) matrix at the indicated outlet temperatures. All PDIs were  $< 0.3$ .  $n = 3$ , error bars show standard deviation, \*\*\* $p < 0.001$ .

This difference was 31 nm for the lipoplexes in lactose matrix and 19 nm for mannitol, and it aligned with the difference observed by Qiu et al. between their freshly prepared and reconstituted spray dried PEG12KL4/mRNA complexes [117]. Nonetheless, considering the time frame in which the lipoplexes solubilise in the lungs and the time of transfection in *in vitro* cell experiments (Chapter 6.2.3.3), the z-average measured directly after redispersion seems to be the most relevant.

The z-average of the freshly reconstituted mRNA lipoplexes of both matrices and spray dried at any outlet temperature fell within the range established by Zhdanov et al. and Zimmermann et al. (Figure 6.18) [14, 48]. Additionally, the zeta potentials of around 30 mV for all reconstituted mRNA lipoplexes indicated stable nanoparticles [106]. Similar zeta potentials were also reported by Qiu et al. and Zimmermann et al. [14, 117]. Upon determining that the z-averages and zeta potentials of the reconstituted spray dried mRNA lipoplexes met the specified range, subsequently *in vitro* cell experiments were conducted to assess the integrity of the spray dried lipoplexes.

### 6.2.3.3. Transfection Efficiency of mRNA Lipoplexes after Spray Drying

After assessing the physical properties of the spray dried powder in terms of morphology, particle size distribution and the size and stability of the reconstituted mRNA lipoplexes, the most crucial property remaining to be evaluated is the biological activity of the mRNA lipoplexes. The integrity of both the mRNA and its lipoplex is crucial to ensure efficient transfection into the cell and satisfactory translation to the encoded protein.

Since mRNA lipoplexes are subjected to thermal stress and shear forces, the mRNA and its lipoplex is at risk of being damaged during spray drying. A highly threatening stress factor is the heat encountered during the drying process, where the outlet temperature represents the maximum temperature to which the mRNA lipoplexes are exposed [38, 81]. In order to determine the optimal spray drying conditions, three increasing outlet temperatures were tested, with the inlet temperature set to 120 °C. To verify the integrity of the spray dried mRNA lipoplexes, the spray dried powder was reconstituted and tested on the lung carcinoma cell lines Calu-3 and A549. As displayed in Figure 6.20, the transfection efficiency of the lactose-based lipoplex powders differs significantly ( $p < 0.001$ ) between the two cell lines.

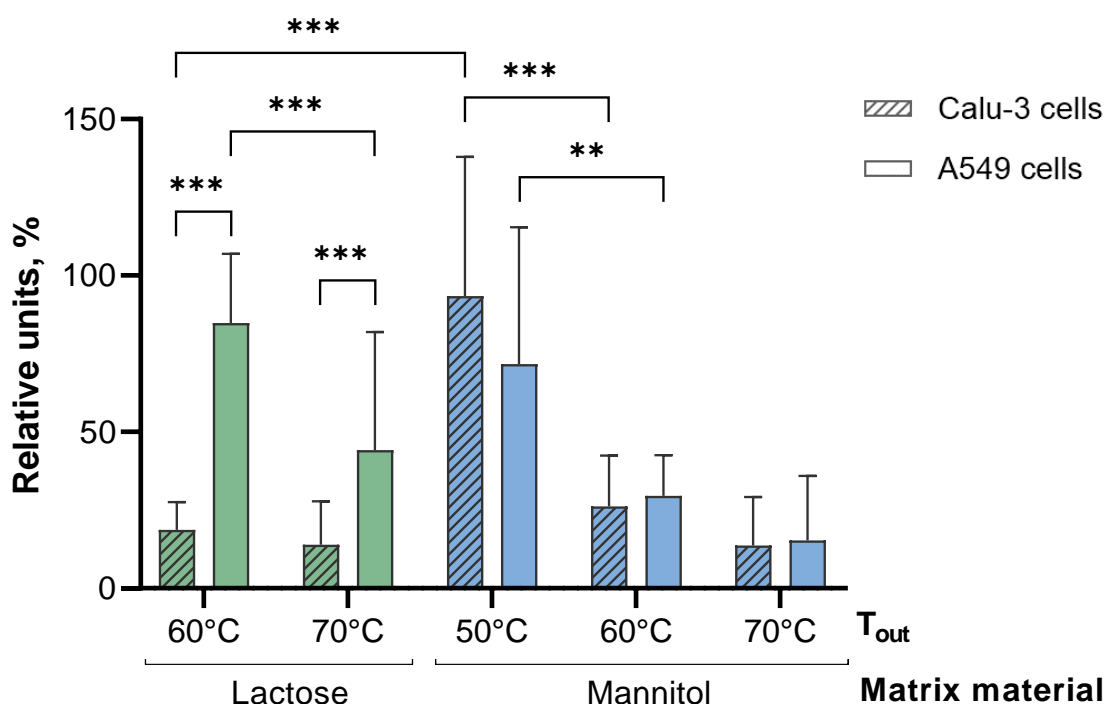


Figure 6.20: Transfection efficiency of mRNA lipoplexes in lactose (green) and mannitol (blue) matrix into Calu-3 and A549 cells after spray drying at outlet temperatures of 50, 60 or 70 °C. Relative units were calculated from luminescence in RLU/mg protein of the sample normalised to the signal of not spray dried lipoplexes. A value of 100% indicates a transfection efficiency as high as the not spray dried control.  $n = 3$ , bars show mean, error bars show standard deviation,  $**p < 0.01$ ;  $***p < 0.001$ .

The A549 cell line showed a significantly higher ( $p < 0.001$ ) transfection efficiency for both outlet temperatures than the Calu-3 cells. The transfection efficiency of spray dried mRNA lipoplexes in lactose matrix in A549 cells was significantly higher ( $p < 0.001$ ) for an outlet temperature of 60 °C than of 70 °C. In comparison, the transfection efficiency in Calu-3 cells did not differ significantly ( $p > 0.05$ ) for both outlet temperatures. One could assume that this observation was due to the difference in transfectability of the two cell lines as described in Chapter 6.1.2. However, each signal was normalised to its not spray dried counterpart transfected into the same cell line. Therefore, it is reasonable to assume that the disparity between the two cell lines can be attributed to the interplay of Calu-3 cells, lactose, lipoplex and the spray drying process. The spray drying process might have led to a reaction between the mRNA, lipids and the reducing sugar lactose, making it more difficult for the lipoplexes to overcome the mucus layer of the Calu-3 cells after spray drying. In contrast, the A549 cells, lacking a mucus layer, still exhibited satisfactory transfection. This observation requires further investigation in a subsequent study. One effective approach could involve using fluorescence-tagged lipids that allow visual tracking of lipoplexes during the transfection process into the cells, such as the cellular uptake study of Qiu et al. [117].

The mannitol-based lipoplex powders displayed a consistent transfection efficiency for both cell lines, with a trend of a higher efficiency at lower outlet temperatures. At an outlet temperature of 50 °C, the Calu-3 cells showed a transfection efficiency of approximately 93%, while the A549 cells achieved about 72% compared to the not spray dried control. Moreover, there were significant differences observed between an outlet temperature of 50 °C and 60 °C for both cell lines (Calu-3 cells:  $p < 0.001$ , A549 cells:  $p = 0.007$ ). These findings align with the anticipation that lower outlet temperatures result in reduced thermal stress, ultimately leading to an increased transfection efficiency.

Upon comparing the two matrices, a significant difference was observed in the Calu-3 cells between the lowest investigated outlet temperatures. For lactose, an outlet temperature of 50 °C was not feasible, as the spray dried powder was stuck on the walls of the collecting vessel, rendering it unrecoverable. In contrast, a satisfactory yield was produced by spray drying the mannitol-based formulation at an outlet temperature of 50 °C. For this set up the mannitol matrix demonstrated a significant advantage ( $p < 0.001$ ) with a transfection efficiency of 93% of the not spray dried control, compared to 18.6% for lactose that was spray dried at an outlet temperature of 60 °C. In their study, Qiu et al. observed that there was no significant impact on transfection efficiency following the spray and freeze drying of their PEG12KL4/mRNA complexes [117]. In this work, I found a minimum loss of transfection efficiency of 7% in Calu-3 cells and 28% in A549 cells. This may be attributed to the differing composition of the transfecting agent, as Qiu et al. used a pegylated peptide, the PEG12KL4

to complex mRNA. However, the transfection efficiencies of 93% in Calu-3 cells and 72% in A549 cells following spray drying were deemed satisfactory for this platform formulation.

Considering this positive outcome and a yield of over 50% during spray drying, mannitol was selected as the matrix for mRNA lipoplexes and an outlet temperature of 50 °C for the spray drying process in the further formulation development. Having determined matrix material and critical process parameters, the next step involved characterising the aerodynamic performance of the resulting spray dried powder.

#### **6.2.3.4. Aerodynamic Characterisation of the Spray Dried mRNA Lipoplex Formulation in Mannitol Matrix**

After characterising all spray dried formulations with respect to their morphology, particle size distribution, as determined by laser diffraction, z-average and zeta potential following reconstitution, and the transfection efficiency of the mRNA lipoplexes, the mannitol-based formulation, spray dried at an outlet temperature of 50°C, was selected for aerodynamic characterisation and further optimisation.

The volume-based diameter which was assessed via laser diffraction allows a first impression of the particle size of inhalable formulations. A crucial parameter to characterise these formulations is the aerodynamic diameter. In order to reach the lungs, particles are considered to require an aerodynamic diameter between 1 and 5 µm [69]. To characterise the aerodynamic performance of the spray dried mRNA lipoplexes in the mannitol matrix the NGI in combination with the mouthpiece, the throat, the preseparator and an RS01 inhaler with low resistance were utilised. The RS01 inhaler, a capsule based inhaler, was selected to define the amount of powder delivered by weighing it into the capsules.

The deposition profile displayed in Figure 6.21 A revealed that approximately 22% of the powder was recovered from the capsules. This might be due to electrostatic interactions between the capsule and the inhaler, leading to an increased charge on the capsule surface, which hinders the formulations from exiting the capsule [146]. The fine particle fraction (FPF) is the fraction of powder with an aerodynamic diameter  $< 5 \mu\text{m}$  with respect to the recovered dose and was determined to be almost 35% (Figure 6.21 B).

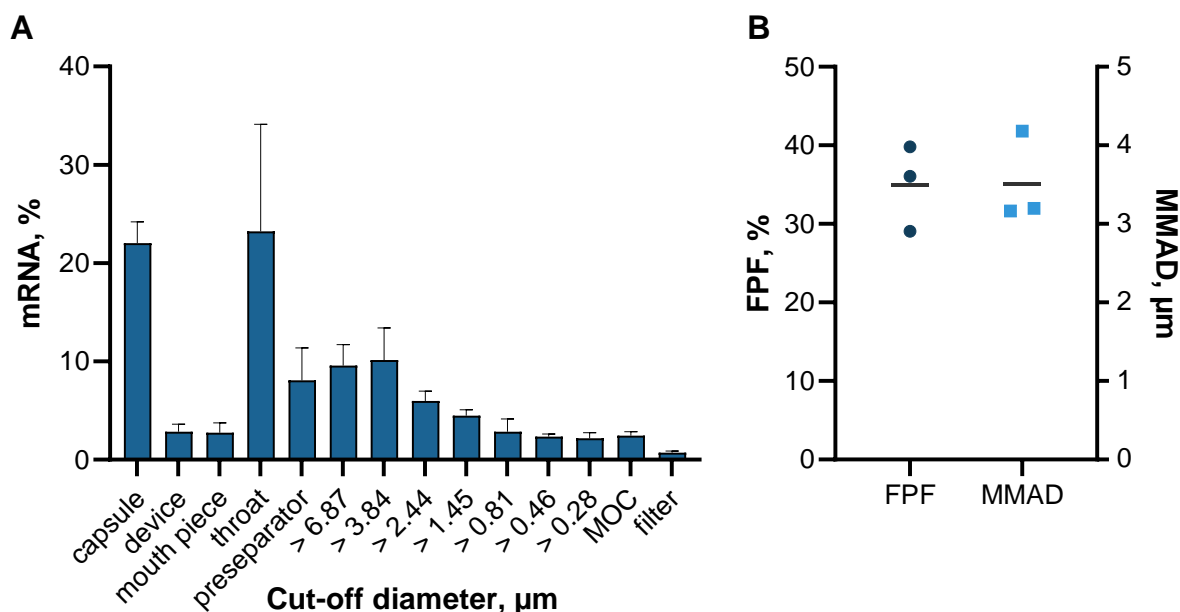


Figure 6.21: (A) Deposition profile of the mRNA lipoplex formulation in mannitol matrix spray dried at an outlet temperature of  $50^\circ\text{C}$  characterised using the NGI in combination with the capsule-based RS01 device. Bars show mean, error bars show standard deviation of 3 NGI measurements. (B) Fine Particle Fraction (FPF) and Mass Median Aerodynamic Diameter (MMAD), symbols show individual values and lines show mean of 3 NGI measurements, calculated using the COPLEY software.

In comparison, the laser diffraction measurement to determine the particle size distribution showed that 90% of the formulation were  $< 4.7 \mu\text{m}$ . The substantial disparity between the volume-based and the aerodynamic diameter underscores their fundamental difference. However, with an FPF of almost 35 % the formulation is comparable to commercially available formulations with glucocorticoids and bronchodilators, also applied by a capsule-based inhaler [94]. Moreover, the mass median aerodynamic diameter (MMAD) was calculated to be  $3.5 \mu\text{m}$ . The MMAD represents the cut-off particle size at which 50% of the aerosol's mass is smaller and the remaining 50% is larger than the specified parameter [129, 147]. For the spray dried mRNA lipoplex formulation that means 50% of the particles are expected to be smaller than  $3.5 \mu\text{m}$ .

In conclusion, to increase the amount of powder being released out of the capsules and to outperform the FPF of the commercially available formulations, optimisation of the formulation itself was necessary and is reported in Chapter 6.3.

#### 6.2.4. Conclusion on Spray Drying mRNA Lipoplexes

In conclusion, this chapter delved into the utilisation of spray drying for developing an inhalable dry powder formulation for mRNA lipoplexes. The investigation started with the significance of choosing appropriate equipment and parameters to ensure the preservation of material integrity and achieve desirable particle characteristics. The selection process for the spray dryer model involved the consideration of the Büchi Nano Spray Dryer B-90 and the Büchi Mini Spray Dryer B-290. Given the value and sensitivity of mRNA, and the objective to produce inhalable particles, the Büchi Mini Spray Dryer B-290 was chosen for its capability to generate small particles with high yields. The choice of tubing material was critical to maintain the integrity of mRNA lipoplexes during the pumping step. Silicone tubing, commonly used in biopharmaceutical production, exhibited a significant reduction in transfection efficiency. This led to the exploration of alternative tubing materials, with EPDM/PP tubing being identified as the tubing that preserved transfection efficiency comparable to the control while demonstrating superior robustness against shear forces during pumping.

The spray drying process involved the evaluation of lactose and mannitol as matrix materials to embed the mRNA lipoplexes. Both were chosen for their approval for inhalation by the FDA, and their ability to readily dissolve upon contact with lung fluid and releasing the incorporated mRNA lipoplexes. The study evaluated different temperatures (50, 60 and 70 °C) to determine the optimal outlet temperature. Mannitol demonstrated suitability for spray drying under all of these conditions, while lactose was not recoverable when spray dried at the lowest outlet temperature due to recrystallisation on the walls of the collecting vessel. The properties of the spray dried powders were comprehensively assessed, including particle morphology, particle size distribution and water content. Scanning electron microscopy revealed spherical particles for all formulations, with lactose-based particles spray dried at an outlet temperature of 60 °C showing some solid bridges likely due to high water content. The particle size distributions, measured via laser diffraction, provided an initial estimate of the number of particles within the inhalable range, as 90% of the particles of all formulations showed a geometric diameter less than 5 µm. Both matrices exhibited monomodal particle size distributions, with the mannitol-based formulation displaying a rather bimodal distribution at lower outlet temperatures.

Upon reconstitution of the spray dried mRNA lipoplexes, the z-average and zeta potential were within the desired range for efficient transfection. However, a slight reduction in particle size was observed compared to prior spray drying, potentially attributed to the forces during the spraying process or the shorter storage time after reconstitution. The analysis of transfection efficiency, crucial for evaluating the biological activity of mRNA lipoplexes, revealed notable differences influenced by matrix and outlet temperature. The observed trends of higher efficiency at lower outlet temperatures aligned with the expectations and highlighted the impact of thermal stress on transfection. In particular, the mannitol-based lipoplex powders exhibited

satisfactory transfection efficiency for both Calu-3 and A549 cell lines. Therefore, the mannitol-based mRNA lipoplexes spray dried at the lowest outlet temperature of 50 °C were chosen for the following aerodynamic assessment. The aerodynamic performance exhibited a MMAD of 3.5 µm falling well within the inhalable range and a FPF of almost 35%, which showed room for improvement. Moreover, a second and more severe optimisation necessity was identified, as approximately 22% of the formulation remained within the capsules, possibly due to electrostatic interactions between the capsules' inner surface and the spray dried powder.

In the pursuit of developing an inhalable dry powder platform for mRNA therapeutics, the project had reached a milestone. The insights gained from this chapter pave the way for continued advancements and innovations in the domain of inhalable formulations for nucleic acid-based therapies. The journey continues with the optimisation of the aerodynamic performance in the next chapter.

### **6.3. Optimising the Aerodynamic Performance**

A high amount of powder remaining in the capsules, may be due to high surface charge of the HPMC capsules when in contact with the device material. This high surface charge leads to electrostatic interactions between the capsule's inner surface and the formulation, hindering the formulation from exiting the capsule [146].

Two different strategies were applied to enhance particle detachment and aerodynamic performance: the introduction of sweeper crystals and increasing surface hydrophobicity through co-spray drying with L-leucine.

#### **6.3.1. Introduction of Sweeper Crystals**

One possibility to increase the detachment of the spray dried particles from the surface of the capsule is the use of so-called sweeper crystals. Sweeper crystals are coarse particles above the inhalable size range. They are meant to sweep the capsule's inner surface clean of remaining powder, allowing it to follow the air flow out of the capsule and therefore increase the delivered dose [77, 148]. The sweeper crystals itself are intended to deposit in the upper airways due to their large particle size.

In a previous study, Etschmann increased the emitted dose of a soft pellet formulation delivered by a capsule-based dry powder inhaler by almost 20% after addition of the lactose quality InhaLac 70 as sweeper crystals [78]. Therefore, in the present study, it was assumed that the mechanism would work analogously with the capsule-based RS01 device and the spray dried mRNA lipoplex formulation.

Following this theory, the spray dried powder from Chapter 6.2 was blended with sweeper crystals of different particle sizes. Hence, the lactose qualities InhaLac 70, 120, 180 and 251 were used in the present study to investigate the performance of different particle sizes as sweeper crystals. In a first step, the particle size of the different lactose qualities was characterised using laser diffraction. Subsequently, the sweeper crystal blends were prepared and analysed for their morphology via scanning electron microscopy and their aerodynamic performance utilising the NGI.

### 6.3.1.1. Particle Size Distribution of Sweeper Crystals and Morphology of Sweeper Crystal Blends

The lactose qualities InhaLac 70, 120, 180 and 251 were used as sweeper crystals and therefore examined using laser diffraction. According to manufacturer specifications InhaLac 251 comprised the smallest particles, followed by InhaLac 180, 120 and 70. While InhaLac 180 is a milled quality, the others are sieved lactose qualities. Hence, a broader particle size distribution and higher span value was expected especially for InhaLac 180. Figure 6.22 and Table 6.4 display the particle size distributions, x50 values and span values of the used lactose qualities, exhibiting the anticipated decrease in x50 values from InhaLac 70 with  $207.37 \pm 5.78 \mu\text{m}$  to InhaLac 251 with  $52.30 \pm 0.42 \mu\text{m}$ .

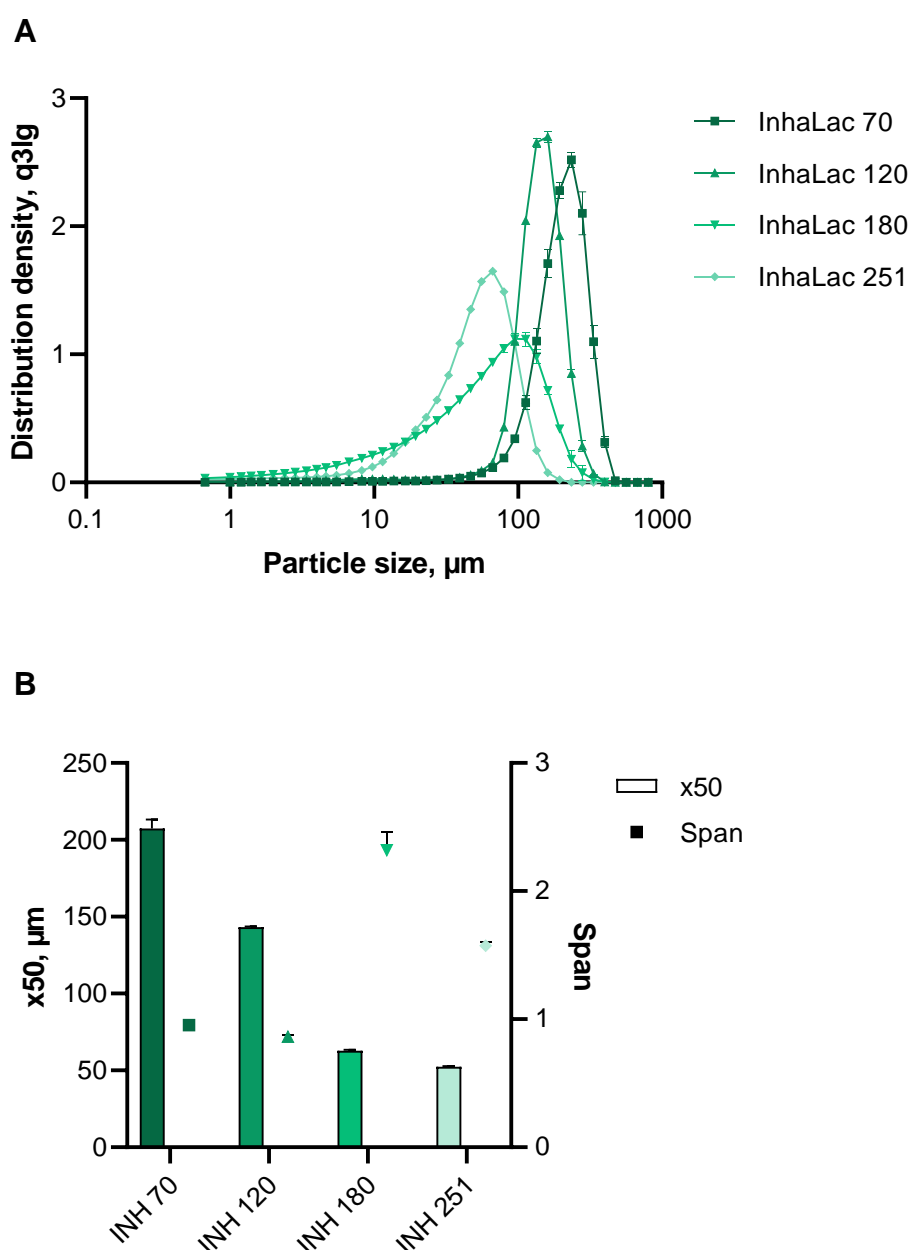


Figure 6.22: (A) Particle size distributions and (B) x50 and span values of the lactose qualities (InhaLac (INH) 70, 120, 180, 251) used as sweeper crystals.  $n = 3$ , error bars show standard deviation.

Table 6.4: Characteristic values of particle size distributions of the lactose qualities (InhaLac 70, 120, 180, 251) used as sweeper crystals using laser diffraction.  $n = 3$ , mean  $\pm$  standard deviation.

| Sample      | x10, $\mu\text{m}$ | x50, $\mu\text{m}$ | x90, $\mu\text{m}$ | Span            |
|-------------|--------------------|--------------------|--------------------|-----------------|
| InhaLac 70  | 114.48 $\pm$ 3.04  | 207.37 $\pm$ 5.78  | 312.43 $\pm$ 7.89  | 0.95 $\pm$ 0.01 |
| InhaLac 120 | 89.31 $\pm$ 0.16   | 143.31 $\pm$ 0.34  | 212.98 $\pm$ 1.69  | 0.86 $\pm$ 0.01 |
| InhaLac 180 | 8.72 $\pm$ 0.75    | 62.72 $\pm$ 0.78   | 154.01 $\pm$ 7.06  | 2.32 $\pm$ 0.14 |
| InhaLac 251 | 15.71 $\pm$ 1.01   | 52.30 $\pm$ 0.42   | 98.02 $\pm$ 0.08   | 1.57 $\pm$ 0.03 |

All InhaLac qualities were significantly (all  $p < 0.001$ ) different in their x50 values. Moreover, InhaLac 180 showed the highest span value with 2.32 and thus, the broadest particle size distribution of all used qualities. InhaLac 251 exhibited the next highest span value (1.57), as it was the smallest sieved quality. The other two sieved qualities, InhaLac 70 and 120, were previously used as sweeper crystals by Etschmann and had narrow particle size distributions with span values of 0.95 and 0.86, respectively [78]. The measured characteristics match well with the manufacturer specifications and showed significant differences in particle size [149–152]. Thus, the chosen lactose qualities were found suitable to investigate a wide spectrum of optimisation possibilities through the introduction of sweeper crystals. As Etschmann achieved the highest increase in delivered dose using InhaLac 70, which has the highest x50 value among the lactose qualities, it was anticipated that this quality would be most successful in increasing the detachment from the capsules.

Subsequently, sweeper crystal blends were prepared in a sweeper crystal to spray dried mannitol microparticles embedding mRNA lipoplexes ratio of 1+2, as this was the most successful combination used by Etschmann. The mixtures were blended for 10 min, sieved using a 300  $\mu\text{m}$  sieve and blended again for 10 min before being visualised via scanning electron microscopy (Figure 6.23) [78].

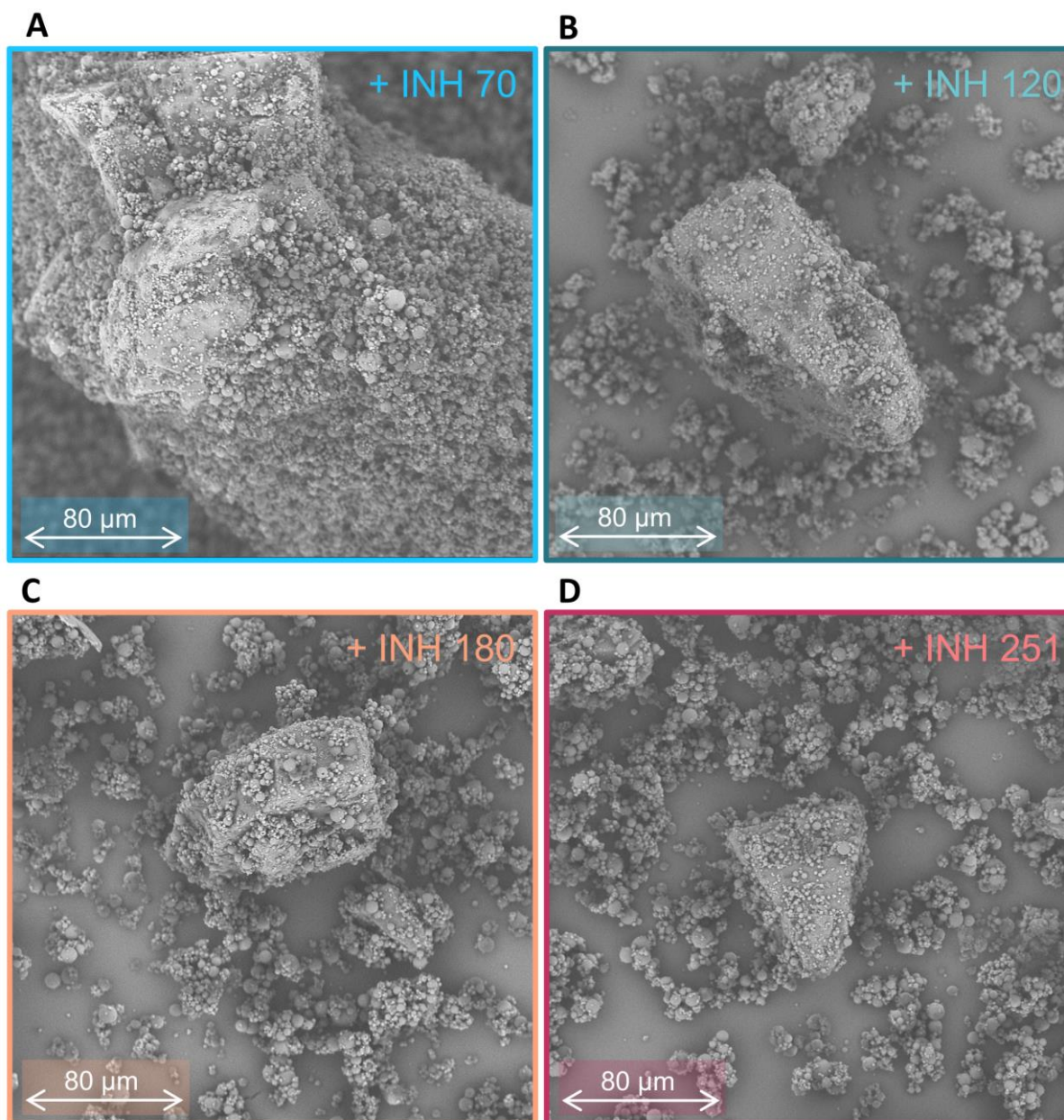


Figure 6.23: Representative scanning electron microscope images of all sweeper crystal formulations. The spray dried mRNA lipoplex formulation with mannitol matrix was blended with InhaLac (INH) 70 (A), InhaLac 120 (B), InhaLac 180 (C) or InhaLac 251 (D).

The examination of the images clearly displayed the differences in size of the sweeper crystals and the typical tomahawk shape of the lactose particles [153]. The spray dried powder, blended with the sweeper crystals, was identified as the smaller particles surrounding and covering the sweeper crystals. In contrast to an adhesive mixture, it was not especially aimed for attachment of the spray dried powder on the surface of the sweeper crystals. However, the InhaLac qualities are found to be densely covered. Whether the sweeper crystals in these blends could enhance detachment from the capsules and made more mRNA formulation available, was determined by aerodynamic performance (Chapter 6.3.1.2).

### 6.3.1.2. Aerodynamic Performance of Sweeper Crystal Formulations

The aerodynamic performance of the sweeper crystal formulations was characterised using the NGI, to determine whether the amount of powder exiting the capsules can be increased and the deposition profile would be altered. For the aerodynamic characterisation 30 mg of the sweeper crystal blends were filled in capsules and compared with the pure spray dried formulation analysed in Chapter 6.2.3.4 with 20 mg per capsule. The deposition profile, fine particle fraction (FPF) and mass median aerodynamic diameter (MMAD) are displayed in Figure 6.24.

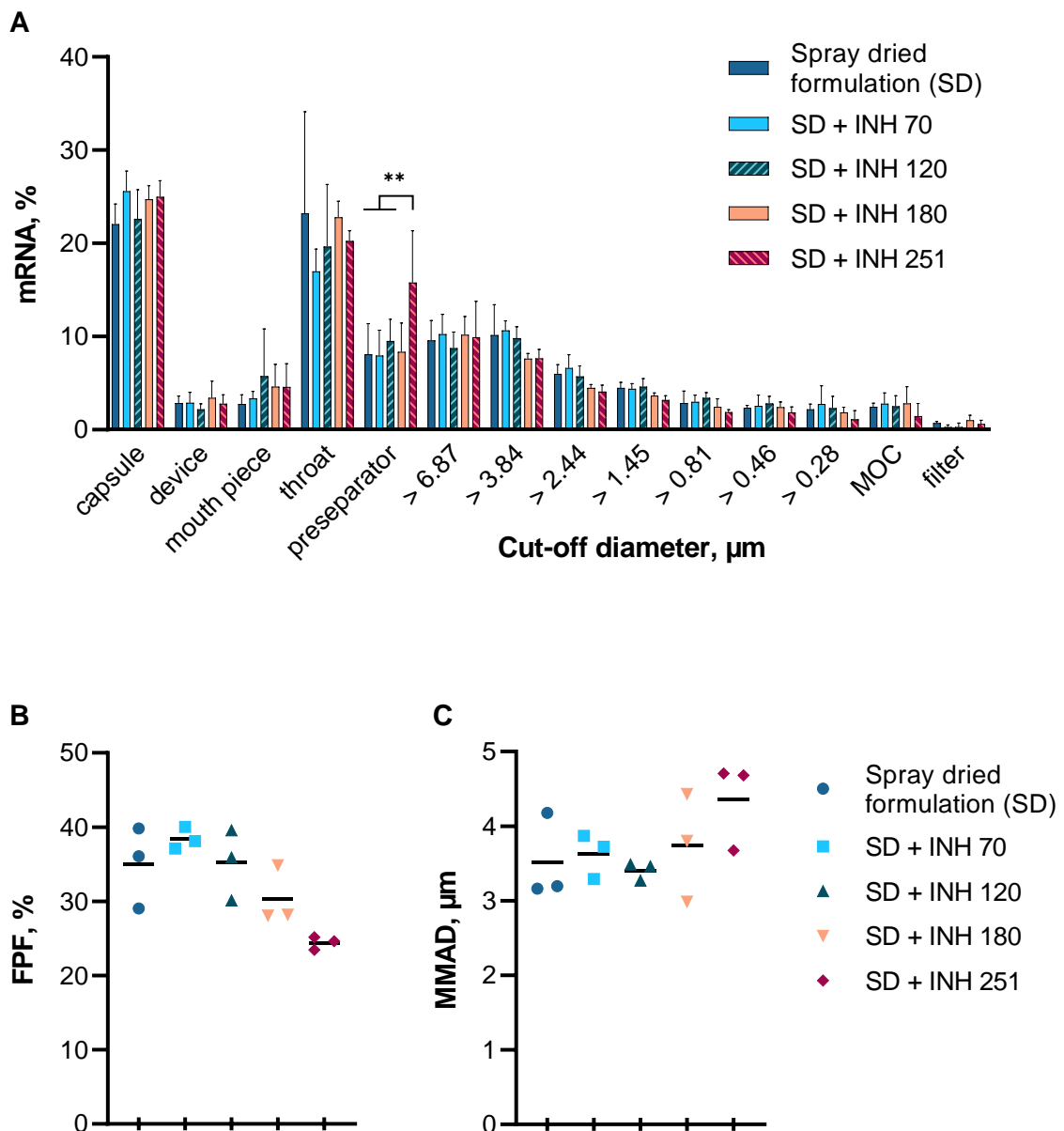


Figure 6.24: Aerodynamic performance of the spray dried formulation (SD) in comparison to all formulations with sweeper crystals (InhaLac 70, 120, 180, 251) using the NGI in combination with the RS01 inhaler, the mouthpiece, the throat and the preseparator. The deposition profiles of all formulations (A), the fine particle fractions (FPF) (B) and the mass median aerodynamic diameter (MMAD) (C) are displayed. Bars (in A) and lines (in B, C) show mean of 3 NGI measurements. Symbols (in B, C) display individual values of 3 NGI measurements. \*\* $p < 0.01$ .

The release of the particles from the capsules was not enhanced by any of the lactose qualities employed as sweeper crystals. Specifically, InhaLac 120 did not change the residue in the capsules ( $p > 0.05$ ), while the other used lactose qualities significantly increased the remaining powder in the capsules (InhaLac 70:  $p = 0.003$ , InhaLac 180:  $p = 0.007$ , InhaLac 251:  $p = 0.006$ ). There was also no positive effect on the FPF or MMAD. InhaLac 251 even showed a decreased FPF compared to the other formulations, possibly due to a strong attachment of the spray dried powder on the sweeper crystal surface. This was confirmed by the significantly higher deposition (all  $p < 0.01$ ) of mRNA from the InhaLac 251 sweeper crystal formulation in the preseparator compared to all the other formulations, as displayed in Figure 6.24 A. All sweeper crystals are intended to deposit in the upper airways, modelled by the throat and the preseparator, while the spray dried formulation, detached from the capsule's inner wall, should follow the airstream deeper into the lungs. However, a considerable amount of the spray dried formulation with addition of InhaLac 251, apparently did not detach from the sweeper crystals and thus deposited in the preseparator as well. All used lactose qualities are often employed in adhesive mixtures, a formulation for low dose inhalation, in which they are meant to carry the active pharmaceutical ingredient (API), facilitating delivery from the device. This is followed by detachment in the airstream, so that the API can reach the deeper parts of the lungs. When developing adhesive mixtures, the balance between detachment from and attachment to the carrier is often a challenge [69]. Besides these interactions, the inhaler utilised for the NGI measurements could be a reason why the introduction of sweeper was unsuccessful. The device used to deliver a dry powder for inhalation, has a substantial influence in the delivery success. Sweeper crystals were successfully employed in formulations that were delivered using the Twincer device [77, 78]. The Twincer was especially designed for high dose inhalation. By dispersing powder with multiple classifiers, it is able to deliver up to 50 mg of powder in one inhalation [76, 78]. In the present study, the capsule-based RS01 inhaler was used with a capsule filling of 30 mg for the sweeper crystal blends and 20 mg for the pure spray dried formulation. These filling masses were chosen to ensure an adequate amount of mRNA for quantification. Even though the powder blend occupied a maximum of one-third of the capsule volume and masses like 45 mg or 50 mg of spray dried powders were successfully used in other studies with capsule-based devices, the large volume in the capsules should not be overlooked as a possible reason for the lack of improvement by sweeper crystals [14, 154, 155].

All in all, the introduction of sweeper crystals in various sizes did not improve the detachment of the spray dried powder from the capsules. However, a noteworthy observation was that capsule filling was facilitated by the larger particles in the formulation in comparison to the pure spray dried powder. As the sweeper crystals approach was not successful in improving the

detachment from the capsules, the next approach was to increase surface hydrophobicity by co-spray drying with L-leucine.

### 6.3.2. Increasing Particle Surface Hydrophobicity

Spray drying offers the possibility to directly include additives in the particles, which introduce certain functionalities. These functionalities can allow humidity protection, stabilisation of the amorphous state or introduction of surface hydrophobicity [69]. Introducing hydrophobicity is commonly conducted by the addition of L-leucine. By adding L-leucine to the spray drying dispersion, particles with enhanced dispersibility can be produced within one step. L-leucine is an amino acid with a hydrophobic side chain. Because of this side chain, L-leucine is poorly soluble in water and crystallises early during spray drying causing an L-leucine enriched shell [69, 95, 156, 157]. This shell reduces surface energy, is thereby improving powder dispersion by reducing cohesive forces among particles and is acting as a dispersion enhancer [96, 97]. Chow et al. spray dried naked siRNA with mannitol and L-leucine. They raised the concern that L-leucine and siRNA could compete to stay on the particle surface due to their surface-active nature and low mobility, respectively. However, they successfully developed formulations with enhanced aerodynamic performance compared to formulations without L-leucine [97]. In the present study, mRNA was encapsulated in lipoplexes. This implies that the entire lipoplex could compete with L-leucine to stay on the particle surface, potentially resulting in a less hydrophobic surface and minimising the enhancing effect.

It was assumed that the spray dried lipoplex powder remained in the capsules due to adhesive forces like electrostatic interactions with the capsule's surface. Since L-leucine increases hydrophobicity and decreases surface energy, the next approach was to co-spray dry with L-leucine and to investigate whether this principle also applied for mRNA lipoplexes and resulted in a reduction of retained powder within the capsules.

In Chapter 6.2.2, spray drying experiments with mRNA lipoplexes in mannitol and lactose matrix were conducted to find the optimal outlet temperature that preserves mRNA lipoplex integrity. Spray drying in a lactose matrix at an outlet temperature of 50 °C raised challenges, as the spray dried powder immediately crystallised on the walls of the collecting vessel, rendering it irrecoverable. Interestingly, after adding L-leucine to the spray drying dispersion, it was possible to produce a recoverable amount of powder in a satisfactory yield also for this choice of parameters. Hence, lactose was reintroduced in the experiments once more.

As a first step in this part of the study, the cytotoxicity of L-leucine was assessed to preclude negative effects on the model cell lines. Furthermore, mRNA lipoplexes in an excipient-leucine-dispersion were physicochemically characterised and tested *in vitro* to ensure equal transfection compared to the samples without L-leucine. Subsequently, spray drying experiments were conducted and the produced powder was characterised in the solid and reconstituted state to compare the properties with those prior to spray drying. Finally, to reveal the detachment enhancing potency of L-leucine and to compare both matrices once again, the aerodynamic performance was assessed.

### 6.3.2.1. Physicochemical Properties and Transfection of mRNA Lipoplexes in Presence of Matrix Excipients and L-Leucine

Since L-leucine is an amino acid with a hydrophobic side chain and surface-active properties, it bears the potential of interacting with hydrophobic elements of the phospholipids DOTAP and DOPE. This interaction could interfere with the formation of lipoplexes and hence, with the transfection of mRNA lipoplexes *in vitro*. Therefore, the physicochemical properties and transfection efficiency of mRNA lipoplexes in the presence of matrix excipients and L-leucine were investigated.

#### 6.3.2.1.1. Cytotoxicity of L-Leucine

5% L-leucine, calculated from the solid content, was chosen to be added to the spray drying solution. This resulted in a concentration of 0.45  $\mu\text{g}/\mu\text{L}$  per well. Therefore, L-leucine concentrations in the range of 0.2 to 1.8  $\mu\text{g}/\mu\text{L}$  were evaluated. The assessment of the concentration dependent cytotoxicity of L-leucine exhibited no significant difference ( $p > 0.05$ ) between the two model cell lines, except for the lowest concentration (Figure 6.25).

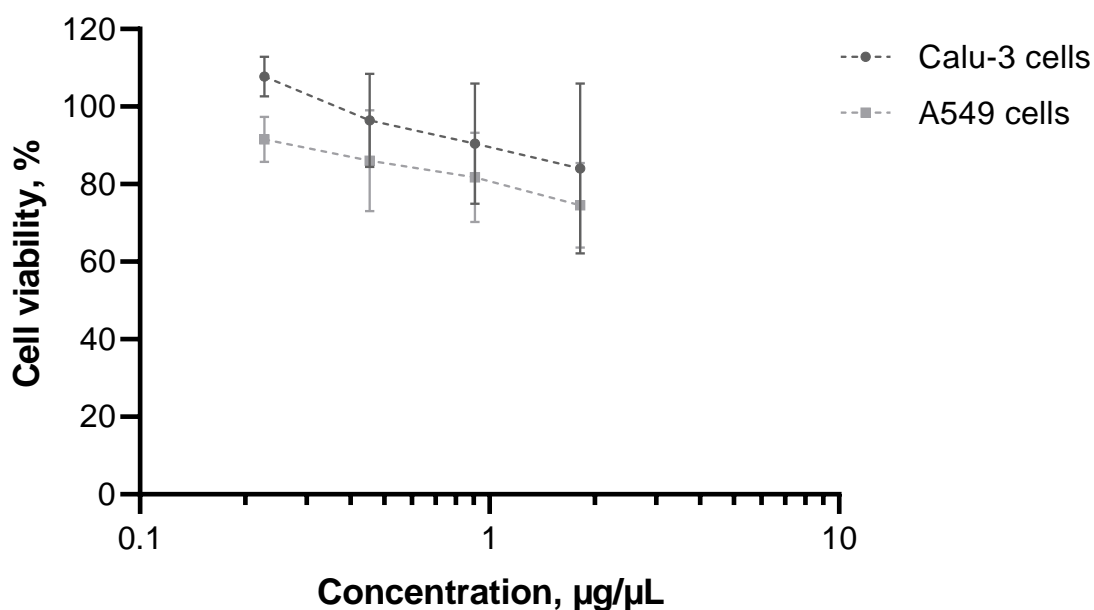


Figure 6.25: Concentration dependent cytotoxicity of L-leucine on Calu-3 and A549 cells after treatment for 5 h using the CellTiter-Glo Assay.  $n = 3$ , symbols show mean, error bars show standard deviation.

All concentrations tested ensured a cell viability above 70% and 0.45  $\mu\text{g}/\mu\text{L}$  per well was well tolerated by both cell lines. With cell viability assured, the next step was to analyse the lipoplex characteristics in the presence of L-leucine.

### 6.3.2.1.2. Physicochemical Characterisation of mRNA Lipoplexes in the Presence of Excipients and L-Leucine

In this section of the study, the physicochemical properties, the z-average, PDI and zeta potential of the mRNA lipoplexes in presence of L-leucine were assessed. It was not easy to predict whether the z-average and PDI would change after the introduction of L-leucine. Being a surface-active amino acid with a hydrophobic side chain, it was possible for L-leucine to interact with the lipids. This interaction could result in an increase or a reduction of both the z-average and the PDI. The zeta potential, however, was expected to stay similar to the samples without L-leucine due to its neutral properties. Upon examining the results, it was found that adding L-leucine to the lipoplex-excipient-dispersions did not significantly alter the z-average, PDI and zeta potential ( $p > 0.05$ ) (Figure 6.26).

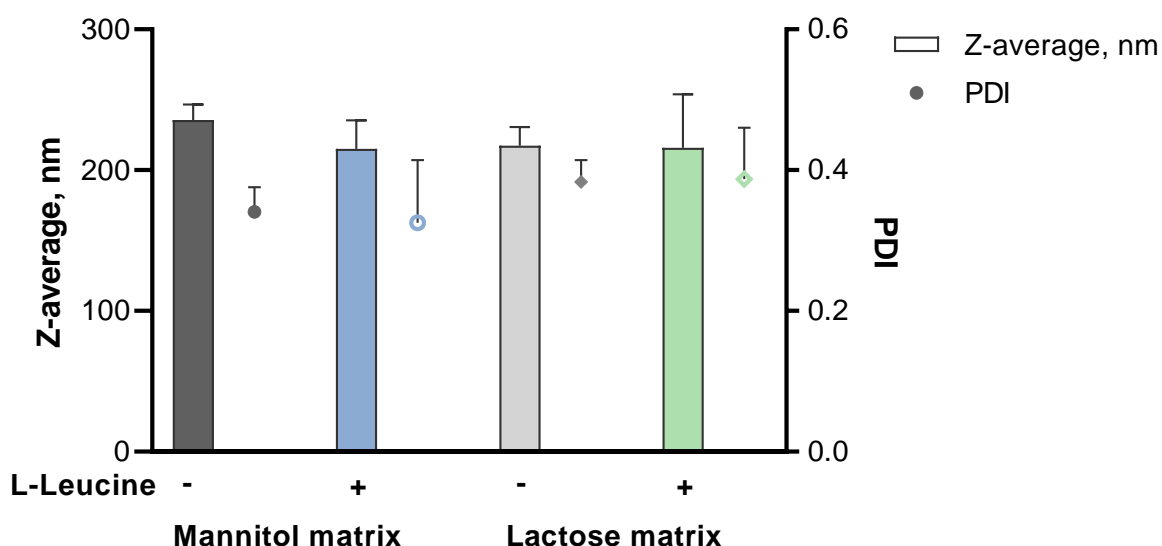


Figure 6.26: Z-average and PDI of mRNA lipoplexes in the presence of lactose or mannitol, with (+) or without (-) the addition of L-leucine.  $n = 3$ , error bars show standard deviation.

After introducing L-leucine, the z-average of all formulations ranged around 220 nm with a PDI lower than 0.4. These values were generally consistent with good transfectability as determined earlier in this study.

### 6.3.2.1.3. Transfection of mRNA Lipoplexes in the Presence of Excipients and L-Leucine

After ensuring that L-leucine has no negative effect on the formation of lipoplexes, the z-average, PDI and zeta potential, it was left to investigate whether the transfection into Calu-3 cells and A549 cells was influenced by the introduction of L-leucine. Since L-leucine was used in studies using siRNA without perturbing transfection, no negative influence was expected in the present study [97]. As previously observed and due to the mucus production of Calu-3 cells, the signals of Calu-3 cells were anticipated to be lower than those of A549 cells. Figure 6.27 compares the transfection efficiency of the lipoplex-excipient-dispersion with and without the addition of L-leucine.

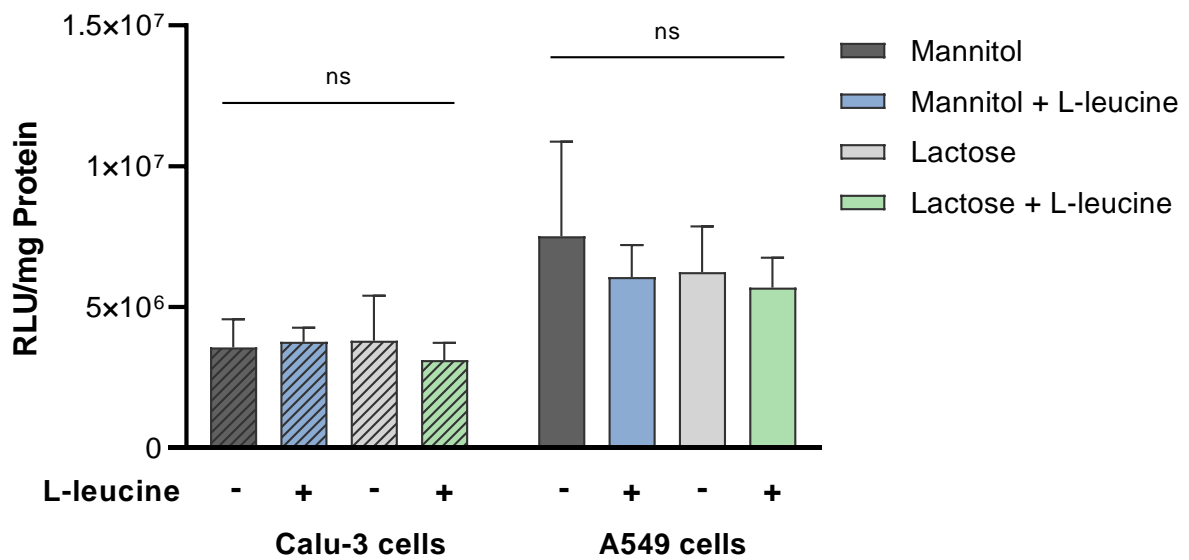


Figure 6.27: Transfection of mRNA lipoplexes in the presence of lactose or mannitol, with (+) or without (-) the addition of L-leucine into Calu-3 and A549 cells. Transfection efficiency was expressed as the mean value of relative light units normalised to total protein.  $n = 3$ , error bars show standard deviation, ns = not significant.

Upon comparing the samples within one cell line, no significant difference was found between both matrices with or without L-leucine ( $p > 0.05$ ). This demonstrates that the introduction of L-leucine does not affect the transfection efficiency of the mRNA lipoplexes in the respective matrix. Hence, spray drying experiments could follow.

### **6.3.2.2. Characterisation of mRNA Lipoplexes after Spray Drying in a Matrix with L-Leucine in the Solid and Reconstituted State**

During spray drying, additives can be directly included into the particles to modify functional properties, such as cohesion and flowability. This makes spray drying a very useful tool for tailoring inhalable dry powder formulations. For inhalation, the produced particles need to remain within the inhalable size range (1 to 5  $\mu\text{m}$ ) to reach the lungs [69]. Therefore, mRNA lipoplexes in a dispersion with mannitol or lactose and 5% L-leucine were spray dried using the same setup as utilised in Chapter 6.2. The mannitol samples containing L-leucine were related to the spray dried mannitol samples without L-leucine. Due to insufficient yield when spray drying the lactose-based formulation at an outlet temperature of 50 °C, the lactose samples were compared to the formulation spray dried at 60 °C. Since the integrity of the mRNA lipoplexes is the most important aspect for the pharmacological effect, the spray dried mRNA lipoplexes were physicochemically characterised (z-average, PDI, zeta potential) and *in vitro* cell experiments were conducted to functionally investigate the transfection efficiency. The assessment of particle size of the solid powder was performed using laser diffraction in a first step and was complemented by aerodynamic characterisation. Furthermore, scanning electron microscope images confirmed the measured particle size and visualised the shape of the particles.

### 6.3.2.2.1. Physicochemical Characterisation of mRNA Lipoplexes after Spray Drying in a Matrix with L-Leucine

The spray dried formulations were reconstituted and analysed for their z-average and PDI. After observing a decrease in z-average and PDI after spray drying the formulations without L-leucine in Chapter 6.2.3.2, this outcome was also expected after the addition of L-leucine. However, Tang et al., for instance, observed aggregation of their siRNA lipoplexes after freeze drying with L-leucine, which did not aggregate without L-leucine [158]. The results of the present experiment did not show any aggregation of the mRNA lipoplexes. The reconstituted mRNA lipoplexes with L-leucine exhibited a significant decrease in z-average and PDI for both matrices, indicating smaller and more monodisperse mRNA lipoplexes (Figure 6.28).

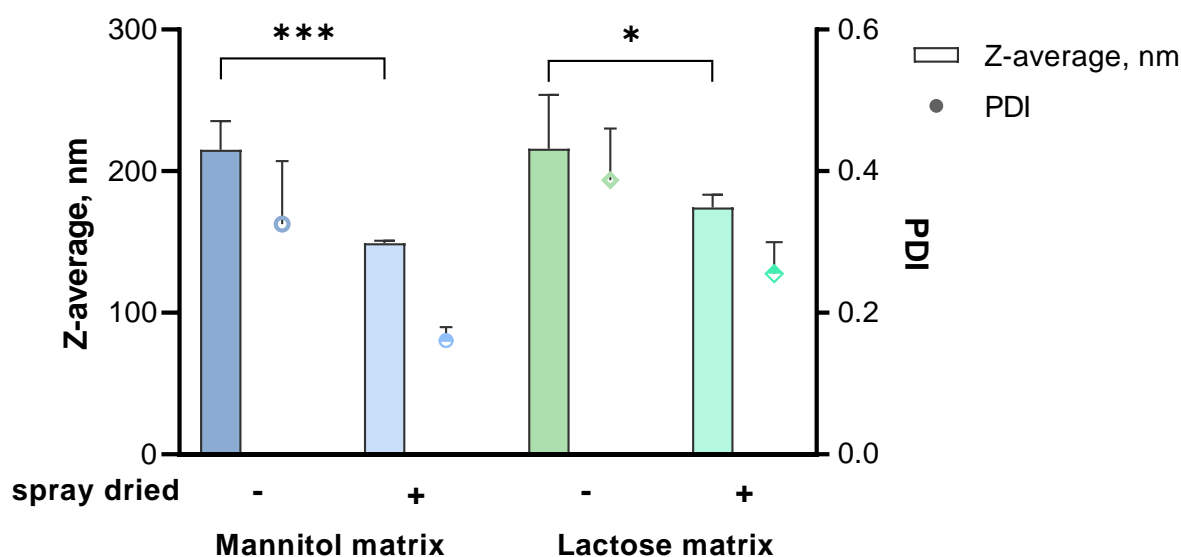


Figure 6.28: Z-average and PDI of mRNA lipoplexes in the presence of matrix material and L-leucine before (-) and after (+) spray drying.  $n = 3$ , error bars show standard deviation, \* $p < 0.05$ ; \*\*\* $p < 0.001$ .

The PDI of the mannitol matrix decreased significantly ( $p < 0.001$ ) from 0.325 before spray drying to 0.161 after spray drying. The decrease of PDI for the lactose-based formulation was also significant ( $p = 0.003$ ). The results for the z-averages showed a significant reduction ( $p < 0.001$ ) from  $215 \pm 20$  nm to  $149 \pm 2$  nm for the mannitol samples and from  $215 \pm 38$  nm to  $174 \pm 9$  nm ( $p = 0.026$ ) for the lactose-based formulations. Examining the mean z-average with standard deviation, a decrease in standard deviation was also clearly visible. A reason for that and the decrease of the PDI might be homogenisation forces during spraying with the two-fluid nozzle as described in Chapter 6.2.3.2. There, the reconstituted lactose dispersions exhibited an average decrease of 71 nm, while the mannitol dispersions showed a difference of 92 nm in z-average compared to the not spray dried samples. In the present experiment, with a decrease in z-average of 66 nm after spray drying, the mRNA lipoplexes spray dried in mannitol matrix also showed a higher difference than those in a lactose matrix with a difference

of 42 nm. Analogously to the spray dried mRNA lipoplexes without L-leucine, the z-average of the spray dried mRNA lipoplexes in the present experiment fell within the range set by Zhdanov et al. for efficient transfection [48]. In order to confirm that mRNA lipoplexes spray dried in a matrix with L-leucine still exhibit sufficient transfection efficiency, *in vitro* testing was conducted as the next step.

#### 6.3.2.2.2. Transfection Efficiency of mRNA Lipoplexes after Spray Drying in a Matrix with L-Leucine

Since spray drying subjects the mRNA lipoplexes to thermal stress and shear forces, it was important to analyse how L-leucine is influencing the integrity of mRNA lipoplexes during spray drying. Transfection experiments with not spray dried mRNA lipoplexes and both excipients did not show a decrease in transfection efficiency after the addition of L-leucine (Chapter 6.3.2.1.3). Hence, it was anticipated that spray drying the mannitol samples would not result in any differences either. In contrast to the mannitol samples, the L-leucine-lactose samples were compared to the lactose samples spray dried at an outlet temperature of 60 °C, due to the previously described recovery issues. Thus, an increase in transfection efficiency was expected for the lactose samples containing L-leucine, as the thermal stress is lower at an outlet temperature of 50 °C compared to 60 °C. The comparison of the transfection efficiencies of the formulations with and without L-leucine did not show a significant difference for the mannitol containing samples in both cell lines ( $p > 0.05$ ) (Figure 6.29).

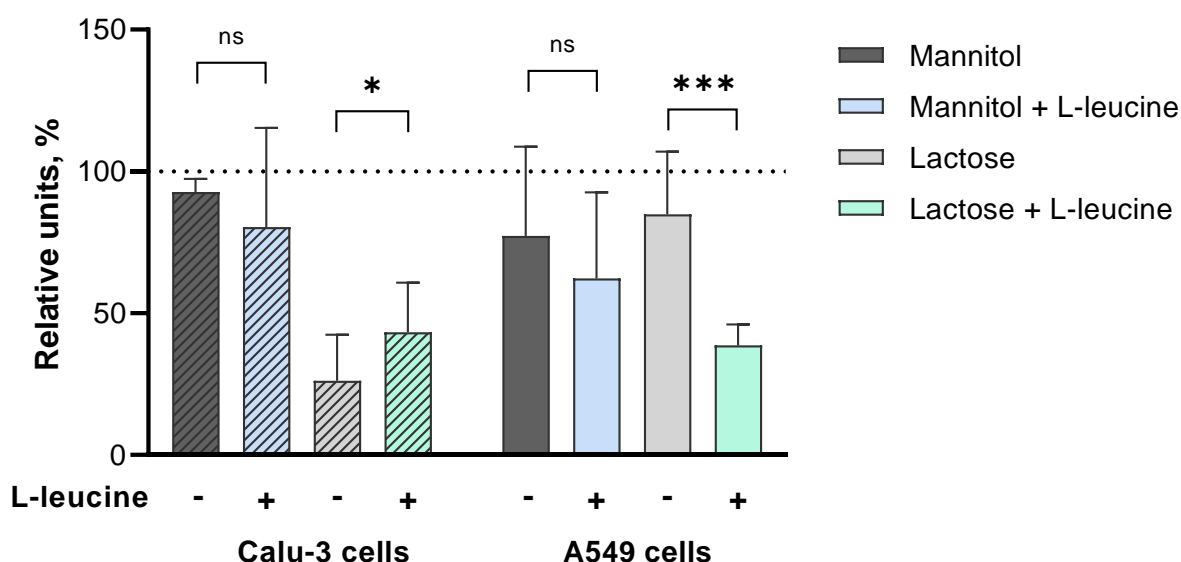


Figure 6.29: Transfection of spray dried mRNA lipoplexes in lactose or mannitol matrix, with or without the addition of L-leucine into Calu-3 and A549 cells. Relative units were calculated from luminescence in RLU/mg protein of sample normalised to the signal of not spray dried lipoplexes in the respective matrix without L-leucine. A value of 100% indicates a transfection efficiency as high as the not spray dried control.  $n = 3$ , error bars show standard deviation, ns = not significant,  $*p < 0.05$ ;  $***p < 0.001$ .

In contrast, the lactose-based samples revealed a significant difference in transfection efficiency after co-spray drying with L-leucine ( $p < 0.001$ ). Interestingly, in Calu-3 cells L-leucine increased the transfection efficiency significantly ( $p = 0.032$ ), while in A549 cells L-leucine resulted in a highly significant decrease ( $p < 0.001$ ). These results indicated once more that mannitol might be the better suited matrix. However, in order to fully evaluate the influence of L-leucine in the formulations spray dried in both matrices, the particle size distribution and aerodynamic performance of the formulations were compared in the next steps.

### 6.3.2.2.3. Particle Size Distribution, Water Content, Yield and Morphology

After the introduction of L-leucine, an increase of hydrophobicity and thus a decrease in water content and an increased yield was expected. The results of the water content measurements of the mannitol sample exhibited a reduction of water content to  $0.13 \pm 0.01\%$ , in contrast to  $0.98 \pm 0.11\%$  without L-leucine (Table 6.5).

Table 6.5: Water content and yield of the spray dried formulations in lactose or mannitol matrix, with (+) or without (-) the addition of L-leucine.  $n = 3$ , mean  $\pm$  standard deviation.

| Matrix   | Sample                 |           | Water content, % | Yield, %          |
|----------|------------------------|-----------|------------------|-------------------|
|          | Outlet temperature, °C | L-Leucine |                  |                   |
| Mannitol | 50                     | -         | $0.98 \pm 0.11$  | $52.58 \pm 11.60$ |
|          |                        | +         | $0.13 \pm 0.01$  | $70.57 \pm 2.18$  |
| Lactose  | 60                     | -         | $6.21 \pm 0.18$  | $37.54 \pm 16.92$ |
|          | 50                     | +         | $7.08 \pm 0.66$  | $64.32 \pm 8.05$  |

For the lactose-based formulation a reduction could not be proven, as no measurements were possible for the sample without L-leucine spray dried at an outlet temperature of 50 °C. However, the water content of the lactose sample with L-leucine was only slightly above the sample spray dried at an outlet temperature of 60 °C without L-leucine.

By adding L-leucine, a substantial increase in the spray drying yield could be achieved. With almost 71% the mannitol-based sample exhibited an approximately 18% higher yield compared to the one without L-leucine, the lactose-based formulation with about 64% showed an increase of almost 27%. This improved yield cannot solely be attributed to decreased water content, as the lactose-based sample with the higher yield exhibited a higher water content. The L-leucine enriched shell, however, led to a less cohesive powder, with almost no powder remaining in the cyclone.

As spray drying was performed analogously to Chapter 6.2, a similar particle size was expected, despite the addition of L-leucine to the spray drying dispersion. However, the introduction of L-leucine resulted in a highly significant increase ( $p < 0.001$ ) in the x50 value for both excipients (Figure 6.30 B, Table 6.6).

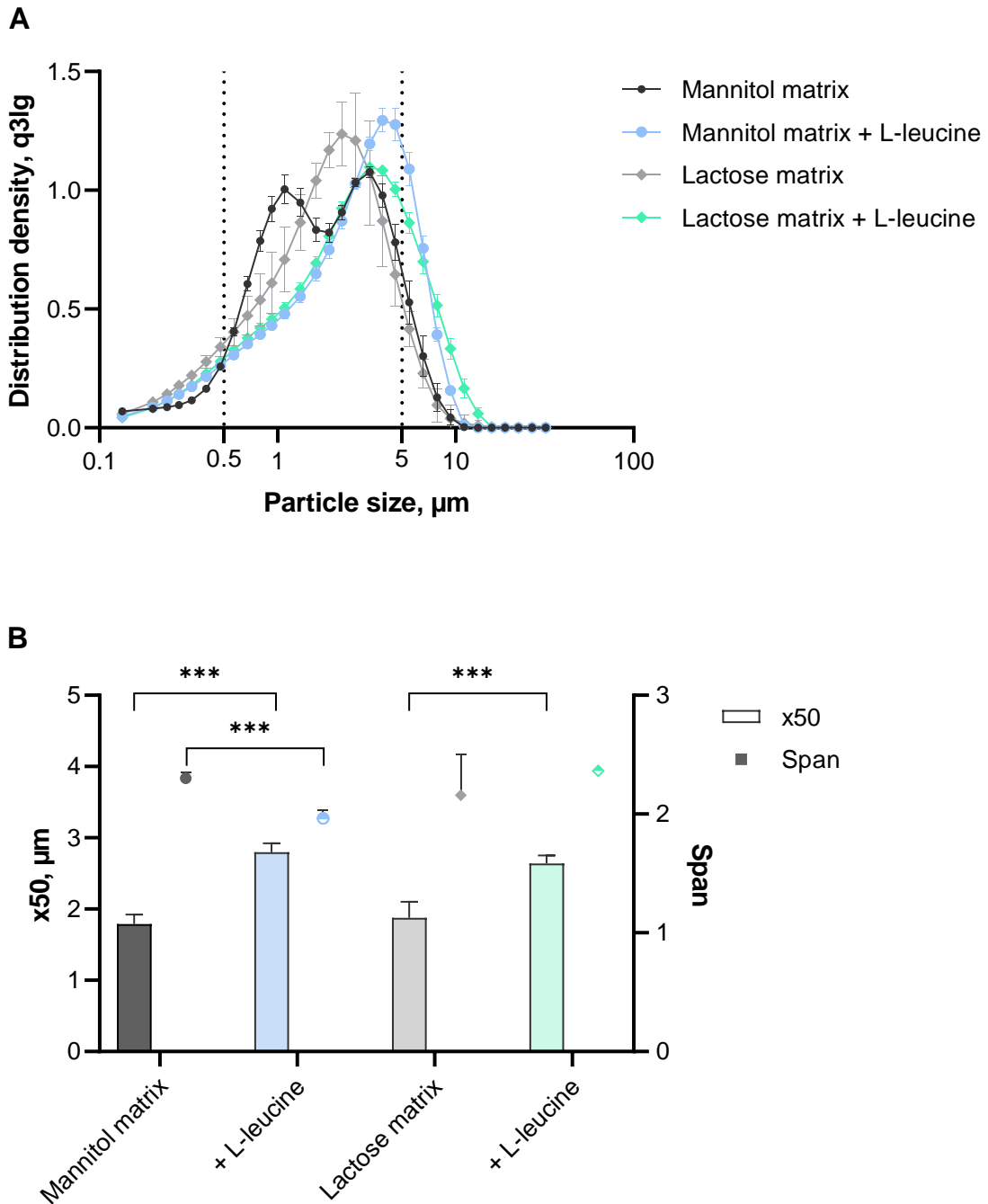


Figure 6.30: (A) Particle size distributions and (B) x50 and span values of the spray dried formulations with mannitol or lactose matrix, with or without the addition of L-leucine,  $n = 3$ , error bars show standard deviation, \*\*\* $p < 0.001$ .

Table 6.6: Characteristic values of the particle size distributions of the spray dried mRNA lipoplex formulations in lactose or mannitol matrix, with (+) or without (-) the addition of L-leucine, measured using laser diffraction.  $n = 3$ , means  $\pm$  standard deviation.

| Matrix   | Sample                           |           | x10, $\mu\text{m}$ | x50, $\mu\text{m}$ | x90, $\mu\text{m}$ | Span            |
|----------|----------------------------------|-----------|--------------------|--------------------|--------------------|-----------------|
|          | Outlet temp., $^{\circ}\text{C}$ | L-Leucine |                    |                    |                    |                 |
| Mannitol | 50                               | -         | $0.59 \pm 0.02$    | $1.79 \pm 0.13$    | $4.7 \pm 0.33$     | $2.30 \pm 0.05$ |
|          |                                  | +         | $0.57 \pm 0.03$    | $2.80 \pm 0.12$    | $6.06 \pm 0.12$    | $1.96 \pm 0.07$ |
| Lactose  | 60                               | -         | $0.48 \pm 0.03$    | $1.88 \pm 0.23$    | $4.48 \pm 0.36$    | $2.16 \pm 0.34$ |
|          | 50                               | +         | $0.56 \pm 0.01$    | $2.64 \pm 0.11$    | $6.80 \pm 0.28$    | $2.36 \pm 0.04$ |

This circumstance is clearly displayed in the particle size distribution graphs (Figure 6.30 A). The peaks of both powders containing L-leucine shifted towards larger particles. This observation was also made by Mangal et al., Wang et al. and Molina et al. who also spray dried their formulations with the addition of 5% (w/w) L-leucine [95, 159–161]. In contrast, Chow et al. reported a decrease in particle size when spray drying with L-leucine proportions starting at 10% [97]. This might be attributed to the particle wrinkling at higher L-leucine concentrations. Consequently, there might be a certain concentration, depending on the spray drying setup, below which the particle size increases and beyond which it decreases. However, it is imperative to recognise that the particle size is governed by a multifaceted interplay of diverse factors. Foremost among these factors are the solid concentration of the spray drying dispersion, process temperature, and the velocity of surface enrichment of L-leucine, coupled with the kinetics of shell formation.

Interestingly, in the present study, the addition of L-leucine to the mannitol dispersion led to a more monomodal particle size distribution, as evidenced by the significantly lower span value ( $p < 0.001$ ) in comparison to the powder without L-leucine. Hence, the addition of L-leucine did not only increase the particle size, but also led to a narrower particle size distribution. However, the x50 values were not significantly different ( $p > 0.05$ ) with  $2.80 \pm 0.12 \mu\text{m}$  for the mannitol-based and  $2.64 \pm 0.11 \mu\text{m}$  for the lactose-based formulation and apart from this within the inhalable range of 1 to 5  $\mu\text{m}$  [69].

The scanning electron microscope images confirmed the measured particle size and predominantly display spherical particles for both matrices (Figure 6.31).

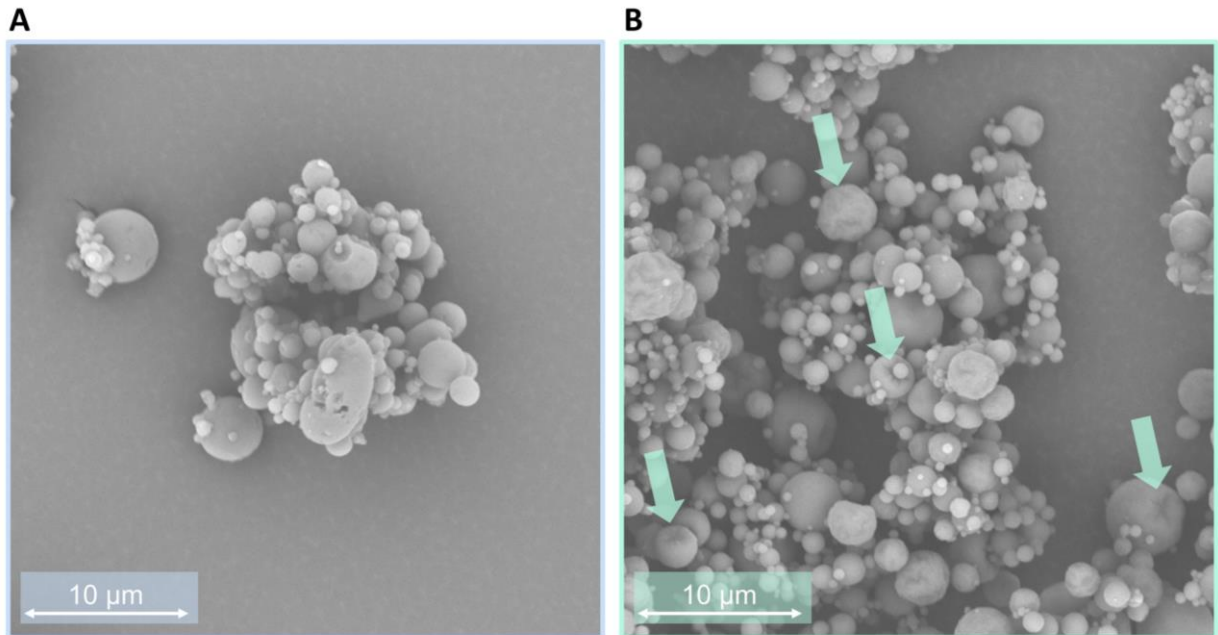


Figure 6.31: Representative scanning electron microscope images of the mRNA lipoplexes spray dried in mannitol (A) and lactose (B) matrix after the addition of L-leucine. Arrows show indications of wrinkling.

Upon comparison with the spray dried particles before the addition of L-leucine, some particles of the lactose-based formulation exhibit first indications of wrinkling. This can be explained by the formation of a L-leucine enriched shell during spray drying. Depending on the thickness and mechanical properties of this shell, the remaining solvent may diffuse through the shell, evaporate through openings in the shell, or cause the hollow particle to collapse or wrinkle [83]. Whether these new surface properties and the produced particle sizes are an advantage for the detachment from the capsules' inner surface and an increased FPF during inhalation, remained to be determined by aerodynamic characterisation.

### 6.3.2.3. Aerodynamic Performance of Spray Dried Formulations with L-Leucine

Two examples where the aerodynamic performance of formulations containing nucleic acids was successfully optimised introducing L-leucine are the studies conducted by Chow et al. and Mohamed et al. [97, 162]. They started with a considerably low FPF (16.9 and 19.96%) and added L-leucine in various ratios to find the most successful formulation which comprised 25% and 50% L-leucine of the total solid content, respectively. In the present study, the FPF of the spray dried mannitol-based formulation without L-leucine exhibited satisfactory 35% and the major obstacle was the attachment of the powder to the capsules' inner surface. Thus, L-leucine was added at a percentage of 5% of the total solid content to the spray drying dispersion. The spray dried powders, comprising mRNA lipoplexes in mannitol or lactose matrix and L-leucine as a dispersion enhancer, were characterised for their aerodynamic performance using the NGI and RS01 inhaler. It was expected that, despite the small amount of L-leucine, the increased hydrophobicity on the particle surface would enhance the detachment from the capsules. The aerodynamic characterisation revealed that the addition of L-leucine resulted in a highly significant reduction (both  $p < 0.001$ ) of the powder that remained in the capsules (Table 6.7, Figure 6.32 A).

Table 6.7: Residue in the capsules and fine particle fraction (FPF) of the spray dried mannitol-based formulation with (+) and without (-) L-leucine and the spray dried lactose-based formulation with (+) L-leucine.  $n = 3$ , mean  $\pm$  standard deviation.

| Matrix   | L-Leucine | Capsules Residue, % | FPF, %           |
|----------|-----------|---------------------|------------------|
| Mannitol | -         | 22.04 $\pm$ 2.16    | 34.98 $\pm$ 5.47 |
|          | +         | 10.14 $\pm$ 0.62    | 45.05 $\pm$ 1.84 |
| Lactose  | +         | 11.57 $\pm$ 1.58    | 44.03 $\pm$ 3.23 |

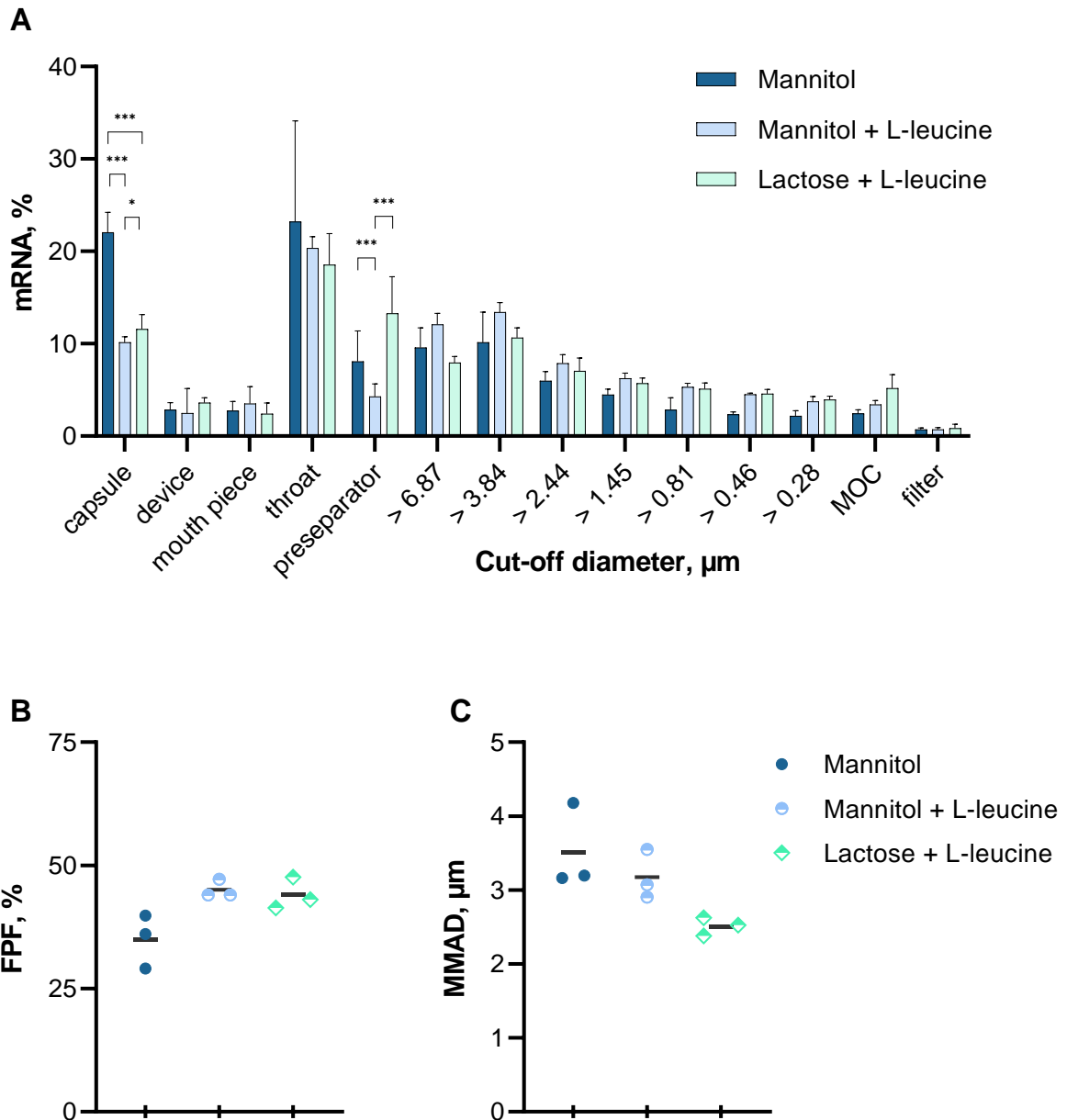


Figure 6.32: Aerodynamic performance of the spray dried formulations using the NGI in combination with the RS01 inhaler, the mouthpiece, the throat and the preseparator. The deposition profiles of the spray dried formulation in mannitol matrix, with or without the addition of L-leucine and in lactose matrix with L-leucine (A), the fine particle fractions (FPF) (B) and the mass median aerodynamic diameters (MMAD) (C) are displayed. A: Bars show mean, error bars depict standard deviation. B, C: Symbols represent individual values and lines show mean of 3 NGI measurements. \* $p < 0.05$ ; \*\*\* $p < 0.001$ .

The residue of the formulation with mannitol matrix was reduced by almost 54% and the residue of the lactose-based formulation approximately by 48%, compared to the mannitol formulation without L-leucine respectively. Thus, the introduction of L-leucine did successfully enhance the detachment from the capsule surface. However, in case of the lactose-based formulation, significantly ( $p < 0.001$ ) more mRNA was found in the preseparator, indicating that particles may have exited the capsules but were probably agglomerating and thus deposited in the preseparator. In contrast, the deposition in the preseparator of the mannitol-based

formulation with L-leucine was decreased by about 47% in comparison to the mannitol formulation without L-leucine. Moreover, the FPF increased by approximately 10% to a FPF of 45% for the mannitol matrix and about 9% to a FPF of 44% for the lactose matrix. After adding L-leucine to the spray drying dispersions, both matrices provided a highly significant reduction ( $p < 0.001$ ) of attached powder in the capsules and considerably increased the FPF. Chow et al. enhanced the FPF of their siRNA polyplexes in mannitol matrix from 16.9% to 45% using 50% (w/w) L-leucine and Mohamed et al. optimised the FPF of miRNA nanoparticles from 19.96 to 51.33% with 25% (w/w) L-leucine [84, 97, 162]. These substantial increases observed were higher than the FPF increase in the present study and were presumably caused by the higher amounts of added L-leucine. However, the present study also reached a satisfactory FPF, higher than most commercial capsule-based inhalers and about 15% higher than Zimmerman et al. described as a very good value for their spray dried siRNA lipid nanoparticles in mannitol or lactose matrix without L-leucine [14, 94]. Therefore, with a successfully enhanced detachment from the capsules and a satisfactory FPF, a decision for a matrix material was left to make. While the detachment from the capsules and the FPF were only slightly in favour for the mannitol-based formulation with L-leucine, it showed a significantly ( $p < 0.001$ ) lower deposition in the preseparator compared to the lactose formulation. However, from an aerodynamic perspective, with only slightly different FPFs, both excipients showed sufficient potential as a matrix when combined with L-leucine. Hence, the decision for a matrix must also take the transfection data and further aspects into account. This matter is discussed in the concluding chapter.

### 6.3.3. Conclusion on Optimising the Aerodynamic Performance and Increasing Detachment

This part of the study aimed to enhance the aerodynamic performance of mRNA lipoplexes spray dried in a mannitol matrix formulation. Identifying the attachment of the spray dried formulation to the capsules' inner surface as a major obstacle to efficient pulmonary delivery, the first attempt to enhance detachment was based on the introduction of sweeper crystals. Sweeper crystals are meant to scrape the capsules' inner surface free from residual powder, allowing it to exit the capsule. Four lactose qualities, differing in particle sizes and span values, were characterised, and blended with the spray dried mRNA lipoplexes in mannitol matrix. The mixtures were then tested for their aerodynamic performance, and it was evaluated, whether the detachment of powder from the capsules was improved. However, despite investigating varying particle sizes, the sweeper crystals did not enhance particle detachment from the capsules. Moreover, InhaLac 251 exhibited a decreased FPF, possibly due to strong attachment of the spray dried powder on the sweeper crystal surface. The capsule-based RS01 inhaler used in this study may have also influenced the outcome, as sweeper crystals have been successful in formulations delivered using other devices [148]. Thus, a sweeper crystal strategy was not suitable to enhance the detachment from the capsules and the FPF of the developed formulation in combination with the used device.

Given the limitations encountered with sweeper crystals, the study turned its attention to increasing surface hydrophobicity through co-spray drying with L-leucine. Prior to introducing L-leucine as further component, a general characterisation of cytotoxicity, transfection and physicochemical properties, similar to the assessment of lipids and matrix materials, was conducted. The cytotoxicity study of L-leucine, along with the physicochemical characterisation and transfection experiments, confirmed its compatibility and precluded negative influences. After co-spray drying mannitol and lactose with L-leucine in the previously chosen setup, the obtained powders were reconstituted and the embedded mRNA lipoplexes were analysed for their physicochemical properties and the transfection efficiency. These mRNA lipoplexes exhibited a decrease in z-average and PDI after spray drying similar to those formulations spray dried without L-leucine. Transfection efficiency studies revealed that while the addition of L-leucine did not significantly ( $p > 0.05$ ) impact transfection for mannitol-based samples, lactose-based samples showed divergent results between the cell lines, which cannot be fully explained currently and need further attention. Particle size distribution analysis indicated an increase in particle size with L-leucine, accompanied by a more monomodal particle size distribution. Scanning electron microscopy images confirmed these changes, with some particles exhibiting indications of wrinkling.

The aerodynamic performance assessment demonstrated that the introduction of L-leucine significantly ( $p < 0.001$ ) reduced the remaining mRNA powder in the capsules. Additionally,

L-leucine led to a considerable increase in FPF for both matrices. The mannitol-based formulation exhibited a greater reduction in residue and resulted in a slightly higher FPF compared to the lactose-based formulation.

Taking both the transfection efficiency and the aerodynamic performance into account, the mannitol matrix in combination with L-leucine demonstrated more consistent results. In comparison to the lactose-based formulation with L-leucine, the mannitol formulation showed stable transfection rates without differences between the model cell lines.

Besides considering transfection efficiency and aerodynamic performance, other crucial aspects have to be taken into account when selecting a matrix material. These factors include the chemical, physical and microbiological stability of the formulation under various storage conditions, for instance. These factors include the chemical, physical, and microbiological stability of the formulation over an extended period. Additionally, potential optimisation steps should be explored. One potential approach for the improvement could involve the addition of further excipients, such as trehalose, a disaccharide commonly used as a cryoprotectant during protein freeze-drying. Its inclusion may also result in enhanced stability in spray dried powders [16]. Enhanced stability was also achieved by Sibum et al. after the addition of trileucine instead of L-leucine [163]. Friis et al. combined trehalose and trileucine for a spray dried lipid nanoparticle formulation for intratracheal delivery of mRNA. Their findings regarding inhaled vaccination exhibited potential in generating an adaptive immune response, however, they have not yet evaluated the stability of the formulation [16]. In conclusion, many potential matrix materials are currently under research, and further data is required to make a final decision on the optimal matrix material or combination.

## 7. Conclusion and Perspectives

To synergise the benefits of mRNA therapeutics, inhalation as a delivery route and a solid-state formulation, it was the aim of this work to incrementally develop a platform capable of protecting mRNA, facilitating transfection, and providing the required aerodynamic performance.

In order to encapsulate mRNA for protection and to facilitate transfection, it was crucial to determine a preparation technique and to characterise the produced mRNA complexes including the assessment of different preparation techniques, cytotoxicity testing and lipoplex composition. As complexing partner, the lipids DOTAP and DOPE were chosen, due to their efficient, non-toxic and well-documented transfection abilities. Liposomes were prepared from DOTAP:DOPE, whereby the probe-type sonicator produced the most favourable liposomes. Those liposomes were complexed with mRNA to produce lipoplexes of different weight ratios, which were subsequently analysed for their transfection efficiency and physicochemical properties (Figure 7.1 A).

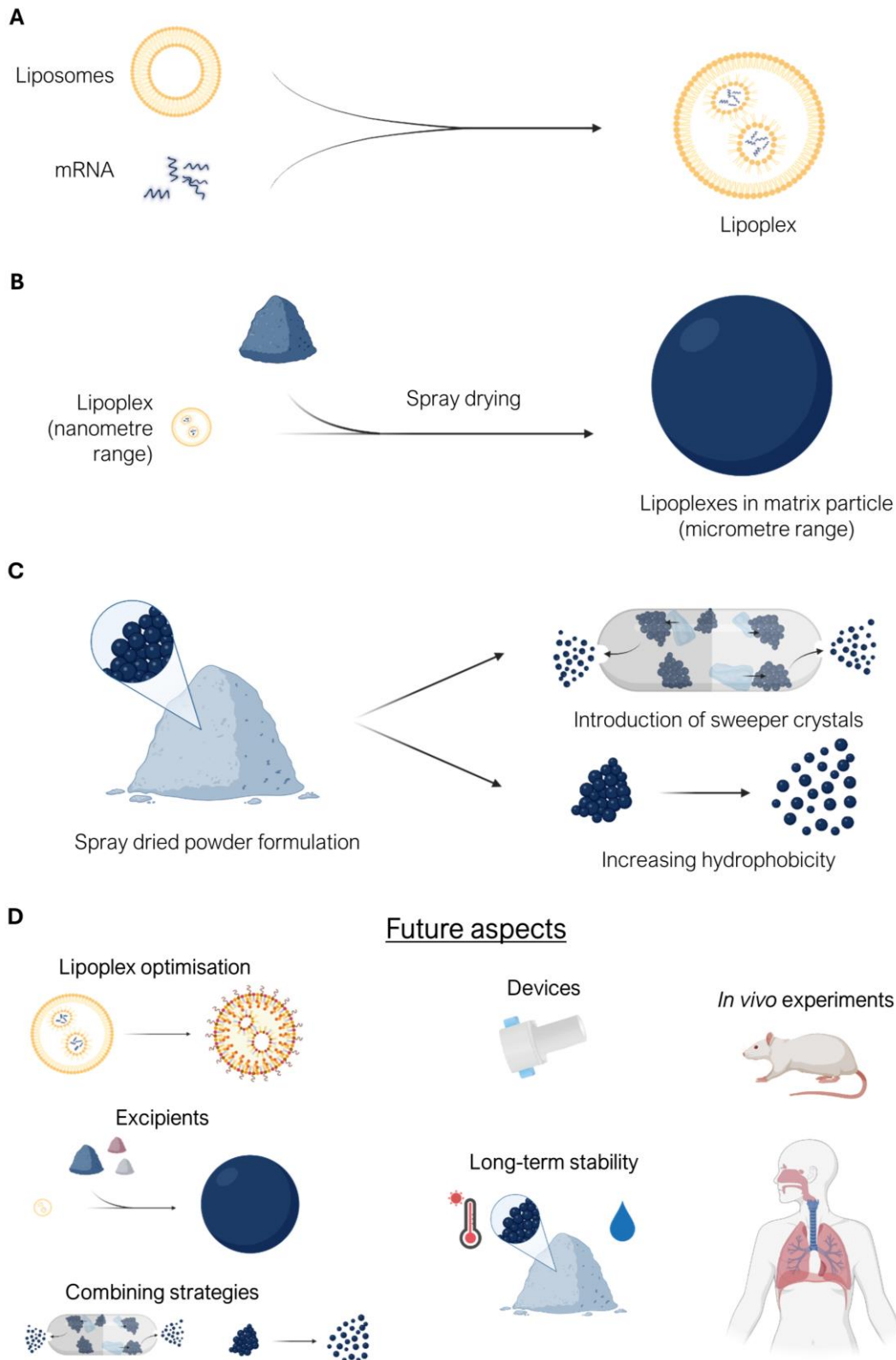


Figure 7.1: Schematic representation of the formulation steps within this work (A-C) and its perspectives (D). (A) Formulation of lipoplexes. (B) By adding a matrix material and spray drying, microparticles are produced that embed the lipoplexes. (C) Optimisation strategies to improve the aerodynamic performance. (D) An overview showing the future aspects of this work, including lipoplex optimisation to enhance transfection and protection, the addition of other excipients and the combination of both employed strategies or other devices to improve the aerodynamic performance. Moreover, long-term stability has to be evaluated and optimised. Finally, in vivo experiments have to be conducted to verify the performance of the formulation. Created with BioRender.com

A weight ratio of lipids to mRNA of 5+1 showed the most efficient transfection and the physicochemical as well as the visual analysis exhibited lipoplexes of the desired properties and size in the lower nanometre range. Additional investigations, including free mRNA assessment and fluorescence displacement assays, supported the choice of the ratio.

After the successful development and characterisation of mRNA lipoplexes, which efficiently deliver mRNA into the model cells, the second part of this work focused on establishing a process to embed the lipoplexes into an inhalable matrix particle (Figure 7.1 B).

Spray drying, a well-established method known for its scalability and ability to process heat-sensitive materials like proteins, was the method of choice for this project [81]. However, although the process parameters were selected to expose the mRNA lipoplexes to as little heat as possible, during the spray drying process mRNA lipoplexes are subjected to thermal stress and shear forces. Therefore, it was particularly important to assess the transfection efficiency of the spray dried lipoplexes as ultimate proof, whether the integrity of the mRNA and its lipoplex was not impaired. Mannitol and lactose were evaluated as matrix materials, with mannitol proving suitable for spray drying under all investigated conditions. Comprehensive assessments of particle morphology, size distribution, and water content levels were conducted, revealing promising initial properties for an inhalable dry powder. Upon reconstitution, the spray dried mRNA lipoplexes demonstrated desired physicochemical properties for efficient transfection. The mannitol-based formulation, spray dried at the lowest investigated outlet temperature exhibited the most efficient transfection *in vitro*. Hence, this formulation was chosen to be aerodynamically characterised. The aerodynamic characterisation showed favourable performance with a fine particle fraction (FPF) of almost 35%. However, a major challenge was discovered, as approximately 22% of the spray dried powder remained in the capsules.

Once this obstacle was identified, two strategies for improving the aerodynamic performance were applied (Figure 7.1 C).

Spray dried formulations within the inhalable range often exhibit poor flowability and pronounced cohesiveness, leading to adhesion to the inner surface of the capsules used in the inhaler to deliver the formulation. To overcome these challenges the first strategy pursued was the addition of coarse particles, so called sweeper crystals, to the spray dried formulation [77]. These particles were intended to clear the surface of the capsules of attached powder, facilitating the escape of the powder from the capsules. Four different lactose qualities were tested but did not result in significant improvements. Instead, it led to decreased FPF for the smaller sweeper crystals, possibly due to strong attachment of the spray dried powder on the sweeper crystal surface. Therefore, sweeper crystals were deemed unsuitable for improving detachment and FPF in this study.

Subsequently, this work focused on increasing the surface hydrophobicity through co-spray drying with L-leucine. Prior to co-spray drying, the assessment of cytotoxicity of L-leucine and the transfection and physicochemical properties of the lipoplexes in presence of L-leucine confirmed compatibility. After co-spray drying, the obtained powders showed an increase in particle size in comparison to the samples without L-leucine. The reconstituted samples exhibited lipoplexes that were slightly smaller than before spray drying and, for the lactose matrix, showed different results between the cell lines upon transfection, while the transfection efficiency of the mannitol-based sample was not affected by spray drying. Aerodynamic characterisation revealed that L-leucine significantly reduced the remaining mRNA powder in the capsules and increased the FPF for both matrices, with the mannitol-based formulation exhibiting slightly superior results with an FPF of 45%.

Considering both, transfection efficiency and aerodynamic performance, the mannitol matrix with L-leucine demonstrated favourable characteristics as dry powder formulation for pulmonary delivery of mRNA therapeutics.

This work demonstrated the feasibility of the development of an inhalable dry powder platform for mRNA therapeutics and forms a solid foundation for further optimisation.

Next steps involve verifying the successful transfection of other mRNAs besides the utilised model mRNA and optimising the preparation process. In particular, the liposome and lipoplex production method, which was established to minimize expended material in this work, requires scaled up. To scale up the production of the lipoplexes, microfluidics, as a continuous production principle would be highly beneficial [46]. However, translating the production method from a thin-film rehydration protocol to microfluidics can result in differences of the liposomes or lipoplexes. Peletta et al. observed a significantly higher hydration of the bilayers of the liposomes produced by thin-film rehydration compared to those prepared using microfluidics, which can influence the complexation of nucleic acids. Therefore, the prepared lipoplexes have to be thoroughly characterised in order to find the most suitable microfluidics method [164].

Additionally, the lipid composition used in this study could be optimised to further increase transfection efficiency and safety (Figure 7.1 D). This includes adding PEG-ylated lipids to control particle size through steric hindrance, decrease immunogenicity and susceptibility to RNases, as well as cholesterol to enhance stability [2, 46, 53]. Moreover, ionisable lipids could be introduced into the formulation. The purpose of ionisable lipids is to enhance the tolerability of the lipids while they are circulating in the bloodstream, as they are zwitterionic at neutral pH [14]. This principle could also increase tolerability in the lungs.

Besides ionisable lipids, numerous other vectors for RNA therapies are currently under investigation, which might also qualify as mRNA carrier in an inhalable dry powder platform [64].

Furthermore, as an important defence mechanism of the respiratory tract, the respiratory mucus has to be considered as a barrier to respiratory gene delivery. Sanders et al. reported that mucus has the ability to bind lipids and destabilise lipoplexes. Therefore, they recommended that the cationic surface should be shielded by neutral and hydrophilic polymers to prevent adherence to the mucus [68]. Consequently, these additional aspects have to be taken into account to optimise the mRNA carrier for respiratory delivery.

In this work, a laboratory spray dryer was used to embed the mRNA lipoplexes within matrix particles of inhalable size. Spray drying offers relatively straightforward scalability. The outlet temperature in this study was set by adjusting the pump rate of the feed, ensuring precise temperature control for the product. However, other strategies exist for controlling the process in an industrial setting. Within a controlled environment, it may be possible to consistently achieve the desired outlet temperature by maintaining a fixed pump rate and adjusting the aspirator. This alternative approach could allow for more predictable and reproducible production periods.

Evaluating the dry powder formulations, an FPF of 45% and a powder residue in the capsule of only 10% for the mannitol-based formulation is a satisfactory achievement. However, to further reduce the loss and increase the FPF, a higher percentage of L-leucine, the addition of other excipients, or a different device employing a different dispersion strategy, such as a dispersion aid like the cyclone in the Novolizer device, could be beneficial. Moreover, a combination of sweeper crystals and L-leucine may lead to an even lower residue in the capsules.

In this work, a dry powder formulation was chosen to enhance stability, as liquids are in general more susceptible to chemical, physical and microbiological instabilities. Preliminary results indicated that the spray dried mRNA lipoplexes, particularly the samples with the lactose-leucine matrix, might remain stable for at least two months when stored at -20 °C. Hence, an additional study to this work should investigate the specific enhancement of stability of the spray dried formulation with various matrices in comparison to liquid formulations in a long-term stability assessment. This could lead to new ideas for improving the stability of the spray-dried mRNA lipoplexes.

After optimising the mRNA carrier and improving the performance and stability of the dry powder formulation, finally, it would be interesting to evaluate if the formulation truly demonstrates its potential in *in vivo* experiments.

In conclusion, this work constitutes a proof of concept for an inhalable dry powder formulation for mRNA therapeutics and a foundation for future research.

## 8. Abstract

Messenger RNA (mRNA) therapeutics have emerged as a revolutionary approach in medicine, offering precise and personalised treatments by leveraging the patient's own cells to produce therapeutic proteins. mRNA therapies hold promise as preventive, curative, and disease-modifying therapies, for a wide range of diseases, including cancer, viral infections, autoimmune and metabolic disorders. Key to the efficacy of mRNA therapeutics is their delivery strategy, given mRNA's susceptibility to degradation by nucleases and environmental stressors. Overcoming these challenges requires innovative delivery strategies that protect mRNA while facilitating its entry into target cells. Intravenous or intramuscular administration, while most common, present limitations, particularly concerning the need for trained healthcare personnel and stability issues of liquid formulations. Inhalation of mRNA therapeutics as a dry powder offers a promising alternative. The large surface area of the lungs, coupled with their relatively low enzymatic environment, provides a favourable site for drug delivery. In addition, inhalation is non-invasive, enhancing patient compliance and reducing the healthcare burden. Therefore, this work focused on the development of an inhalable dry powder platform for mRNA therapeutics, aiming to combine protection, efficient transfection, and good aerodynamic performance. The formulation process was initiated with the preparation of liposomes from the lipids DOTAP and DOPE, followed by the encapsulation of mRNA within these liposomes to form lipoplexes. These two well-studied lipids were chosen to focus the study on the development and optimisation of the dry powder formulation. After determining the optimal lipoplex composition, a spray drying process was established to obtain a dry powder of inhalable microparticles, which embed the lipoplexes within a matrix and maintain the biological activity of the mRNA. Mannitol and lactose were investigated as matrix materials, with mannitol exhibiting the most successful transfection efficiency combined with promising aerodynamic characteristics. A major obstacle was the significant powder residue in the capsule-based inhaler used for delivering the formulation. To overcome this challenge, two optimisation strategies were employed with the aim of minimising the amount of residual powder and improving the aerodynamic performance. The first one was the introduction of sweeper crystals, which did not show the hoped-for success. However, the second strategy, which involved co-spray drying with L-leucine increased the hydrophobicity of the particles, resulted in a reduced powder residue in the capsules and an improved aerodynamic performance with a fine particle fraction of 45%.

In summary, a process has been established encompassing every step from mRNA encapsulation to the production of an inhalable powder with specifically tailored properties. Through the step-by-step development of the platform, this work demonstrated comprehensive proof of concept and laid the foundation for the focused development of an inhalable dry

powder platform for mRNA therapeutics with an excellent aerodynamic performance and high transfection efficiency.

## 9. Zusammenfassung

Messenger RNA (mRNA)-Therapeutika sind ein revolutionärer Ansatz in der Medizin, der präzise und personalisierte Behandlungen ermöglicht, indem er die eigenen Zellen des Patienten zur Produktion therapeutischer Proteine nutzt. Auf mRNA basierende Therapien versprechen präventive, kurative und krankheitsmodifizierende Therapien für eine Vielzahl von Krankheiten, darunter Krebs, Virusinfektionen, Autoimmun- und Stoffwechselstörungen. Entscheidend für die Wirksamkeit von mRNA-Therapeutika ist ihre Applikationsstrategie, da mRNA empfindlich gegenüber dem Abbau durch Nukleasen und Umweltstressfaktoren ist. Um diese Herausforderung zu meistern, sind innovative Verabreichungsstrategien erforderlich, die die mRNA schützen und ihr gleichzeitig den Eintritt in die Zielzellen ermöglichen. Die intravenöse oder intramuskuläre Applikation ist zwar am weitesten verbreitet, hat aber ihre Grenzen, insbesondere durch den Bedarf an geschultem medizinischem Personal und die Stabilitätsprobleme, die mit flüssigen Formulierungen einhergehen. Die Inhalation von mRNA-Therapeutika in Form von Pulvern bietet eine vielversprechende Alternative. Die große Oberfläche der Lunge in Verbindung mit einem relativ enzymarmen Milieu stellt einen vorteilhaften Ort für die Applikation von Medikamenten dar. Außerdem ist die Inhalation eine nicht invasive Applikationsmethode, die die Therapietreue und Compliance der Patienten erhöht und den Zugang zu Therapien erleichtert.

Der Fokus dieser Arbeit lag daher auf der Entwicklung einer inhalierbaren Pulverplattform für mRNA-Therapeutika, die den Schutz der mRNA mit effizienter Transfektion und optimalen aerodynamischen Eigenschaften verbindet. Der erste Schritt im Formulierungsprozess war die Herstellung von Liposomen aus den Lipiden DOTAP und DOPE, gefolgt von der Komplexierung der mRNA in diesen Liposomen zur Bildung von Lipoplexen. Diese beiden gut untersuchten Lipide wurden ausgewählt, um den Schwerpunkt dieser Arbeit auf die Entwicklung und Optimierung der Pulverformulierung zu legen. Nach der Bestimmung der optimalen Lipoplexzusammensetzung wurde ein Sprühtrocknungsverfahren entwickelt, um die Lipoplexe in einem Matrixpartikel im inhalierbaren Größenbereich einzubetten und die biologische Aktivität der mRNA zu erhalten. Als Matrixmaterialien wurden Mannitol und Laktose untersucht. Mit der Mannitolmatrix wurde die beste Transfektionseffizienz in Kombination mit vielversprechenden aerodynamischen Eigenschaften erreicht. Eine Herausforderung waren die erheblichen Pulverrückstände in den Kapseln nach der Inhalation mit dem kapselbasierten Inhalator. Um die Menge an Pulverrückständen zu minimieren und die aerodynamischen Eigenschaften weiter zu verbessern, wurden zwei Optimierungsstrategien angewandt und bewertet. Die erste Strategie war die Einführung von Sweeper Crystals, die jedoch nicht den erhofften Erfolg brachte. Der zweite Ansatz allerdings, Sprühtrocknung mit L-Leucin, um die Hydrophobie der Partikeloberfläche zu erhöhen, reduzierte erheblich den Pulverrückstand in den Kapseln und steigerte die Feinpartikelfraktion auf 45%.

In dieser Arbeit wurde also sukzessive ein Prozess etabliert, der sich von der mRNA Komplexierung bis zur Optimierung der inhalierbaren Pulverformulierung erstreckt. Durch die schrittweise Entwicklung hat diese Arbeit gezeigt, dass das Konzept funktioniert und den Grundstein für die gezielte Entwicklung einer inhalierbaren Pulverplattform für mRNA-Therapeutika mit ausgezeichneten aerodynamischen Eigenschaften und hoher Transfektionseffizienz gelegt.

## 10. Appendix

### 10.1. Abbreviations

Table 10.1: Abbreviations

|      |         |  |                                      |
|------|---------|--|--------------------------------------|
| A    | API     | Active pharmaceutical ingredient                         |                                      |
|      | ATCC    | American Type Culture Collection                         |                                      |
|      | ATP     | Adenosine triphosphate                                   |                                      |
| C    | CFTR    | Cystic fibrosis transmembrane conductor regulator        |                                      |
| D    | DD      | DOTAP:DOPE   |                                      |
|      | DLS     | Dynamic light scattering                                 |                                      |
|      | DNA     | Deoxyribonucleic acid                                    |                                      |
|      | DOPE    | 1,2-dioleoyl-sn-glycero-3-phosphoethanolamine            |                                      |
|      | DOTAP   | 1,2-dioleoyloxypropyl-N,N,N-trimethylammonium chloride). |                                      |
|      | DPI     | Dry powder inhaler                                       |                                      |
|      | E       | EC50   | Half-maximal effective concentration |
| E    | ED      | Emitted dose   |                                      |
|      | EDTA    | Ethylenediaminetetraacetic acid                          |                                      |
|      | EMA     | European Medicines Agency                                |                                      |
|      | EMEM    | Minimum essential medium eagle                           |                                      |
|      | EPDM/PP | Ethylene-propylene-diene/polypropylene                   |                                      |
|      | F       | F-12K  | Ham's F-12 K medium                  |
|      |         | FBS  | Fetal bovine serum                   |
| FDA  |         | Food and Drug Administration                             |                                      |
| FLuc |         | Firefly Luciferase                                       |                                      |
| FPD  |         | Fine particle dose                                       |                                      |
| FPF  |         | Fine particle fraction                                   |                                      |
| H    |         | HELOS  | Helium Laser Optical System          |
|      | HIV     | Human Immunodeficiency Virus                             |                                      |
| M    | MDI     | Metered dose inhaler                                     |                                      |
|      | MMAD    | Mass median aerodynamic diameter                         |                                      |
|      | MOC     | Micro-orifice collector                                  |                                      |
|      | MOC     | Micro-orifice collector                                  |                                      |
|      | mRNA    | Messenger ribonucleic acid                               |                                      |
| N    | NGI     | Next Generation Impactor                                 |                                      |
|      | nk mRNA | Naked mRNA   |                                      |

---

|   |            |   |
|---|------------|---|
| P | PBS        | Phosphate buffered saline                                   |
|   | PDI        | Polydispersity index  |
|   | PEG        | Polyethylene glycol   |
|   | PEI        | Polyethyleneimine   |
|   | Ph. Eur.   | European Pharmacopoeia                                      |
|   | pMDI       | Pressurised metered dose inhaler                            |
| R | RNA        | Ribonucleic acid  |
|   | RNAi       | RNA interference  |
| S | SARS-CoV-2 | Severe acute respiratory syndrome coronavirus 2             |
|   | SEM        | Scanning electron microscopy                                |
|   | siRNA      | Small interfering RNA                                       |
| T | TAE        | Tris-acetate EDTA   |
|   | TEM        | Transmission electron microscopy                            |
| X | x10/50/90  | Particle diameter, where 10/50/90% of particles are smaller |

## 10.2. Substances

Table 10.2: Substances employed in this work with the respective suppliers.

| Substance           | Supplier code   | LOT                     | Supplier   |
|---------------------|---|-------------------------|--|
| A549 cells          | CCL-185   | Passage number 8 to 12  | ATCC, Manassas, USA                                |
| Bradford Assay      | Pierce Coomassie (Bradford) Protein-Assay Kit<br>23200  |                         | Thermo Fisher Scientific Inc., Waltham, USA        |
| Bright-Glo          | Bright-Glo Luciferase Assay System<br>E2610   | 439912                  | Promega GmbH, Walldorf, Germany                    |
| Brij 35             |   | 007D0224                | Uniqema, Corda International plc, Snaith, England  |
| Calu-3 cells        | HTB-55  | Passage number 48 to 65 | ATCC, Manassas, USA                                |
| capsules            | Vcaps Plus, Capsugel Size: 3<br>V43.900   | 53414041                | Lonza Inc., Morristown, USA                        |
| Cell culture medium | Minimum Essential Medium Eagle, with Earle's salts, L-glutamine and sodium bicarbonate<br>M4655 |                         | Sigma-Aldrich, Merck KGaA, Darmstadt, Germany      |
| Cell culture medium | Ham's F-12K (Kaighn's) Medium<br>21127022   |                         | Gibco, Thermo Fisher Scientific Inc., Waltham, USA |
| CellTiter-Glo       | CellTiter-Glo Luminescent Cell Viability Assay<br>G7570   |                         | Promega GmbH, Walldorf, Germany                    |
| Chloroform          | Chloroform Rotisolv HPLC<br>7331.2  | 1211791                 | Carl Roth, Karlsruhe, Germany                      |
| DOTAP:DOPE          | Transfection Reagent 1<br>790310P-500MG-Avanti  | A-157                   | Avanti Polar Lipids, Birmingham, USA               |
| Ethanol             | Ethanol (96 %), HPLC Quality  |                         | Merck KGaA, Darmstadt, Germany                     |
| Fetal bovine serum  | F7524   | BCCB7222<br>1643900     | Sigma-Aldrich, Merck KGaA, Darmstadt, Germany      |

| Substance                                | Supplier code  | LOT         | Supplier                          |   |
|--|--|-------------|-----------------------------------|---|
| <b>Firefly Luciferase mRNA</b>           | FLuc, ~1680 nt Off-The-Shelf, dsRNA reduced Cap1 upgrade 150nt Poly-A tail |             | RiboPro B.V., Oss The Netherlands |   |
| <b>Glycerol</b>                          | Glycerol technical grade   | 211339.1214 | 952433                            | AppliChem, Darmstadt, Germany                           |
| <b>Heparin</b>                           | Heparin-Natrium-5000-ratiopharm  | 3170642     | X44442A                           | ratiopharm GmbH, Ulm, Germany                           |
| <b>InhaLac 120</b>                       |  | 13005024    | L10191705566<br>34A538            | Meggle GmbH & Co. KG, Wasserburg am Inn, Germany        |
| <b>InhaLac 180</b>                       |  | 13008788    | L10596706301<br>54A538            | Meggle GmbH & Co. KG, Wasserburg am Inn, Germany        |
| <b>InhaLac 251</b>                       |  | 13007221    | L10492705295<br>62A538            | Meggle GmbH & Co. KG, Wasserburg am Inn, Germany        |
| <b>InhaLac 70</b>                        |  | 13006558    | L10198705824<br>17A538            | Meggle GmbH & Co. KG, Wasserburg am Inn, Germany        |
| <b>Lipofectamine 2000</b>                |  | 11668030    | 2264843                           | Invitrogen, Thermo Fisher Scientific Inc., Waltham, USA |
| <b>L-Leucine</b>                         |  | L8912-100G  | SLBW8571                          | Sigma-Aldrich, Merck KGaA, Darmstadt, Germany           |
| <b>Loading Dye</b>                       | DNA Gel Loading Dye (6X)   | R0611       |                                   | Thermo Fisher Scientific Inc., Waltham, USA             |
| <b>Lysis buffer</b>                      | 5X Passive Lysis Buffer  | 99912       |                                   | Biotium Inc., Fremont, USA                              |
| <b>Mannitol</b>                          | D(-)-Mannit  | 4175.3      | 481314364                         | Carl Roth, Karlsruhe, Germany                           |
| <b>Non-essential amino acid solution</b> | MEM Non-essential Amino Acid Solution (100x)                               | M7145-100ML | RNBL3006                          | Sigma-Aldrich, Merck KGaA, Darmstadt, Germany           |
| <b>Opti-MEM</b>                          | Opti-MEM Reduced Serum Medium  | 31985070    |                                   | Gibco, Thermo Fisher Scientific Inc., Waltham, USA      |

|                          | Substance   | Supplier code | LOT | Supplier  |
|--------------------------|---|---------------|-----|---|
| PBS                      | Dulbecco's Phosphate Buffered Saline, Modified, without calcium chloride and magnesium chloride | D8537         |     | Sigma-Aldrich, Merck KGaA, Darmstadt, Germany           |
| Penicillin-streptomycin  | Penicillin-streptomycin (100x)  | P4333-100ML   |     | Sigma-Aldrich, Merck KGaA, Darmstadt, Germany           |
| RNA Ladder               | RiboRuler High Range RNA Ladder   | SM1823        |     | Thermo Fisher Scientific Inc., Waltham, USA             |
| RNase-free water         | UltraPure DNase/RNase-Free Distilled Water  | 10977035      |     | Invitrogen, Thermo Scientific Inc., Waltham, USA        |
| Sodium pyruvate solution | Sodium pyruvate solution 100 mM   | S8636-100ML   |     | Sigma-Aldrich, Merck KGaA, Darmstadt, Germany           |
| SYBR Gold                | SYBR™ Gold Nucleic Acid Gel Stain (10,000X Concentrate in DMSO)                                 | S11494        |     | Invitrogen, Thermo Fisher Scientific Inc., Waltham, USA |
| TAE buffer               | UltraPure TAE-Puffer, 10X   | 15558-042     |     | Invitrogen, Thermo Fisher Scientific Inc., Waltham, USA |
| Trypan blue              | Trypan Blue solution 0.4%   | T8154-100ML   |     | Sigma-Aldrich, Merck KGaA, Darmstadt, Germany           |
| Trypsin                  | Trypsin-EDTA solution, 0.25%  | T4049         |     | Sigma-Aldrich, Merck KGaA, Darmstadt, Germany           |
| Uranylacetat Dihydrat    |   | 1.08473       |     | Merck KGaA, Darmstadt, Germany                          |

### 10.3. Equipment and Software

Table 10.3: Equipment employed in this work with the respective suppliers.

|                          | Equipment  | Manufacturer   |
|--------------------------|--|--|
| Cell culture plates      | TC-plate 96 well, Standard, F                      | Sarstedt AG & Co. KG, Nümbrecht, Germany                   |
| Cell culture plates      | Microplate, 384 well, F-bottom, white, Ref. 781080 | Greiner Bio-One GmbH, Frickenhausen, Germany               |
| Centrifuge               | Biofuge 28 RS                                      | Heraeus GmbH, Hanau, Germany                               |
| CITDAS Software V3.1     | n/a  | Copley Scientific, Nottingham, UK                          |
| Dehumidifier             | B-296  | Büchi Labortechnik GmbH, Flawil, Switzerland               |
| Density meter            | density meter DMA 48                               | Anton Paar Germany GmbH, Ostfildern, Germany               |
| Dynamic light scattering | Zetasizer ZS Nano                                  | Malvern Panalytical GmbH, Kassel, Germany                  |
| GraphPad Prism           | GraphPad Prism 10.2.                               | GraphPad Software, Boston, USA                             |
| Imager for gel imaging   | ChemoStar 21 TS Intas                              | INTAS Science Imaging Instruments GmbH, Göttingen, Germany |
| Incubator                | HERAcell 150                                       | Thermo Fisher Scientific Inc., Waltham, USA                |
| Karl-Fischer Titrator    | Karl-Fischer Titrator V20                          | Mettler Toledo AG, Analytical, Schwerzenbach, Switzerland  |
| Laser diffractometer     | HELOS in combination with RODOS module             | Sympatec GmbH, Clausthal-Zellerfeld, Germany               |
| Microsoft Excel          | Microsoft Excel for Microsoft 365                  | Microsoft Corporation, Redmond, USA                        |
| Next Generation Impactor | n/a  | Copley Scientific Ltd., Nottingham, UK                     |

|   | <b>Equipment</b>                                   | <b>Manufacturer</b>   |
|---|--|---|
| <b>PAQXOS</b>                               | PAQXOS 5.2.1                                       | Sympatec GmbH, Clausthal-Zellerfeld, Germany                    |
| <b>Plate reader</b>                         | Tecan Spark  | Tecan Group Ltd., Männedorf, Switzerland                        |
| <b>Plate shaker</b>                         | IKA VORTEX 4 basic                                 | IKA-Werke GmbH & CO. KG, Staufen, Germany                       |
| <b>Plates for Fluorescence measurements</b> | Microplate, 96 well, F-bottom, black, Ref. 675076  | Sarstedt AG & Co. KG, Nümbrecht, Germany                        |
| <b>Plates for Luminescence measurements</b> | Microplate, 96 well, Half area, white, Ref. 675075 | Greiner Bio-One GmbH, Frickenhausen, Germany                    |
| <b>RS01 Inhaler</b>                         | Low resistance                                     | Plastiap, part of Berry Global Inc., Evansville, USA            |
| <b>Scanning electron microscope</b>         | Phenom World XL                                    | Thermo Fisher Scientific Inc., Waltham, USA                     |
| <b>Sonication bath</b>                      | Transsonic 460/H                                   | Elma Schmidbauer GmbH, Singen, Germany                          |
| <b>Probe-type Sonicator</b>                 | Sonoplus HD 4100                                   | Bandelin electronic GmbH & Co. KG, Berlin, Germany              |
| <b>Spray Dryer</b>                          | Mini Spray Dryer B-290                             | Büchi Labortechnik GmbH, Flawil, Switzerland                    |
| <b>Sputter coater</b>                       | BAL-Tec SCP 050 Sputter Coater                     | Leica Microsystems GmbH, Wetzlar, Germany                       |
| <b>TEM</b>                                  | JEOL 1400 Plus TEM                                 | JEOL Germany, Munich, Germany                                   |
| <b>TEM camera</b>                           | TemCam-F416 camera                                 | TVIPS, Munic, Germany   |
| <b>TEM Carbon grid</b>                      | CF300-CU Carbon Film 300 Mesh                      | Electron Microscopy Sciences, Science Services, Munich, Germany |

|   | <b>Equipment</b>          | <b>Manufacturer</b>                                  |
|---|---------------------------|--|
| <b>Tubes for pumping and spray drying experiments</b> | Tygon 2375 NSF-51         | Saint-Gobain Performance Plastics, Charny, France    |
|   | Tygon F-4040-A            | Saint-Gobain Performance Plastics, Charny, France    |
|   | EPDM/PP (RCT 333647)      | Reichelt Chemietechnik GmbH+Co., Heidelberg, Germany |
|   | silicone tubing (9205001) | Erich Eydam KG, Kiel, Germany                        |
| <b>Turbula blender</b>                                | n/a                       | Willy A. Bachofen AG, Muttenz, Switzerland           |
| <b>Viscosimeter</b>                                   | SV-10 Vibro-Viscosimeter  | A&D Company Ltd., Tokio, Japan                       |
| <b>Zetasizer Nano software</b>                        |                           | Malvern Panalytical GmbH, Kassel, Germany            |

## 11. References

1. Schoenmaker, L., Witzigmann, D., Kulkarni, J.A., Verbeke, R., Kersten, G., Jiskoot, W., Crommelin, D.J.A.: mRNA-lipid nanoparticle COVID-19 vaccines: Structure and stability. *International Journal of Pharmaceutics* **2021**, 601, 120586, doi: 10.1016/j.ijpharm.2021.120586
2. Rohner, E., Yang, R., Foo, K.S., Goedel, A., Chien, K.R.: Unlocking the promise of mRNA therapeutics. *Nat Biotechnol* **2022**, 40(11), 1586–1600, doi: 10.1038/s41587-022-01491-z
3. COMIRNATY. FDA, Thu, 7 December 2023. <https://www.fda.gov/vaccines-blood-biologics/comirnaty>. Accessed 17 February 2024
4. SPIKEVAX. FDA, Thu, 21 September 2023. <https://www.fda.gov/vaccines-blood-biologics/spikevax>. Accessed 17 February 2024
5. Weng, Y., Li, C., Yang, T., Hu, B., Zhang, M., Guo, S., Xiao, H., Liang, X.-J., Huang, Y.: The challenge and prospect of mRNA therapeutics landscape. *Biotechnol Adv* **2020**, 40, 107534, doi: 10.1016/j.biotechadv.2020.107534
6. Adapted vaccine targeting BA.4 and BA.5 Omicron variants and original SARS-CoV-2 recommended for approval | European Medicines Agency **2024**. <https://www.ema.europa.eu/en/news/adapted-vaccine-targeting-ba4-and-ba5-omicron-variants-and-original-sars-cov-2-recommended-approval>. Accessed 3 March 2024
7. Pather, S., Madhi, S.A., Cowling, B.J., Moss, P., Kamil, J.P., Ciesek, S., Muik, A., Türeci, Ö.: SARS-CoV-2 Omicron variants: burden of disease, impact on vaccine effectiveness and need for variant-adapted vaccines. *Frontiers in immunology* **2023**, 14, 1130539, doi: 10.3389/fimmu.2023.1130539
8. Jöhler, S.M., Rejman, J., Guan, S., Rosenecker, J.: Nebulisation of IVT mRNA Complexes for Intrapulmonary Administration. *PLoS One* **2015**, 10(9), e0137504, doi: 10.1371/journal.pone.0137504
9. Tavernier, G., Andries, O., Demeester, J., Sanders, N.N., Smedt, S.C. de, Rejman, J.: mRNA as gene therapeutic: how to control protein expression. *J Control Release* **2011**, 150(3), 238–247, doi: 10.1016/j.jconrel.2010.10.020
10. Lv, H., Zhang, S., Wang, B., Cui, S., Yan, J.: Toxicity of cationic lipids and cationic polymers in gene delivery. *Journal of Controlled Release* **2006**, 114(1), 100–109, doi: 10.1016/j.jconrel.2006.04.014
11. Zheng, M., Librizzi, D., Kılıç, A., Liu, Y., Renz, H., Merkel, O.M., Kissel, T.: Enhancing in vivo circulation and siRNA delivery with biodegradable polyethylenimine-graft-polycaprolactone-block-poly(ethylene glycol) copolymers. *Biomaterials* **2012**, 33(27), 6551–6558, doi: 10.1016/j.biomaterials.2012.05.055

12. Hellfritzsich, M., Scherließ, R.: Mucosal Vaccination via the Respiratory Tract. *Pharmaceutics* **2019**, 11(8), doi: 10.3390/pharmaceutics11080375
13. Labiris, N.R., Dolovich, M.B.: Pulmonary drug delivery. Part I: physiological factors affecting therapeutic effectiveness of aerosolized medications. *Br J Clin Pharmacol* **2003**, 56(6), 588–599, doi: 10.1046/j.1365-2125.2003.01892.x
14. Zimmermann, C.M., Baldassi, D., Chan, K., Adams, N.B.P., Neumann, A., Porras-Gonzalez, D.L., Wei, X., Kneidinger, N., Stoleriu, M.G., Burgstaller, G., Witzigmann, D., Luciani, P., Merkel, O.M.: Spray drying siRNA-lipid nanoparticles for dry powder pulmonary delivery. *J Control Release* **2022**, 351, 137–150, doi: 10.1016/j.jconrel.2022.09.021
15. Qiu, Y., Chow, M.Y.T., Liang, W., Chung, W.W.Y., Mak, J.C.W., Lam, J.K.W.: From Pulmonary Surfactant, Synthetic KL4 Peptide as Effective siRNA Delivery Vector for Pulmonary Delivery. *Mol Pharm* **2017**, 14(12), 4606–4617, doi: 10.1021/acs.molpharmaceut.7b00725
16. Friis, K.P., Gracin, S., Oag, S., Leijon, A., Sand, E., Lindberg, B., Lázaro-Ibáñez, E., Lindqvist, J., Whitehead, K.A., Bak, A.: Spray dried lipid nanoparticle formulations enable intratracheal delivery of mRNA. *J Control Release* **2023**, 363, 389–401, doi: 10.1016/j.jconrel.2023.09.031
17. Rowe, S.M., Zuckerman, J.B., Dorgan, D., Lascano, J., McCoy, K., Jain, M., Schechter, M.S., Lommatzsch, S., Indihar, V., Lechtzin, N., McBennett, K., Callison, C., Brown, C., Liou, T.G., MacDonald, K.D., Nasr, S.Z., Bodie, S., Vaughn, M., Meltzer, E.B., Barbier, A.J.: Inhaled mRNA therapy for treatment of cystic fibrosis: Interim results of a randomized, double-blind, placebo-controlled phase 1/2 clinical study. *J Cyst Fibros* **2023**, 22(4), 656–664, doi: 10.1016/j.jcf.2023.04.008
18. Dr. Isabelle Viktoria Maucher (Apothekerin): Der Corona-Impfstoff BNT162b2 (COMIRNATY). *Vidal MMI Germany GmbH*, 21 December 2020. <https://www.gelbe-liste.de/nachrichten/zulassung-corona-impfstoff-bnt162b2-deutschland>. Accessed 20 February 2024
19. Kim, B.-K., Hwang, G.-B., Seu, Y.-B., Choi, J.-S., Jin, K.S., Doh, K.-O.: DOTAP/DOPE ratio and cell type determine transfection efficiency with DOTAP-liposomes. *Biochim Biophys Acta* **2015**, 1848(10 Pt A), 1996–2001, doi: 10.1016/j.bbamem.2015.06.020
20. Goleij, P., Babamohamadi, M., Rezaee, A., Sanaye, P.M., Tabari, M.A.K., Sadreddini, S., Arefnezhad, R., Motedayyen, H.: Chapter Three - Types of RNA therapeutics. In: Chu, D.-T., van Than, T. (eds.) *Progress in Molecular Biology and Translational Science : RNA Therapeutics Part A*, vol. 203, pp. 41–63. Academic Press **2024**
21. Schoenberg, D.R., Maquat, L.E.: Regulation of cytoplasmic mRNA decay. *Nat Rev Genet* **2012**, 13(4), 246–259, doi: 10.1038/nrg3160

22. Penalva, L.O.F.: mRNA Degradation. In: Dubitzky, W., Wolkenhauer, O., Cho, K.-H., Yokota, H. (eds.) *Encyclopedia of systems biology*. With 148 tables, p. 1460. Springer Reference, New York, NY **2013**
23. Parker, R., Song, H.: The enzymes and control of eukaryotic mRNA turnover. *Nat Struct Mol Biol* **2004**, 11(2), 121–127, doi: 10.1038/nsmb724
24. Shepherd, S.J., Warzecha, C.C., Yadavali, S., El-Mayta, R., Alameh, M.-G., Wang, L., Weissman, D., Wilson, J.M., Issadore, D., Mitchell, M.J.: Scalable mRNA and siRNA Lipid Nanoparticle Production Using a Parallelized Microfluidic Device. *Nano Lett* **2021**, 21(13), 5671–5680, doi: 10.1021/acs.nanolett.1c01353
25. Decroly, E., Ferron, F., Lescar, J., Canard, B.: Conventional and unconventional mechanisms for capping viral mRNA. *Nat Rev Microbiol* **2011**, 10(1), 51–65, doi: 10.1038/nrmicro2675
26. Liu, C., Shi, Q., Huang, X., Koo, S., Kong, N., Tao, W.: mRNA-based cancer therapeutics. *Nat Rev Cancer* **2023**, 23(8), 526–543, doi: 10.1038/s41568-023-00586-2
27. Kim, D.Y., Atasheva, S., McAuley, A.J., Plante, J.A., Frolova, E.I., Beasley, D.W.C., Frolov, I.: Enhancement of protein expression by alphavirus replicons by designing self-replicating subgenomic RNAs. *Proc Natl Acad Sci U S A* **2014**, 111(29), 10708–10713, doi: 10.1073/pnas.1408677111
28. McKay, P.F., Hu, K., Blakney, A.K., Samnuan, K., Brown, J.C., Penn, R., Zhou, J., Bouton, C.R., Rogers, P., Polra, K., Lin, P.J.C., Barbosa, C., Tam, Y.K., Barclay, W.S., Shattock, R.J.: Self-amplifying RNA SARS-CoV-2 lipid nanoparticle vaccine candidate induces high neutralizing antibody titers in mice. *Nat Commun* **2020**, 11(1), 3523, doi: 10.1038/s41467-020-17409-9
29. Huysmans, H., Zhong, Z., Temmerman, J. de, Mui, B.L., Tam, Y.K., Mc Cafferty, S., Gitsels, A., Vanrompay, D., Sanders, N.N.: Expression Kinetics and Innate Immune Response after Electroporation and LNP-Mediated Delivery of a Self-Amplifying mRNA in the Skin. *Molecular Therapy - Nucleic Acids* **2019**, 17, 867–878, doi: 10.1016/j.omtn.2019.08.001
30. Blakney, A.K., Ip, S., Geall, A.J.: An Update on Self-Amplifying mRNA Vaccine Development. *Vaccines* **2021**, 9(2), doi: 10.3390/vaccines9020097
31. Rosa, S.S., Prazeres, D.M.F., Azevedo, A.M., Marques, M.P.C.: mRNA vaccines manufacturing: Challenges and bottlenecks. *Vaccine* **2021**, 39(16), 2190–2200, doi: 10.1016/j.vaccine.2021.03.038
32. Qin, S., Tang, X., Chen, Y., Chen, K., Fan, N., Xiao, W., Zheng, Q., Li, G., Teng, Y., Wu, M., Song, X.: mRNA-based therapeutics: powerful and versatile tools to combat diseases. *Sig Transduct Target Ther* **2022**, 7(1), 166, doi: 10.1038/s41392-022-01007-w
33. Brian P O’Sullivan, Steven D Freedman: Cystic fibrosis

34. Verbeke, R., Lentacker, I., Smedt, S.C. de, Dewitte, H.: The dawn of mRNA vaccines: The COVID-19 case. *J Control Release* **2021**, 333, 511–520, doi: 10.1016/j.jconrel.2021.03.043
35. Hu, B., Zhong, L., Weng, Y., Peng, L., Huang, Y., Zhao, Y., Liang, X.-J.: Therapeutic siRNA: state of the art. *Sig Transduct Target Ther* **2020**, 5(1), 101, doi: 10.1038/s41392-020-0207-x
36. European Medicines Agency: Onpattro, INN: patisiran. [https://www.ema.europa.eu/de/documents/overview/onpattro-epar-medicine-overview\\_de.pdf](https://www.ema.europa.eu/de/documents/overview/onpattro-epar-medicine-overview_de.pdf). Accessed 14 February 2024
37. Klingler, M.: Neueinführung Onpattro bei hATTR. *Vidal MMI Germany GmbH*, 17 October 2018. <https://www.gelbe-liste.de/neue-medikamente/neueinfuehrung-onpattro-hattr>. Accessed 19 February 2024
38. Chheda, U., Pradeepan, S., Esposito, E., Strezsak, S., Fernandez-Delgado, O., Kranz, J.: Factors Affecting Stability of RNA - Temperature, Length, Concentration, pH, and Buffering Species. *Journal of Pharmaceutical Sciences* **2024**, 113(2), 377–385, doi: 10.1016/j.xphs.2023.11.023
39. Kowalski, P.S., Rudra, A., Miao, L., Anderson, D.G.: Delivering the Messenger: Advances in Technologies for Therapeutic mRNA Delivery. *Molecular Therapy* **2019**, 27(4), 710–728, doi: 10.1016/j.ymthe.2019.02.012
40. Wadhwa, A., Aljabbari, A., Lokras, A., Foged, C., Thakur, A.: Opportunities and Challenges in the Delivery of mRNA-based Vaccines. *Pharmaceutics* **2020**, 12(2), doi: 10.3390/pharmaceutics12020102
41. Hajj, K.A., Whitehead, K.A.: Tools for translation: non-viral materials for therapeutic mRNA delivery. *Nat Rev Mater* **2017**, 2(10), 1–17, doi: 10.1038/natrevmats.2017.56
42. Guevara, M.L., Persano, S., Persano, F.: Lipid-Based Vectors for Therapeutic mRNA-Based Anti-Cancer Vaccines. *Current Pharmaceutical Design* **2019**, 25(13), 1443–1454, doi: 10.2174/1381612825666190619150221
43. Akinc, A., Maier, M.A., Manoharan, M., Fitzgerald, K., Jayaraman, M., Barros, S., Ansell, S., Du, X., Hope, M.J., Madden, T.D., Mui, B.L., Semple, S.C., Tam, Y.K., Ciufolini, M., Witzigmann, D., Kulkarni, J.A., van der Meel, R., Cullis, P.R.: The Onpattro story and the clinical translation of nanomedicines containing nucleic acid-based drugs. *Nat Nanotechnol.* **2019**, 14(12), 1084–1087, doi: 10.1038/s41565-019-0591-y
44. FDA approves first-of-its kind targeted RNA-based therapy to treat a rare disease. *FDA*, Tue, 24 March 2020. <https://www.fda.gov/news-events/press-announcements/fda-approves-first-its-kind-targeted-rna-based-therapy-treat-rare-disease>. Accessed 17 February 2024

45. Suzuki, Y., Ishihara, H.: Difference in the lipid nanoparticle technology employed in three approved siRNA (Patisiran) and mRNA (COVID-19 vaccine) drugs. *Drug Metab Pharmacokinet* **2021**, 41, 100424, doi: 10.1016/j.dmpk.2021.100424
46. Jürgens, D.C., Deßloch, L., Porras-Gonzalez, D., Winkeljann, J., Zielinski, S., Munschauer, M., Hörner, A.L., Burgstaller, G., Winkeljann, B., Merkel, O.M.: Lab-scale siRNA and mRNA LNP manufacturing by various microfluidic mixing techniques – an evaluation of particle properties and efficiency. *OpenNano* **2023**, 12, 100161, doi: 10.1016/j.onano.2023.100161
47. Da Sun, Lu, Z.-R.: Structure and Function of Cationic and Ionizable Lipids for Nucleic Acid Delivery. *Pharm Res* **2023**, 40(1), 27–46, doi: 10.1007/s11095-022-03460-2
48. Zhdanov, R.I., Podobed, O.V., Vlassov, V.V.: Cationic lipid-DNA complexes-lipoplexes-for gene transfer and therapy. *Bioelectrochemistry* **2002**, 58(1), 53–64, doi: 10.1016/S1567-5394(02)00132-9
49. Li, Y., Bhindi, R., Deng, Z.J., Morton, S.W., Hammond, P.T., Khachigian, L.M.: Inhibition of vein graft stenosis with a c-jun targeting DNAzyme in a cationic liposomal formulation containing 1,2-dioleoyl-3-trimethylammonium propane (DOTAP)/1,2-dioleoyl-sn-glycero-3-phosphoethanolamine (DOPE). *Int J Cardiol* **2013**, 168(4), 3659–3664, doi: 10.1016/j.ijcard.2013.05.092
50. Sun, H., Zhang, Y., Wang, J., Su, J., Zhou, D., Yu, X., Xu, Y., Yang, W.: Application of Lung-Targeted Lipid Nanoparticle-delivered mRNA of soluble PD-L1 via SORT Technology in Acute Respiratory Distress Syndrome. *Theranostics* **2023**, 13(14), 4974–4992, doi: 10.7150/thno.86466
51. Gilleron, J., Querbes, W., Zeigerer, A., Borodovsky, A., Marsico, G., Schubert, U., Manygoats, K., Seifert, S., Andree, C., Stöter, M., Epstein-Barash, H., Zhang, L., Koteliansky, V., Fitzgerald, K., Fava, E., Bickle, M., Kalaidzidis, Y., Akinc, A., Maier, M., Zerial, M.: Image-based analysis of lipid nanoparticle-mediated siRNA delivery, intracellular trafficking and endosomal escape. *Nat Biotechnol* **2013**, 31(7), 638–646, doi: 10.1038/nbt.2612
52. Wittrup, A., Ai, A., Liu, X., Hamar, P., Trifonova, R., Charisse, K., Manoharan, M., Kirchhausen, T., Lieberman, J.: Visualizing lipid-formulated siRNA release from endosomes and target gene knockdown. *Nat Biotechnol* **2015**, 33(8), 870–876, doi: 10.1038/nbt.3298
53. Yu, B., Wang, X., Zhou, C., Teng, L., Ren, W., Yang, Z., Shih, C.-H., Wang, T., Lee, R.J., Tang, S., Lee, L.J.: Insight into mechanisms of cellular uptake of lipid nanoparticles and intracellular release of small RNAs. *Pharm Res* **2014**, 31(10), 2685–2695, doi: 10.1007/s11095-014-1366-7

- 
54. Szebeni, J., Kiss, B., Bozó, T., Turjeman, K., Levi-Kalisman, Y., Barenholz, Y., Kellermayer, M.: Insights into the Structure of Comirnaty Covid-19 Vaccine: A Theory on Soft, Partially Bilayer-Covered Nanoparticles with Hydrogen Bond-Stabilized mRNA-Lipid Complexes. *ACS Nano* **2023**, 17(14), 13147–13157, doi: 10.1021/acsnano.2c11904
55. Hermosilla, J., Alonso-García, A., Salmerón-García, A., Cabeza-Barrera, J., Medina-Castillo, A.L., Pérez-Robles, R., Navas, N.: Analysing the In-Use Stability of mRNA-LNP COVID-19 Vaccines Comirnaty™ (Pfizer) and Spikevax™ (Moderna): A Comparative Study of the Particulate. *Vaccines* **2023**, 11(11), 1635, doi: 10.3390/vaccines11111635
56. Kubota, K., Onishi, K., Sawaki, K., Li, T., Mitsuoka, K., Sato, T., Takeoka, S.: Effect of the nanoformulation of siRNA-lipid assemblies on their cellular uptake and immune stimulation. *Int J Nanomedicine* **2017**, 12, 5121–5133, doi: 10.2147/IJN.S136426
57. Microfluidic design: Minimizing Internal Volumes - Translume **2023**. <https://www.translume.com/quality/itar/item/209-microfluidic-design-minimizing-internal-volumes>. Accessed 4 March 2024
58. Bergese, P., Hamad-Schifferli, K. (eds.): Nanomaterial interfaces in biology. Methods and protocols. Springer protocols, vol. 1025. Humana Press, New York **2013**
59. Musielak, E., Feliczak-Guzik, A., Nowak, I.: Synthesis and Potential Applications of Lipid Nanoparticles in Medicine. *Materials (Basel)* **2022**, 15(2), doi: 10.3390/ma15020682
60. Taetz, S., Bochot, A., Surace, C., Arpicco, S., Renoir, J.-M., Schaefer, U.F., Marsaud, V., Kerdine-Roemer, S., Lehr, C.-M., Fattal, E.: Hyaluronic acid-modified DOTAP/DOPE liposomes for the targeted delivery of anti-telomerase siRNA to CD44-expressing lung cancer cells. *Oligonucleotides* **2009**, 19(2), 103–116, doi: 10.1089/oli.2008.0168
61. Bogaert, B., Sauvage, F., Guagliardo, R., Muntean, C., van Nguyen, P., Pottie, E., Wels, M., Minnaert, A.-K., Rycke, R. de, Yang, Q., Peer, D., Sanders, N., Remaut, K., Paulus, Y.M., Stove, C., Smedt, S.C. de, Raemdonck, K.: A lipid nanoparticle platform for mRNA delivery through repurposing of cationic amphiphilic drugs. *J Control Release* **2022**, 350, 256–270, doi: 10.1016/j.jconrel.2022.08.009
62. Scherließ, R., Bock, S., Bungert, N., Neustock, A., Valentin, L.: Particle engineering in dry powders for inhalation. *Eur J Pharm Sci* **2022**, 172, 106158, doi: 10.1016/j.ejps.2022.106158
63. Anderson, S., Atkins, P., Bäckman, P., Cipolla, D., Clark, A., Daviskas, E., Disse, B., Entcheva-Dimitrov, P., Fuller, R., Gonda, I., Lundbäck, H., Olsson, B., Weers, J.: Inhaled Medicines: Past, Present, and Future. *Pharmacol Rev* **2022**, 74(1), 48–118, doi: 10.1124/pharmrev.120.000108

- 
64. Chow, M.Y.T., Qiu, Y., Lam, J.K.W.: Inhaled RNA Therapy: From Promise to Reality. *Trends in Pharmacological Sciences* **2020**, 41(10), 715–729, doi: 10.1016/j.tips.2020.08.002
65. Newman, S., Anderson, P.: Respiratory drug delivery. Essential theory and practice. Respiratory Drug Delivery Online, Richmond, Virginia **2009**
66. Bechtold-Peters, K., Luessen, H. (eds.): Pulmonary drug delivery: Basics, applications and opportunities for small molecules and biopharmaceutics. Apv - pharma reflexions, vol. 2. ECV Editio-Cantor-Verl., Aulendorf **2007**
67. Xu, Y., Thakur, A., Zhang, Y., Foged, C.: Inhaled RNA Therapeutics for Obstructive Airway Diseases: Recent Advances and Future Prospects. *Pharmaceutics* **2021**, 13(2), doi: 10.3390/pharmaceutics13020177
68. Sanders, N., Rudolph, C., Braeckmans, K., Smedt, S.C. de, Demeester, J.: Extracellular barriers in respiratory gene therapy. *Adv Drug Deliv Rev* **2009**, 61(2), 115–127, doi: 10.1016/j.addr.2008.09.011
69. Boer, A.H. de, Thalberg, K.: Chapter 5 - Dry powder inhalers (DPIs). In: Kassinos, S. (ed.) Inhaled Medicines. Optimizing Development Through Integration of in Silico, in Vitro and in Vivo Approaches, pp. 99–146. Elsevier Science & Technology, San Diego **2021**
70. Bundesinstitut für Arzneimittel und Medizinprodukte (ed.): Europäisches Arzneibuch 11. Ausgabe, Grundwerk 2023. Amtliche deutsche Ausgabe (Ph. Eur. 11.0), 4th edn. Deutscher Apotheker Verlag, Stuttgart **2023**
71. Patton, J.S.: Mechanisms of macromolecule absorption by the lungs. *Adv Drug Deliv Rev* **1996**, 19(1), 3–36, doi: 10.1016/0169-409X(95)00113-L
72. Carvalho, T.C., Peters, J.I., Williams, R.O.: Influence of particle size on regional lung deposition--what evidence is there? *International Journal of Pharmaceutics* **2011**, 406(1-2), 1–10, doi: 10.1016/j.ijpharm.2010.12.040
73. Labiris, N.R., Dolovich, M.B.: Pulmonary drug delivery. Part II: the role of inhalant delivery devices and drug formulations in therapeutic effectiveness of aerosolized medications. *Br J Clin Pharmacol* **2003**, 56(6), 600–612, doi: 10.1046/j.1365-2125.2003.01893.x
74. Boer, A.H. de, Thalberg, K.: Chapter 4 - Metered dose inhalers (MDIs). In: Kassinos, S. (ed.) Inhaled Medicines. Optimizing Development Through Integration of in Silico, in Vitro and in Vivo Approaches, pp. 65–97. Elsevier Science & Technology, San Diego **2021**
75. Y.T. Chow, M., K.W. Lam, J.: Dry Powder Formulation of Plasmid DNA and siRNA for Inhalation. *Current Pharmaceutical Design* **2015**, 21(27), 3854–3866

- 
76. Hoppentocht, M., Akkerman, O.W., Hagedoorn, P., Frijlink, H.W., Boer, A.H. de: The Cyclops for pulmonary delivery of aminoglycosides; a new member of the Twincer™ family. *Eur J Pharm Biopharm* **2015**, 90, 8–15, doi: 10.1016/j.ejpb.2015.01.012
  77. Boer, A.H. de, Hagedoorn, P., Westerman, E.M., Le Brun, P.P.H., Heijerman, H.G.M., Frijlink, H.W.: Design and in vitro performance testing of multiple air classifier technology in a new disposable inhaler concept (Twincer) for high powder doses. *Eur J Pharm Sci* **2006**, 28(3), 171–178, doi: 10.1016/j.ejps.2005.11.013
  78. Etschmann, C.: Development of a Softpellet Formulation for Inhaled High-Dose Therapy. Dissertation, Kiel University **2021**
  79. Malcolmson, R.J., Embleton, J.K.: Dry powder formulations for pulmonary delivery. *Pharmaceutical Science & Technology Today* **1998**, 1(9), 394–398, doi: 10.1016/S1461-5347(98)00099-6
  80. Vehring, R.: Pharmaceutical Particle Engineering via Spray Drying. *Pharm Res* **2008**, 25(5), 999–1022, doi: 10.1007/s11095-007-9475-1
  81. Broadhead, J., Edmond Rouan, S.K., Rhodes, C.T.: The spray drying of pharmaceuticals. *Drug Dev Ind Pharm* **1992**, 18(11-12), 1169–1206, doi: 10.3109/03639049209046327
  82. Munir, M., Jena, L., Kett, V.L., Dunne, N.J., McCarthy, H.O.: Spray drying: Inhalable powders for pulmonary gene therapy. *Biomaterials Advances* **2022**, 133, 112601, doi: 10.1016/j.msec.2021.112601
  83. Vehring, R., Foss, W.R., Lechuga-Ballesteros, D.: Particle formation in spray drying. *Journal of Aerosol Science* **2007**, 38(7), 728–746, doi: 10.1016/j.jaerosci.2007.04.005
  84. Alhajj, N., O'Reilly, N.J., Cathcart, H.: Leucine as an excipient in spray dried powder for inhalation. *Drug Discov Today* **2021**, 26(10), 2384–2396, doi: 10.1016/j.drudis.2021.04.009
  85. FDA: FDA. Inactive Ingredients Database. <https://www.fda.gov/drugs/drug-approvals-and-databases/inactive-ingredients-database-download>. Accessed 11 November 2023
  86. Ramanathan, A., Robb, G.B., Chan, S.-H.: mRNA capping: biological functions and applications. *Nucleic Acids Res* **2016**, 44(16), 7511–7526, doi: 10.1093/nar/gkw551
  87. Kramps, T., Elbers, K.: RNA Vaccines, vol. 1499. Springer New York, New York, NY **2017**
  88. Shawkat, H., Westwood, M.-M., Mortimer, A.: Mannitol: a review of its clinical uses. *Continuing Education in Anaesthesia Critical Care & Pain* **2012**, 12(2), 82–85, doi: 10.1093/bjaceaccp/mkr063
  89. Mannitol: Uses, Interactions, Mechanism of Action | DrugBank Online **2024**. <https://go.drugbank.com/drugs/DB00742>. Accessed 13 February 2024

- 
90. Fronczek, F.R., Kamel, H.N., Slattery, M.: Three polymorphs (alpha, beta, and delta) of D-mannitol at 100 K. *Acta Cryst C* **2003**, 59(Pt 10), O567-70, doi: 10.1107/S0108270103018961
91. Hulse, W.L., Forbes, R.T., Bonner, M.C., Getrost, M.: The characterization and comparison of spray-dried mannitol samples. *Drug Dev Ind Pharm* **2009**, 35(6), 712–718, doi: 10.1080/03639040802516491
92. Flume, P.A., Amelina, E., Daines, C.L., Charlton, B., Leadbetter, J., Guasconi, A., Aitken, M.L.: Efficacy and safety of inhaled dry-powder mannitol in adults with cystic fibrosis: An international, randomized controlled study. *J Cyst Fibros* **2021**, 20(6), 1003–1009, doi: 10.1016/j.jcf.2021.02.011
93. Gänzle, M.G., Haase, G., Jelen, P.: Lactose: Crystallization, hydrolysis and value-added derivatives. *International Dairy Journal* **2008**, 18(7), 685–694, doi: 10.1016/j.idairyj.2008.03.003
94. Demoly, P., Hagedoorn, P., Boer, A.H. de, Frijlink, H.W.: The clinical relevance of dry powder inhaler performance for drug delivery. *Respir Med* **2014**, 108(8), 1195–1203, doi: 10.1016/j.rmed.2014.05.009
95. Mangal, S., Meiser, F., Tan, G., Gengenbach, T., Denman, J., Rowles, M.R., Larson, I., Morton, D.A.V.: Relationship between surface concentration of L-leucine and bulk powder properties in spray dried formulations. *Eur J Pharm Biopharm* **2015**, 94, 160–169, doi: 10.1016/j.ejpb.2015.04.035
96. Mangal, S., Meiser, F., Lakio, S., Morton, D., Larson, I.: The role of physico-chemical and bulk characteristics of co-spray dried L-leucine and polyvinylpyrrolidone on glidant and binder properties in interactive mixtures. *International Journal of Pharmaceutics* **2015**, 479(2), 338–348, doi: 10.1016/j.ijpharm.2015.01.001
97. Chow, M.Y.T., Qiu, Y., Lo, F.F.K., Lin, H.H.S., Chan, H.-K., Kwok, P.C.L., Lam, J.K.W.: Inhaled powder formulation of naked siRNA using spray drying technology with l-leucine as dispersion enhancer. *International Journal of Pharmaceutics* **2017**, 530(1-2), 40–52, doi: 10.1016/j.ijpharm.2017.07.013
98. Foster, K.A., Avery, M.L., Yazdanian, M., Audus, K.L.: Characterization of the Calu-3 cell line as a tool to screen pulmonary drug delivery. *International Journal of Pharmaceutics* **2000**, 208(1-2), 1–11, doi: 10.1016/S0378-5173(00)00452-X
99. ATCC: Calu-3 Product Sheet (HTB-55) **2023**
100. Ong, H.X., Traini, D., Young, P.M.: Pharmaceutical applications of the Calu-3 lung epithelia cell line. *Expert Opinion on Drug Delivery* **2013**, 10(9), 1287–1302, doi: 10.1517/17425247.2013.805743
101. ATCC: A549 Product Sheet (CRM-CCL-185) **2023**. <https://www.atcc.org/products/crm-ccl-185>. Accessed 25 December 2023

- 
102. Foster, K. A., et al.: Characterization of the A549 Cell Line as a Type II Pulmonary Epithelial Cell Model for Drug Metabolism. *Experimental Cell Research* **1998**(243), 359–366, doi: 10.1006/excr.1998.4172
103. Malvern Panalytical: Manual: Zetasizer Nano user manual (English) MAN0485 **2013**
104. An Introduction to Dynamic Light Scattering (DLS) | Malvern Panalytical **2024**.  
<https://www.malvernpanalytical.com/de/learn/knowledge-center/technical-notes/tn101104dynamiclightscatteringintroduction>. Accessed 13 February 2024
105. Gilroy, E.L., Hicks, M.R., Smith, D.J., Rodger, A.: Viscosity of aqueous DNA solutions determined using dynamic light scattering. *Analyst* **2011**, 136(20), 4159–4163, doi: 10.1039/C1AN15475C
106. Bhattacharjee, S.: DLS and zeta potential - What they are and what they are not? *J Control Release* **2016**, 235, 337–351, doi: 10.1016/j.jconrel.2016.06.017
107. Qiu, Y., Clarke, M., Wan, L.T.L., Lo, J.C.K., Mason, A.J., Lam, J.K.W.: Optimization of PEGylated KL4 Peptide for siRNA Delivery with Improved Pulmonary Tolerance. *Mol Pharm* **2021**, 18(6), 2218–2232, doi: 10.1021/acs.molpharmaceut.0c01242
108. Arnold, P., Lückstädt, W., Li, W., Boll, I., Lokau, J., Garbers, C., Lucius, R., Rose-John, S., Becker-Pauly, C.: Joint Reconstituted Signaling of the IL-6 Receptor via Extracellular Vesicles. *Cells* **2020**, 9(5), 1307, doi: 10.3390/cells9051307
109. Promega Corporation: CellTiter-Glo® Luminescent Cell Viability Assay Technical Bulletin, TB288 **2023**. <https://ch.promega.com/-/media/files/resources/protocols/technical-bulletins/0/celltiter-glo-luminescent-cell-viability-assay-protocol.pdf>. Accessed 27 December 2023
110. Lövborg, H., Wojciechowski, J., Larsson, R., Węsierska-Gądek, J.: Action of a Novel Anticancer Agent, CHS 828, on Mouse Fibroblasts Increased Sensitivity of Cells Lacking Poly (ADP-Ribose) Polymerase-1. *Cancer Res* **2002**, 62(15), 4206–4211
111. Reichmuth, A.M., Oberli, M.A., Jaklenec, A., Langer, R., Blankschtein, D.: mRNA vaccine delivery using lipid nanoparticles. *Ther Deliv* **2016**, 7(5), 319–334, doi: 10.4155/tde-2016-0006
112. Lappalainen, K., Jääskeläinen, I., Syrjänen, K., Urtti, A., Syrjänen, S.: Comparison of cell proliferation and toxicity assays using two cationic liposomes. *Pharm Res* **1994**, 11(8), 1127–1131, doi: 10.1023/A:1018932714745
113. Behr, J.-P.: Gene Transfer with Synthetic Cationic Amphiphiles: Prospects for Gene Therapy. *Bioconjugate Chemistry* **1994**
114. Debus, H., Baumhof, P., Probst, J., Kissel, T.: Delivery of messenger RNA using poly(ethylene imine)-poly(ethylene glycol)-copolymer blends for polyplex formation: biophysical characterization and in vitro transfection properties. *J Control Release* **2010**, 148(3), 334–343, doi: 10.1016/j.jconrel.2010.09.007

- 
115. Akbarzadeh, A., Rezaei-Sadabady, R., Davaran, S., Joo, S.W., Zarghami, N., Hanifehpour, Y., Samiei, M., Kouhi, M., Nejati-Koshki, K.: Liposome: classification, preparation, and applications. *Nanoscale Res Lett* **2013**, 8(1), 102, doi: 10.1186/1556-276X-8-102
116. Bohr, A., Tsapis, N., Foged, C., Andreana, I., Yang, M., Fattal, E.: Treatment of acute lung inflammation by pulmonary delivery of anti-TNF- $\alpha$  siRNA with PAMAM dendrimers in a murine model. *Eur J Pharm Biopharm* **2020**, 156, 114–120, doi: 10.1016/j.ejpb.2020.08.009
117. Qiu, Y., Man, R.C.H., Liao, Q., Kung, K.L.K., Chow, M.Y.T., Lam, J.K.W.: Effective mRNA pulmonary delivery by dry powder formulation of PEGylated synthetic KL4 peptide. *J Control Release* **2019**, 314, 102–115, doi: 10.1016/j.jconrel.2019.10.026
118. Ciani, L., Ristori, S., Salvati, A., Calamai, L., Martini, G.: DOTAP/DOPE and DC-Chol/DOPE lipoplexes for gene delivery: zeta potential measurements and electron spin resonance spectra. *Biochim Biophys Acta* **2004**, 1664(1), 70–79, doi: 10.1016/j.bbamem.2004.04.003
119. Khatri, N., Baradia, D., Vhora, I., Rathi, M., Misra, A.: Development and characterization of siRNA lipoplexes: Effect of different lipids, in vitro evaluation in cancerous cell lines and in vivo toxicity study. *AAPS PharmSciTech* **2014**, 15(6), 1630–1643, doi: 10.1208/s12249-014-0193-9
120. Merkel, O.M., Rubinstein, I., Kissel, T.: siRNA delivery to the lung: what's new? *Adv Drug Deliv Rev* **2014**, 75, 112–128, doi: 10.1016/j.addr.2014.05.018
121. Pires, P., Simões, S., Nir, S., Gaspar, R., Düzgünes, N., Pedroso de Lima, M.C.: Interaction of cationic liposomes and their DNA complexes with monocytic leukemia cells. *Biochim Biophys Acta* **1999**, 1418(1), 71–84, doi: 10.1016/S0005-2736(99)00023-1
122. Ma, B., Zhang, S., Jiang, H., Zhao, B., Lv, H.: Lipoplex morphologies and their influences on transfection efficiency in gene delivery. *J Control Release* **2007**, 123(3), 184–194, doi: 10.1016/j.jconrel.2007.08.022
123. Dokka, S., Toledo, D., Shi, X., Castranova, V., Rojanasakul, Y.: Oxygen radical-mediated pulmonary toxicity induced by some cationic liposomes. *Pharm Res* **2000**, 17(5), 521–525, doi: 10.1023/A:1007504613351
124. Florea, B.I., Meaney, C., Junginger, H.E., Borchard, G.: Transfection efficiency and toxicity of polyethylenimine in differentiated Calu-3 and nondifferentiated COS-1 cell cultures. *AAPS J* **2002**, 4(3), E12, doi: 10.1208/ps040312
125. Stewart, C.E., Torr, E.E., Mohd Jamili, N.H., Bosquillon, C., Sayers, I.: Evaluation of differentiated human bronchial epithelial cell culture systems for asthma research. *Journal of Allergy* **2012**, 2012, 943982, doi: 10.1155/2012/943982

- 
126. Liang, W., Chan, A.Y.L., Chow, M.Y.T., Lo, F.F.K., Qiu, Y., Kwok, P.C.L., Lam, J.K.W.: Spray freeze drying of small nucleic acids as inhaled powder for pulmonary delivery. *Asian J Pharm Sci* **2018**, 13(2), 163–172, doi: 10.1016/j.ajps.2017.10.002
127. Thermo Fisher Scientific: Lipofectamine 2000.  
<https://www.thermofisher.com/order/catalog/product/de/de/11668019>. Accessed 9 April 2024
128. Dana, H., Chalbatani, G.M., Mahmoodzadeh, H., Karimloo, R., Rezaiean, O., Moradzadeh, A., Mehmandoust, N., Moazzen, F., Mazraeh, A., Marmari, V., Ebrahimi, M., Rashno, M.M., Abadi, S.J., Gharagouzlo, E.: Molecular Mechanisms and Biological Functions of siRNA. *International Journal of Biomedical Science : IJBS* **2017**, 13(2), 48–57
129. Bosquillon, C., Lombry, C., Pr eat, V., Vanbever, R.: Influence of formulation excipients and physical characteristics of inhalation dry powders on their aerosolization performance. *Journal of Controlled Release* **2001**, 70(3), 329–339, doi: 10.1016/S0168-3659(00)00362-X
130. Steiner, D., Schumann, L.V., Bunjes, H.: Processing of Lipid Nanodispersions into Solid Powders by Spray Drying. *Pharmaceutics* **2022**, 14(11), doi: 10.3390/pharmaceutics14112464
131. B UCHI Labortechnik GmbH: Application\_Booklet\_Nano\_Spray\_Drying
132. B UCHI Labortechnik GmbH: Particle collector of the Nano Spray Dryer B-90.  
<https://www.buchi.com/de/produkte/instrumente/nano-spray-dryer-b-90-hp>. Accessed 11 December 2023
133. Keil, T.W.M., Deiringer, N., Friess, W., Merkel, O.M.: Evaluation of adsorption of DNA/PEI polyplexes to tubing materials. *Eur J Pharm Biopharm* **2022**, 179, 58–64, doi: 10.1016/j.ejpb.2022.08.014
134. Saint-Gobain Performance Plastics: Tygon Ultra Chemical Resistant Tubing, Formulation 2375, Saint-Gobain Performance Plastics.  
<https://www.cmscientific.com/info-sheets/Tygon2375.pdf>. Accessed 13 December 2023
135. FDA: CFR - Code of Federal Regulations Title 21 **2023**.  
<https://www.accessdata.fda.gov/scripts/cdrh/cfdocs/cfcr/cfrsearch.cfm?fr=177.1520>. Accessed 15 December 2023
136. OPTUBUS GmbH: datasheet-tube-tygon-f-4040-a.  
<https://www.optubus.de/files/datasheets/datasheet-tube-tygon-f-4040-a.pdf>. Accessed 15 December 2023
137. Trenkel, M.: Effects of excipients in nasal powder formulations for systemic drug delivery. Dissertation, Kiel University **2023**

138. Scherliess, R.: The MTT assay as tool to evaluate and compare excipient toxicity in vitro on respiratory epithelial cells. *International Journal of Pharmaceutics* **2011**, 411(1-2), 98–105, doi: 10.1016/j.ijpharm.2011.03.053
139. Carrillo, C., Sánchez-Hernández, N., García-Montoya, E., Pérez-Lozano, P., Suñé-Negre, J.M., Ticó, J.R., Suñé, C., Miñarro, M.: DNA delivery via cationic solid lipid nanoparticles (SLNs). *Eur J Pharm Sci* **2013**, 49(2), 157–165, doi: 10.1016/j.ejps.2013.02.011
140. Jüptner, A.: Einfluss von Dosiersystemen auf sprühgetrocknete Pulver zur Applikation im Respirationstrakt. Dissertation, Kiel University **2022**
141. Hellfritzschn, M.: Zinc oxide in formulation for respiratory vaccination. Dissertation, Kiel University **2021**
142. Maas, S.G., Schaldach, G., Littringer, E.M., Mescher, A., Griesser, U.J., Braun, D.E., Walzel, P.E., Urbanetz, N.A.: The impact of spray drying outlet temperature on the particle morphology of mannitol. *Powder Technology* **2011**, 213(1-3), 27–35, doi: 10.1016/j.powtec.2011.06.024
143. HAQUE, M.K., ROOS, Y.H.: Water Plasticization and Crystallization of Lactose in Spray-dried Lactose/Protein Mixtures. *Journal of Food Science* **2004**, 69(1), FEP23-FEP29, doi: 10.1111/j.1365-2621.2004.tb17863.x
144. Grohgan, H., Lee, Y.-Y., Rantanen, J., Yang, M.: The influence of lysozyme on mannitol polymorphism in freeze-dried and spray-dried formulations depends on the selection of the drying process. *International Journal of Pharmaceutics* **2013**, 447(1-2), 224–230, doi: 10.1016/j.ijpharm.2013.03.003
145. Vicente, J., Pinto, J., Menezes, J., Gaspar, F.: Fundamental analysis of particle formation in spray drying. *Powder Technology* **2013**, 247, 1–7, doi: 10.1016/j.powtec.2013.06.038
146. Pinto, J.T., Wutscher, T., Stankovic-Brandl, M., Zellnitz, S., Biserni, S., Mercandelli, A., Kobler, M., Buttini, F., Andrade, L., Daza, V., Ecenarro, S., Canalejas, L., Paudel, A.: Evaluation of the Physico-mechanical Properties and Electrostatic Charging Behavior of Different Capsule Types for Inhalation Under Distinct Environmental Conditions. *AAPS PharmSciTech* **2020**, 21(4), 128, doi: 10.1208/s12249-020-01676-2
147. Jaafar-Maalej, C., Andrieu, V., Elaissari, A., Fessi, H.: Assessment methods of inhaled aerosols: technical aspects and applications. *Expert Opinion on Drug Delivery* **2009**, 6(9), 941–959, doi: 10.1517/17425240903117244
148. Heida, R., Akkerman, R., Jacob Silva, P.H., Lakerveld, A.J., Ortiz, D., Bigogno, C., Gasbarri, M., van Kasteren, P.B., Stellacci, F., Frijlink, H.W., Huckriede, A.L.W., Hinrichs, W.L.J.: Development of an inhalable antiviral powder formulation against respiratory

- syncytial virus. *J Control Release* **2023**, 357, 264–273, doi: 10.1016/j.jconrel.2023.03.059
149. MEGGLE Pharma: InhaLac® 70 Produkt Detail - MEGGLE Pharma - Excipients & Technology **2024**. <https://www.meggle-pharma.de/de/lactose/20-inhalac-70.html>. Accessed 12 January 2024
150. MEGGLE Pharma: InhaLac® 120 Produkt Detail - MEGGLE Pharma - Excipients & Technology **2024**. <https://www.meggle-pharma.de/de/lactose/21-inhalac-120.html>. Accessed 12 January 2024
151. MEGGLE Pharma: InhaLac® 180 Produkt Detail - MEGGLE Pharma - Excipients & Technology **2024**. <https://www.meggle-pharma.de/de/lactose/34-inhalac-180.html>. Accessed 12 January 2024
152. MEGGLE Pharma: InhaLac® 251 Produkt Detail - MEGGLE Pharma - Excipients & Technology **2024**. <https://www.meggle-pharma.de/de/lactose/26-inhalac-251.html>. Accessed 12 January 2024
153. Raghavan, S.L., Ristic, R.I., Sheen, D.B., Sherwood, J.N., Trowbridge, L., York, P.: Morphology of Crystals of  $\alpha$ -Lactose Hydrate Grown from Aqueous Solution. *J. Phys. Chem. B* **2000**, 104(51), 12256–12262, doi: 10.1021/jp002051o
154. Keil, T.W., Zimmermann, C., Baldassi, D., Adams, F., Friess, W., Mehta, A., Merkel, O.M.: Impact of crystalline and amorphous matrices on successful spray drying of siRNA polyplexes for inhalation of nano-in-microparticles. *Advanced Therapeutics* **2021**, 4(6), 2100073, doi: 10.1002/adtp.202100073
155. Son, Y.-J., Miller, D.P., Weers, J.G.: Optimizing Spray-Dried Porous Particles for High Dose Delivery with a Portable Dry Powder Inhaler. *Pharmaceutics* **2021**, 13(9), 1528, doi: 10.3390/pharmaceutics13091528
156. Rabbani, N.R., Seville, P.C.: The influence of formulation components on the aerosolisation properties of spray-dried powders. *Journal of Controlled Release* **2005**, 110(1), 130–140, doi: 10.1016/j.jconrel.2005.09.004
157. Schoubben, A., Vivani, R., Paolantoni, M., Perinelli, D.R., Gioiello, A., Macchiarulo, A., Ricci, M.: D-leucine microparticles as an excipient to improve the aerosolization performances of dry powders for inhalation. *Eur J Pharm Sci* **2019**, 130, 54–64, doi: 10.1016/j.ejps.2019.01.018
158. Tang, M., Hattori, Y.: Effect of using amino acids in the freeze-drying of siRNA lipoplexes on gene knockdown in cells after reverse transfection. *Biomedical Reports* **2021**, 15(3), 72, doi: 10.3892/br.2021.1448
159. Molina, C., Kaialy, W., Nokhodchi, A.: The crucial role of leucine concentration on spray dried mannitol-leucine as a single carrier to enhance the aerosolization performance of

- Albuterol sulfate. *Journal of Drug Delivery Science and Technology* **2019**, 49, 97–106, doi: 10.1016/j.jddst.2018.11.007
160. Li, L., Sun, S., Parumasivam, T., Denman, J.A., Gengenbach, T., Tang, P., Mao, S., Chan, H.-K.: L-Leucine as an excipient against moisture on in vitro aerosolization performances of highly hygroscopic spray-dried powders. *Eur J Pharm Biopharm* **2016**, 102, 132–141, doi: 10.1016/j.ejpb.2016.02.010
161. Wang, X., Wan, W., Lu, J., Quan, G., Pan, X., Liu, P.: Effects of L-leucine on the properties of spray-dried swellable microparticles with wrinkled surfaces for inhalation therapy of pulmonary fibrosis. *International Journal of Pharmaceutics* **2021**, 610, 121223, doi: 10.1016/j.ijpharm.2021.121223
162. Mohamed, A., Pekoz, A.Y., Ross, K., Hutcheon, G.A., Saleem, I.Y.: Pulmonary delivery of Nanocomposite Microparticles (NCMPs) incorporating miR-146a for treatment of COPD. *International Journal of Pharmaceutics* **2019**, 569, 118524, doi: 10.1016/j.ijpharm.2019.118524
163. Sibum, I., Hagedoorn, P., Kluitman, M.P.G., Kloezen, M., Frijlink, H.W., Grasmeijer, F.: Dispersibility and Storage Stability Optimization of High Dose Isoniazid Dry Powder Inhalation Formulations with L-Leucine or Trileucine. *Pharmaceutics* **2019**, 12(1), 24, doi: 10.3390/pharmaceutics12010024
164. Peletta, A., Prompetchara, E., Tharakhet, K., Kaewpang, P., Buranapraditkun, S., Yostreat, N., Manopwisedjaroen, S., Thitithanyanont, A., Avaro, J., Krupnik, L., Neels, A., Ruxrungham, K., Ketloy, C., Borchard, G.: Translating a Thin-Film Rehydration Method to Microfluidics for the Preparation of a SARS-CoV-2 DNA Vaccine: When Manufacturing Method Matters. *Pharmaceutics* **2022**, 14(7), 1427, doi: 10.3390/pharmaceutics14071427









## Erklärung gemäß §8 und §9 der Promotionsordnung

Hiermit erkläre ich gemäß §9 der Promotionsordnung der Mathematisch-Naturwissenschaftlichen Fakultät der Christian-Albrechts-Universität zu Kiel, dass es sich bei der vorliegende Dissertation - abgesehen von der Beratung durch den Betreuer - nach Inhalt und Form um eine eigenständig und nur mit den angegebenen Hilfsmitteln verfasste Arbeit auf Grundlage eigenständiger, wissenschaftlicher Leistungen handelt. Die Arbeit wurde unter Einhaltung der Regeln guter wissenschaftlicher Praxis der Deutschen Forschungsgemeinschaft erstellt.

Weiterhin versichere ich, dass mir noch kein akademischer Grad entzogen wurde, sowie, dass die vorliegende Arbeit an keiner anderen Stelle im Rahmen eines Prüfungsverfahrens vorgelegen hat.

---

Jana Karin Schembera

Erklärung gemäß §8 und §9 der Promotionsordnung

## Danksagung

Zum Abschluss meiner Promotionszeit möchte ich mich bei einer Reihe wunderbarer Menschen bedanken, die mich auf meinem Weg begleitet und unterstützt haben.

Ein herzliches Dankeschön möchte ich meiner Doktormutter, Prof. Dr. Regina Scherließ aussprechen. Vielen Dank, dass Du mir ermöglicht hast, dieses spannende Thema zu bearbeiten. Durch Dein Vertrauen, Deinen ermutigenden Input und Deine Unterstützung könnte ich nicht nur diese Arbeit anfertigen, sondern mich auch persönlich und beruflich weiterentwickeln. Danke!

Lieben Dank an alle ehemaligen und derzeitigen festangestellten Mitarbeitenden des pharmazeutischen Instituts und der pharmazeutischen Technologie. Einige von Euch haben mich nun angefangen mit meiner Hiwi-Zeit bis zum Beenden meiner Promotion stetig begleitet. Ich danke Euch für Eure Unterstützung und Eure offenen Ohren.

Vielen Dank an alle ehemaligen und derzeitigen Mitglieder des Arbeitskreises für eine wundervolle Zeit, mit viel Lachen, schönen Unternehmungen und (un)konstruktiven Gesprächen. Ich hätte mir keine besseren KollegInnen während den Höhen und Tiefen meiner Promotion vorstellen können und habe mich immer sehr wohl gefühlt.

Danke auch an alle, die meine Arbeit Korrektur gelesen haben, für Eure Genauigkeit und Euer Feedback. Auch Danke an meine Hiwis für Eure Unterstützung im Labor.

Ein sehr großer Dank geht an meine Familie. Danke für Eure bedingungslose Unterstützung und dafür, dass Ihr immer an mich glaubt. Dadurch war das erst alles möglich.

Von ganzem Herzen möchte ich Daniel danken. Danke für Dein Verständnis, Deine Geduld, die Aufmunterungen und dass Du mir immer mit Rat und Tat zur Seite stehst.